Stochastic Models of Aggregation with Injection

高安，美佐子

(Degree)
博士（理学）

(Date of Degree)
1993-03-31

(Date of Publication)
2008-06-04

(Resource Type)
doctoral thesis

(Report Number)
甲1212

(JaLCDOI)
https://doi.org/10.11501/3092492

(URL)
https://hdl.handle.net/20.500.14094/D1001212

博士論文

Stochastic Models of Aggregation with Injection

（注入のある凝集系の統計的モデル）

平成５年　3月

神戸大学大学院自然科学研究科

高安　美佐子

DOCTORAL DISSERTATION

Stochastic Models of Aggregation with Injection

Misako TAKAYASU

Division of Material Science,
The Graduate School of Science and Technology,
Kobe University,
Rokkodai, Nada, Kobe 657, Japan

March, 1993

To my daughter Léna.

Contents

Acknowledgements

My principal debt of gratitude is to Prof. K. Ito who provided me with a scientific atmosphere for working in this exciting field and gave me many opportunities to discuss frankly with many people. I would like to very much thank him for many discussions and continuous encouragements.

I would also like to thank Prof. H. E. Stanley and the members of his group who provided me with interesting discussions during my stay in Boston University as a research fellow. Specially, I would like to thank Dr. A. Provata and Dr. G. Huber for productive and stimulating coworks.

I wish to thank many people at the Department of Earthsciences at Kobe University, in many different ways; Dr. A. Yu. Tretyakov for helpful discussions and careful reading the manuscript, Prof. T. Mukai and Dr. M. Matsuzaki for many discussions concerned with interplanetary and geophysical aspects of aggregation phenomena.

I am also very much indebted to my parents for their moral surpport. Special gratitude to my husband, Prof. H. Takayasu. I would have never achieved my study without his encouragements.

Chapter 1

Introduction

1.1 Approaches to non-equilibrium irreversible processes

The first step toward statistical mechanics was taken in 1736 by J. Bernoulli who tried to derive Boyle-Charles law for rarefied gas by Newtonian mechanics. Since then, great efforts were made by physicists to reconstruct thermodynamics by considering microscopic pictures of molecular motion. Macroscopic empirical laws under thermal equilibrium condition were successfully explained by ensembles of molecular dynamical quantities. In 1877, L. Boltzmann interpreted the second law of thermodynamics, i.e., the irreversible increase of entropy, as a stochastic process of equipartition of energy by elastic collisions of molecules. Though the dynamical processes on microscopical level are reversible, the macroscopic irreversibility is obtained. In the middle of this century a general theory of near-equilibrium systems for which the deviation from the thermal equilibrium is approximated by the first order of expansion terms has been achieved. The formalism is well-known as the linear response theory. However, it is not applicable to far-from-equilibrium systems where responses are nonlinear.

On the other hand, the study of far-from-equilibrium has been attracting much attention in the last two decays. (The historical progress of statistical physics from thermal equilibrium to far-from-equilibrium is shown schematically in Fig.1.1). Though many macroscopic phenomena in nature, such as turbulence, lightning, earthquakes, fracture, erosion, and formation of clouds, aerosols, and interstellar dusts are typical problems of far-from-equilibrium, no unified view has been established.

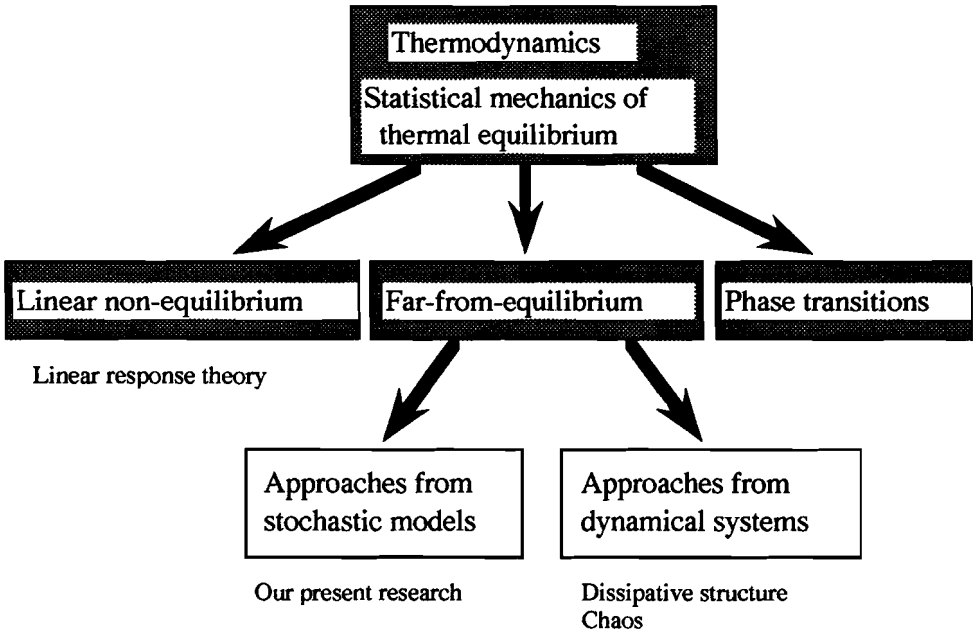

Fig.1.1 Schematic views of thermodynamics to far-from-equilibrium statistical physics.

These problems in nature involve essential difference from thermal equilibrium systems. First, at the macroscopic level the systems do not satisfy the detailed balance and equipartition principles. Second, the system is usually open to an outside source. In order to describe such systems it is necessary to take into account of the injection and dissipation processes. At present stage, we do not know a universal distribution for far-from-equilibrium such as the canonical distribution for thermal equilibrium.

Let us consider an approach by computer analysis. Here we consider a typical far-from-equilibrium problem, aggregation of macroscopic sticky grains, which is the basic process of forming dusts in atmosphere or in outer space. If we try to simulate such

systems by microscopic view we have to include typically an order of $1mol$ molecules to represent one macroscopic particle at local equilibrium. At a collision of two macroscopic particles we will be required a lot of CPU time to observe the fusion of incident macroscopic particles, and still more calculation will be needed until the system reaches a new thermal equilibrium. Further, we have to calculate millions of collisions of macroscopic particles in order to obtain the distribution of particle sizes. Obviously, this is far beyond the capacity of present computers.

By changing the point of view, we can visualize the far-from-equilibrium systems by directly considering in macroscopic terms. Namely, we can make a model of far-from-equilibrium by assuming irreversible rules for the macroscopic dynamics. For example, we are able to make a model for aerosol formation by thinking of particles' coagulation process, neglecting details of microscopic conditions. In such a way, we may explain the mechanism of some universal behavior on macroscopic level found in the natural irreversible systems.

One of the early attempts to use this approach was reported by *T. A. Witten* and *L. M. Sander*(1981) who modeled a pattern formed by cathode deposition of positive metalic ions in an electrolite containing in a small concentration. When a randomly diffusing ion hits the electrode or the already deposited metal on its surface, it immediately sticks to the surface by electrostatic attraction. A randomly branching pattern (see Fig.1.2a) obtained in this experiment is realized by a simple model called *diffusion-limited-aggregation*(DLA): Put a seed particle at the origin of a lattice. Another particle launched far away from origin randomly walks on the lattice. When it arrives at an adjacent site to the seed particle it

stops and forms one more seed particle, and another diffusing particle is launched. Repeating this process, we obtain a branched pattern(Fig.1.2b) which realizes the main features of the deposition pattern obtained experimentally.

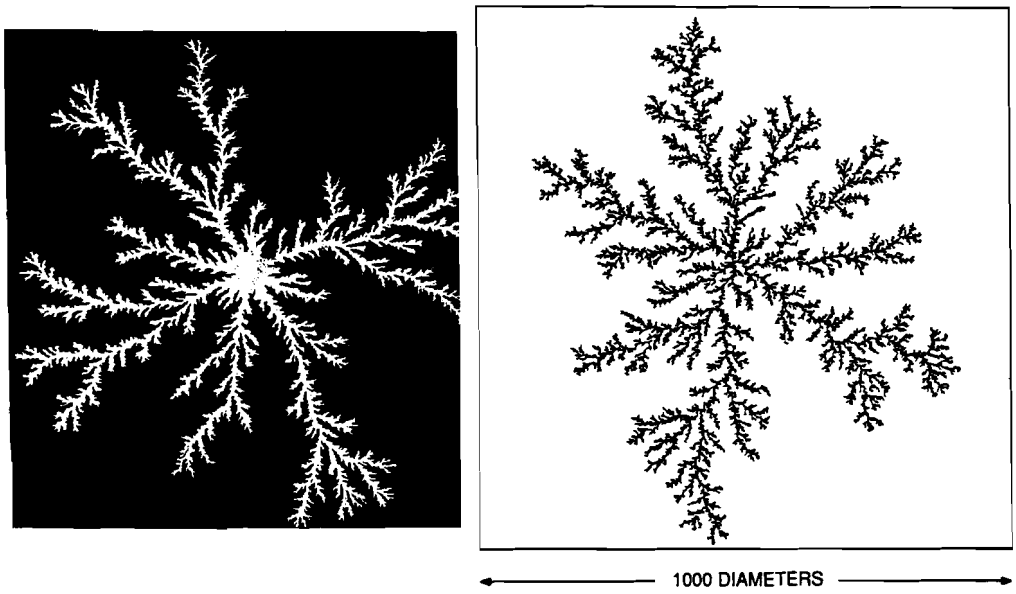

Fig.1.2a Branched structure formed on a centrally positioned zinc electrode by cathdic deposition. [*M. Matsusita, M. Sano, Y. Hayakawa, H. Honjo, and Y. Sawada*(1984)]

b Simulation of a two-dimensional aggregation of particles according to DLA rules. It was composed of 50,000 particles. [*P. Meakin*(1985)]

Randomly branching structures in DLA process and similar models show statistically self-similar appearance. Namely, we cannot tell the statistical difference in shape between a large branch and its component small branches if we enlarge the small ones. We can formulate such self-similar characteristic by a power-

law function since power-law is the only function that has the scale invariance. If a function $n(r)$ is scale-invariant then $n(r)$ satisfies $n(r) \propto n(kr)$ for all positive k. That is, if $n(r)$ is scale-invariant then $n(r)$ should satisfy the functional relation; $n(kr) = n(k)n(r)$ for all positive k and r, from the symmetry of k and r. This equation is the Cauchy's function equation whose only continuous solution(apart from the trivial $n(r)=0$ for all positive r) is; $n(r) = r^{\alpha}$ for some real number α [see *G. Korvin* (1992)]. The self-similarity of DLA is characterized as follows: If we consider a circle of radius r from the origin then the number of particles within the circle, $n(r)$, is scaled as

$$n(r) \propto r^{D} , \qquad (4.1.1)$$

where D is a fractional exponent which is called the *fractal dimension* [*B. B. Mandelbrot* (1975)] and the self-similar geometrical patterns of this kind are called fractals. In the case of DLA the fractal dimension is estimated by computer analysis as D =1.70±0.06 for two-dimensional lattice [*P. Meakin* (1983)].

Scale invariance and fractal geometry are the typical macroscopic feature of far-from-equilibrium systems observed in nature. Yet, we do not know how the self-similarity is achieved. We can say that power-law distributions and fractal geometries are, in a sense, macroscopic peculiarities of *irreversible* systems corresponding to the empirical laws of classical thermodynamics.

The concept of fractal is not only used to describe geometrical self-similar patterns, but also to the phenomena whose distributions follow power-laws, which are typically observed in far-from-equilibrium systems. In the following chapters we

consider the processes of particles' coagulation, but mostly concentrating on the mechanism of forming power-law size distributions in open systems.

1.2 Random aggregating systems observed in nature

In this section we discuss open aggregating particle systems in nature and the corresponding stochastic models.

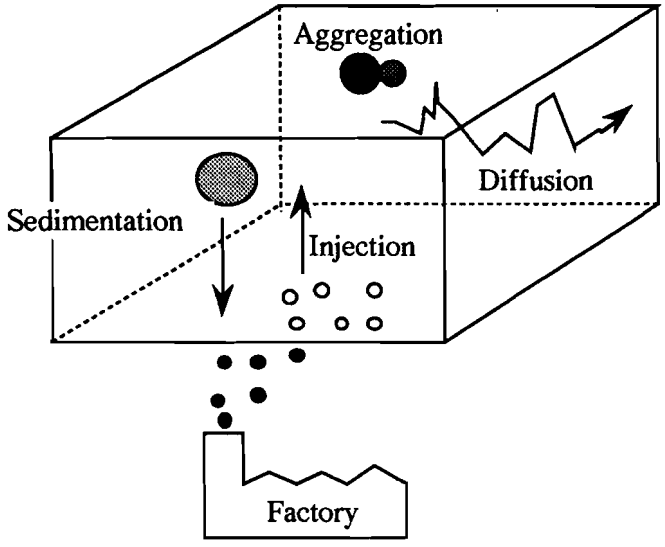

Fig.1.3 Mechanism of aerosol formation in air.

Let us consider aggregation of aerosols. The typical sizes of aerosol are of diameter 10Å(size of a cluster of molecules) to 100μm(size of a fog waterdrop or a particle of fine dust). Since aerosols are small enough they are regarded as particles randomly floating in air, and coagulate with certain probability when they collide. Diffusion and coagulation are repeated until a fully

developed particle, which starts sedimentation, is formed. Beside, small particles are continuously supplied by car fumes and smokes from industrial factories. Fig.1.3 shows a mechanism of aerosol development schematically.

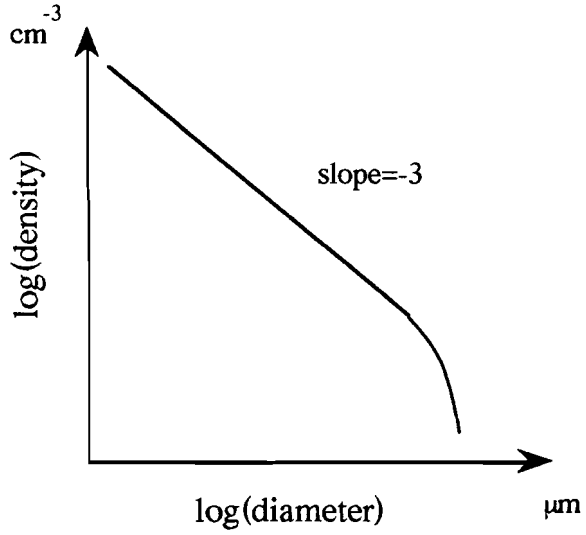

Fig.1.4 A schematic diagram for particle size distribution in aerosols.

Effect of aggregation, sedimentation, and supply of small particles balance to realize a steady state. As shown in Fig.1.4, the steady state size distribution has a power-law range, and, due to sedimentation, a fast decay at the large size range. It has been reported that in actual observation, the diameter distribution for aerosols follows a power-law with an exponent close to -3. Namely, $N(r) \propto r^{-3}$, where $N(r)$ denotes the density of aerosols of diameter r [*Takahashi, T.* (1987)]. Let us discuss in more detail about this power-law distribution.

The system described above is called a *random aggregating system*. In order to concentrate on to the power-law size distribution, here we consider only coagulation and injection of small particles. For convenience we neglect the sedimentation process. If such random aggregating system is closed and no particle is supplied, then the total number of particles decays monotonically with time in the irreversible aggregating process. (In the next chapter we will show that the decay follows a power-law for a particular case of Scheidegger's river model; a model of simplified randomly aggregating particles system in which particles of different sizes diffuse in the same manner.) As a result, the steady state will be a trivial configuration in which all particles gather into one large particle. As we see, the system is required to be open in order to reach a non-trivial steady state.

By injecting small particles continuously, a steady size distribution of fractional power-laws can be observed. It has been shown for Scheidegger's river model that this power-law is stable, namely, the system recovers the same distribution regardless of any perturbation(see chapter 2.5). The power-law is supported by the balance of increasing the number of small particles by injection and decreasing it by aggregation process. In other words, if we single out a particle of any size it grows larger and larger by repeating coalescence, but the number of particles of a given size is kept constant by aggregation of newly injected small particles. Moreover, for a given rate of supply of small particles the aggregation rate is naturally controlled by the injection rate of small particles so that the power-law is maintained for any injection rate(see Fig.1.5), although the mean-size of particles increases with time. We call this condition which is characterized

by a stable power-law as a *statistically steady state* distinguishing from usual steady states in which mean values converge as time develops.

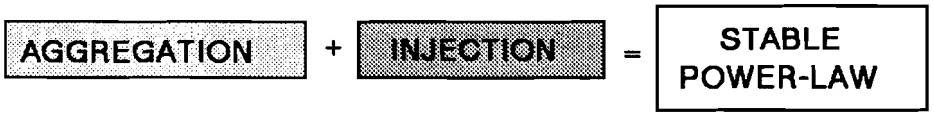

Fig.1.5 A stable power-law is obtained by the balance of aggregation process and injection of particles.

The classical understanding of aggregation kinetics is given by the rate equation approach proposed by *M. von Smoluchowski* (1917). The basic assumptions of his theory are the followings:

i) The reaction rate K_{ij} for two particles of mass i and j is the same for any pair of particles having masses i and j.

ii) The concentration of particles with a given mass can be represented by its spatial average. Thus the spatial dependence of all quantities is neglected, consequently, the results of this approach give the values of the mean-field theory.

iii) The system is sufficiently diluted so that the reaction rate between two types of particles is not influenced by the presence of other particles.

The so-called Smoluchowski equation is found by writing the population balance of both the gains and losses due to collisions under above assumptions. It can be written as follows;

$$\frac{\partial}{\partial t} n_k(t) = \frac{1}{2} \sum_{i+j=k} K_{ij} n_i(t) n_j(t) - n_k(t) \sum_{j=1}^{\infty} K_{kj} n_j(t) + I_k - R_k n_k(t), \quad (1.2.1)$$

where $n_k(t)$ denotes the concentration of particles having mass k at time t, I_k denotes the concentration of particles having mass k injected at time t, and R_k denotes the sedimentation rate of particles having mass k at time t. The first term at the right hand side expresses the number of particles of mass k increased by aggregation, formed by particles having mass i and j coalescing to form a particle of mass $k=i+j$. The second term shows the number of particles of mass k decreased by aggregation of particles having mass k and the other particles. The third term and the last term correspond to injection and sedimentation rate, respectively. Eq(1.2.1) has been studied extensively for decades and it can explain power-law size distributions widely observed in aggregation process. The collision matrix K_{ij} is determined by the physics of the aggregation process. For aggregation of diffusing spherical particles K_{ij} is known to be expressed as $K_{ij} \propto (i^{1/3}+j^{1/3})(i^{-1/3}+j^{-1/3})$. The exact solutions were known only for the case of $K_{ij} \propto 1$ [*M. von Smoluchowski* (1916)], $K_{ij} \propto i+j$ [*J. B. Mcleod* (1962)], and $K_{ij} \propto ij$ [*R. M. Ziff* (1980)]. The Eq.(1.2.1) involves essential difficulties of nonlinearity. The exact solutions for many other cases with complicated collision matrices are still unknown.

In the next chapter, we introduce a special model for which the size distribution and the other statistical properties are rigorously analyzed not only in the mean-field case but also in one-dimension with spatial effects taken into account. We mathematically show that our model has a stable power-law distribution under any

perturbation and derive the functional forms of relaxation to the power-law. Critical dimensions and the exponents of the size distribution depending on the injection types are discussed.

In chapter 3, we introduce some extended models and analyze their statistical properties. The models introduced in this chapter are an aggregation of exponentially growing particles with injection, a random advection dynamics in which a portion of the particles are distributed to neighboring sites, and a modified version of Scheidegger's model where particles' jumping rates depend on their mass.

In the last chapter, we discuss the spatial correlation of aggregation with injection system. The author introduces two new general methods to analyze the correlation of spatial and temporal data. We show that these methods are powerful even for violently fluctuated data which are often encountered in far-from-equilibrium systems.

Chapter 2

Scheidegger's river model

2.1 The model and the basic equations

In the previous chapter, we reviewed some examples of far from equilibrium irreversible systems found in nature, which automatically organize steady states with power-law distributions. In this section we introduce a simple model of random aggregating particles. We will find that even a simplified model can reproduce some peculiarities of non-trivial self-organizing processes found in nature.

2.1.1 The model

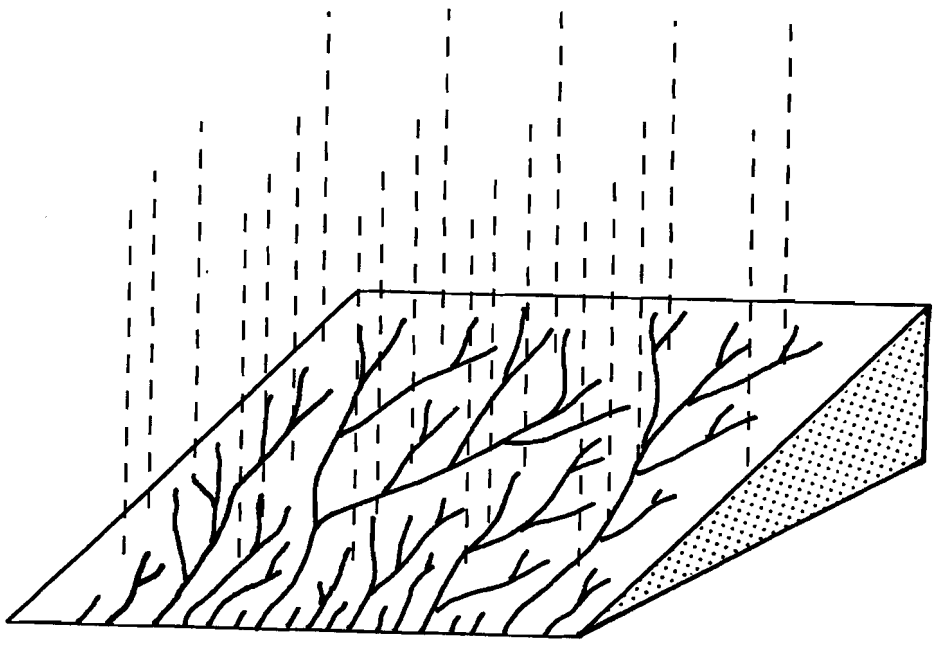

Fig.2.1 Rivers pattern on the slope.

Let us picture a slope of paved road under rain with many pebbles uniformly distributed on the surface (see Fig.2.1). Raindrops fall uniformly and they flow along the slope. When a stream of water encounters one of the pebbles on the surface it slides down to the left or to the right randomly. When two streams happen to gather at the same spot, they coalesce and continue to glide down the road, randomly diverted by the pebbles without penetration into the ground. Once a path has been created, all later raindrops that come upon it follow the same route. If the surface is large enough, after some time we see a hierarchy of little streams and rivulets. Fig.2.2 shows a similar phenomenon observed in a real system. The branched pattern appears on the surface of a glass by the flow of watery yogurt instead of raindrop in above description [*H. Takayasu and M. Takayasu* (1988)].

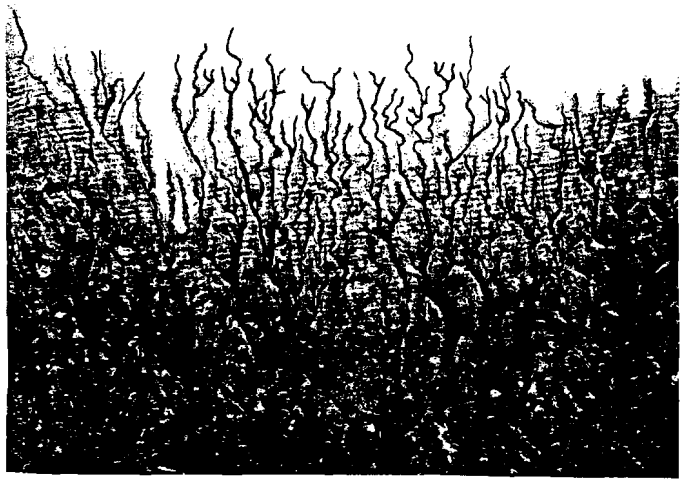

Fig.2.2 River-like pattern made of yogurt on the rough glass.

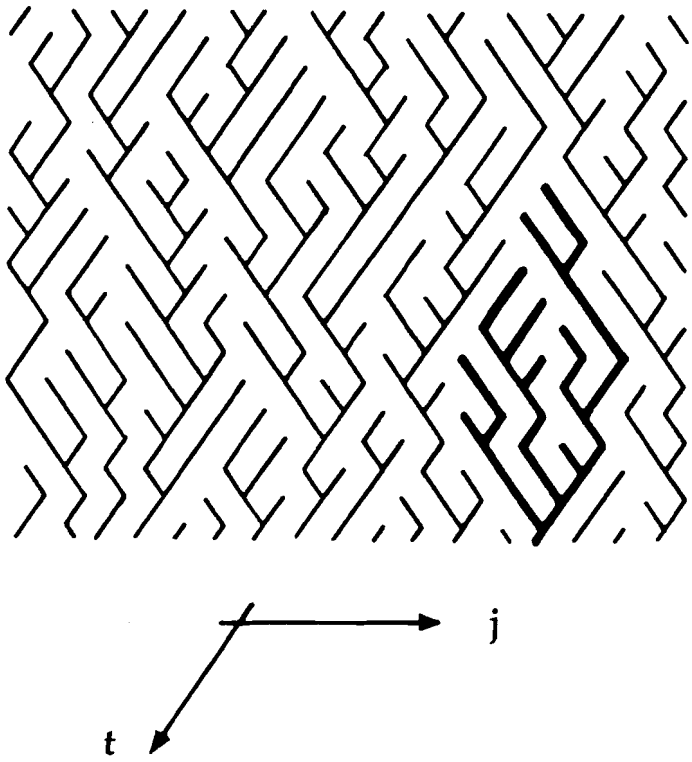

Fig.2.3 An example of a space-time configuration of sticky random walkers in one-dimension with injection.

We can formulate the most essential points of this picture as a random aggregating particle system in discretized space-time. In order to avoid complexity, here, we consider ideal massive particles(material particles) that one can ignore its volume in the model. Consider a process in which at every time step massive particles on sites of a one-dimensional lattice randomly jump to neighboring sites, while a unit mass particle is added to each site of the lattice. When particles meet at a site they coagulate to form a new particle with mass conserved. Fig.2.3 shows the trajectories of

particles in space-time. It involves branched structures which coincide with the river patterns under the rain introduced in the beginning of this chapter. The particles at the latest time step are at the bottom of this figure, and each of them has mass equal to the area of the drainage basin of corresponding branched structure since we inject a unit mass particle per one time step at every site. The ridges of the drainage basins corresponding to the particles at the latest time step are shown in Fig.2.4. Thus, we can visualize a configuration of sizes of mass in one-dimensional space.

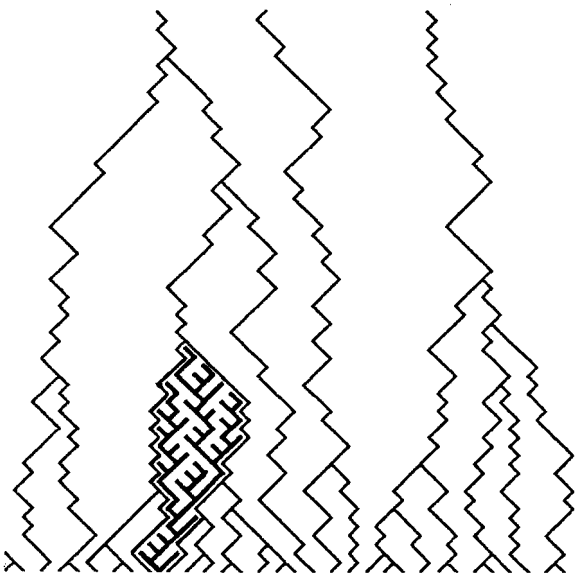

Fig.2.4 The ridges of the drainage basins.

This basic model, so called the basic Scheidegger's river model, was originally proposed by a hydrologist, *A. E. Scheidegger*, in 1967

in the interest of studying river networks. In 1986 it was reinvented as a model of random aggregating particle system by physicists in order to explore a basic step toward a statistical physics for systems far-from-equilibrium [*H. Takayasu and I. Nishikawa* (1986)].

The model can be extended to include the case that the dynamical variables have both positive and negative values instead of considering only positive quantity such as mass. We can interpret this extension as each particle having a positive or negative "charge", and such charges are added algebraically when two particles aggregate [*H. Takayasu* (1989)].

Let $m(j,t)$ be the charge of a particle on site j at the t-th time step. The aggregation process can be represented by the following stochastic equation for $m(j,t)$:

$$m(j, t+1)=\sum_{k} W_{jk}(t)\, m(k,t)+I(j, t) \quad , \tag{2.1.1}$$

where $I(j,t)$ denotes the charge of a particle injected at the j-th site at time t, and $W_{jk}(t)$ is a random variable which is equal to 1 when the particle on the k-th site jumps on the j-th site and is equal to zero otherwise. Since one particle cannot go to two different sites in a single time step, $W_{jk}(t)$ must be normalized: $\sum_j W_{jk}(t)=1$. In the following analysis we shall consider two simple cases:

(A) $W_{jj}(t)=1$ with probability 1/2, $W_{jj-1}(t)=1$ with probability 1/2, and $W_{jk}(t)=0$ for $k \neq j, j-1$.

(B) $W_{jk}(t)=1$ with probability $1/N$, where N is the total number of sites, which will tend to infinity in our analysis.

Under a periodic boundary condition case (A) can be regarded as an aggregating Brownian particles' model, which is evident if we observe from a coordinate moving with a constant velocity of 1/2. Case (B) corresponds to the mean-field limit. We study the statistical steady state properties in cases (A) and (B) under following three different types of injection:

(I) Independent random positive and negative injection(including the case of the basic model).

(II) Random pair creation injection.

(III) Positive and negative fractal injection.

Also, we study the relaxation process in cases (A) and (B) with no injection. In the random injection case, we inject randomly charged particles independently at every site at every time step. In the pair creation case, we inject pairs of particles with positive and negative charges simultaneously, but randomly, on pairs of adjacent sites [For example, a pair injection onto the j-th and $(j+1)$-th sites is given by $I(j, t)=-I(j+1, t)$.]. This special case is particularly interesting since it sheds light on the problem of the critical dimension of the model (see section 2.7). For pair injection, each time step is completed when all sites have, on average, two injected positive and negative particles. In positive and negative fractal injection case, we study the cases of weighted input (symmetric power-law input) and spatially fractal input.

In the following sections we will see that the distribution of the charge m in the statistically steady state has a power-law tail depending both on the type of the injection and on the spatial dimension. Especially, from the study of fractal injection, we will find

that the exponent of power-law distribution in statistically steady state can take continuous values depending both on the input exponent and the dimensionality of the input subspace (see section 2.3.3). And for non-injected closed system, the total number of particles decays following a power law with respect to time.

The time evolution of the charge distribution can be analyzed by introducing an r-body characteristic function (see Appendix (1)),

$$Z_r(\varrho, t) = \langle exp\ [\, i\varrho \sum_{j=1}^{r} m\ (j, t)\,] \rangle \quad , \tag{2.1.2}$$

where $\langle \cdots \rangle$ denotes the average over all realizations of $\{W_{jk}(t)\}$ and $\{I\ (j, t)\}$.

2.1.2 Basic equations in one-dimension with random positive and negative injection

We have the following evolution equation, for $Z_r(\varrho, t)$ from Eq.(2.1.1),

$$Z_r(\varrho, t+1) = \langle exp\ \{\, i\varrho \sum_{j=1}^{r} \sum_{k} W_{jk} m\ (k, t) + i\varrho \sum_{j=1}^{r} I\ (j, t)\,\} \rangle \quad . \tag{2.1.3}$$

Let us consider the total mass of successive r sites, $M_r(t) = m(k+1, t) + m(k+2, t) + \cdots + m(k+r, t)$, on one-dimensional lattice. As we follow the time evolution, the difference between $M_r(t)$ and $M_r(t+1)$ is due to the behavior of two particles, $m(k, t)$

and $m(k+r,t)$, at both edges of the r successive sites. We can consider three different possibilities for the movement of particles at the edges; either $m(k,t)$ or $m(k+r,t)$ move into the r successive sites at $t+1$ with probability 1/4 respectively, both particles move into the r successive sites at $t+1$ with probability 1/4, and both particles do not move into the r successive sites at $t+1$ with possibility 1/4. Now part of the average , $< \cdots >$, in Eq.(2.1.3) can be written explicitly as follows [*H. Takayasu, I. Nishikawa, and H. Tasaki* (1988)];

$$Z_r(\varrho, t+1) = \frac{<exp\ \{i\varrho \sum_{j=k+1}^{k+r} I(j,t)\}>}{4} [<exp\ \{i\varrho \sum_{j=k}^{k+r} m(j,t)\}> + <exp\ \{i\varrho \sum_{j=k}^{k+r-1} m(j,t)\}> + <exp\ \{i\varrho \sum_{j=k+1}^{k+r} m(j,t)\}> + <exp\ \{i\varrho \sum_{j=k+1}^{k+r-1} m(j,t)\}>] \quad . \tag{2.1.4}$$

Using the translational invariance, we have

$$Z_r(\varrho, t+1) = \frac{1}{4} \Phi(\varrho)^r [Z_{r+1}(\varrho,t) + 2Z_r(\varrho,t) + Z_{r-1}(\varrho,t)] \quad , \tag{2.1.5}$$

where $\Phi(\varrho) \equiv <exp\ \{i\varrho I(j,t)\}>$ is the characteristic function for the injection process, which can be expanded as

$$\Phi(\varrho) = 1 + i<I(j,t)>\varrho - <I(j,t)^2>\varrho^2/2 + \cdots \quad . \tag{2.1.6}$$

Eq.(2.1.5) gives a set of linear equations with r =1, 2, $\cdots$, N-1. By definition of the r-body characteristic function, $Z_r(\varrho, t)$, in Eq.(2.1.2), one of the boundary conditions becomes

$$Z_0(\varrho, t) = 1 \quad . \tag{2.1.7}$$

For r=N, $Z_N(\varrho, t)$ is the characteristic function for the total charge of the system, so that the other boundary condition is,

$$Z_N(\varrho, t) = \Phi(\varrho)^{tN} \cdot Z_N(\varrho, 0) \quad . \tag{2.1.8}$$

Eqs.(2.1.7) and (2.1.8) are valid for all cases we are going to consider.

2.1.3 Basic equations in one-dimension with pair-creation injection

In the case of pair-creation injection, positive and negative injections cancel for j=2 to r-1 in Eq.(2.1.4). Therefore, the injections which are effective to the r-body are those two particles at the edges of the r successive sites. Then we have the following evolution equation for r=1,2,$\cdots$:

$$Z_r(\varrho, t+1) = \frac{1}{4} \Phi(\varrho)^2 [Z_{r+1}(\varrho, t) + 2Z_r(\varrho, t) + Z_{r-1}(\varrho, t)] \quad . \tag{2.1.9}$$

2.1.4 Basic equations in one-dimension with fractal injection

We address here the most general case of "fractal input". By the term fractal input we mean that the injection of particles does not take place on entire space of $d=1$ but only on a subspace of dimension $d_f \leq 1$. For example, in one-dimensional aggregation we can have input on subspace realized on a Cantor set, or any other fractal set with dimension less than 1. Introducing the fractal input we should be careful not to break the translational invariance which is essential in our analysis. To keep the system uniform in the statistical sense we shift the fractal subspace randomly at each time step. In this way we recover the statistical uniformity of the system although the injection at each time step is not uniform. Under these assumptions for input, the evolution equation for the r-body characteristic function takes the form,

$$Z_r(\varrho, t+1) = \frac{1}{4} \Phi(\varrho)^{cr^{df}} \{Z_{r+1}(\varrho, t) + 2Z_r(\varrho, t) + Z_{r-1}(\varrho, t)\}, \quad (2.1.10)$$

since the number of newly injected particles on r-body is denoted by cr^{df} , where c is a constant. In the case that the input on each site follows a power-law distribution of the form

$$p(I) = p(-I) \propto |I|^{-1-\beta}, \quad 0<\beta \leq 2, \quad (2.1.11)$$

the characteristic function of the injection for small values of ϱ is approximately given by

$$\Phi(\varrho) = exp\left\{-\frac{c}{2}|\varrho|^{\beta}\right\} \approx 1 - \frac{1}{2}c|\varrho|^{\beta}, \quad \varrho \to 0 \quad , \tag{2.1.12}$$

and is always real due to the symmetric nature of the input, Eq.(2.1.11).

2.1.5 Basic equations in the mean-field case

The evolution equation for the mean-field case of random positive and negative injection can be written as

$$Z_1(\varrho, t+1) = \Phi(\varrho) \sum_{r=0}^{N} a_r Z_1(\varrho, t)^r \quad , \tag{2.1.13}$$

where

$$a_r \equiv \binom{N}{r} \left(\frac{1}{N}\right)^r \left(1 - \frac{1}{N}\right)^{N-r} \quad , \tag{2.1.14}$$

since the probability that arbitrary r sites hop into a site in one time step can be calculated as a_r. This equation is, in a sense, valid also for pair creation injection and fractal injection, but not rigorously since the cases of pair input and fractal input are not well defined on a lattice in which all sites can be regarded as nearest neighbors. In the limit $N \to \infty$ the right-hand side of Eq.(2.1.13) converges to an exponential function, namely

$$Z_1(\varrho, t+1) = \Phi(\varrho) \cdot exp\{Z_1(\varrho, t) - 1\} . \tag{2.1.15}$$

2.2 Solution for no injection case

To clarify the contribution of random injection in forming a statistically steady state, let us first discuss the system without injection as a comparison [*H. Takayasu, M. Takayasu, A. Provata, and G. Huber* (1991)].

2.2.1 In one-dimensional system

The evolution equation for $Z_r(\varrho, t)$ is given by Eq.(2.1.5) with $\Phi(\varrho) = \langle exp\ \{i\varrho\, 0\}\rangle = 1$,

$$Z_r(\varrho, t+1) = \frac{1}{4}\{Z_{r+1}(\varrho, t) + 2Z_r(\varrho, t) + Z_{r-1}(\varrho, t)\} . \tag{2.2.1}$$

This equation can be considered a diffusion equation in (r, t) space. Due to the linearity of Eq.(2.2.1), the solution is given as

$$Z_r(\varrho, t) = \sum_{r'=-t+r}^{t+r} G_{r,r'}(t)\cdot Z_{r'}(\varrho, 0) , \tag{2.2.2}$$

where $G_{r,r'}(t)$ is the Green function for Eq.(2.2.1),

$$G_{r,r'}(t) = \frac{1}{4^t}\begin{pmatrix} 2t \\ t-r-r' \end{pmatrix} , \tag{2.2.3}$$

and $Z_r(\varrho, t)$ for negative r is defined as

$$Z_r(\varrho, t) = 2 - Z_{-r}(\varrho, t) \quad , \tag{2.2.4}$$

which ensures the boundary condition Eq.(2.1.7). $G_{r,r'}(t)$ gives the probability that a random walker starting at $(r',0)$ reaches (r, t). For large t, Eq.(2.2.3) can be approximated by a Gaussian function:

$$G_{r,r'}(t) \cong \frac{1}{\sqrt{\pi t}} exp\ \{ - \frac{(r - r')^2}{t} \} , \qquad t \to \infty \quad , \tag{2.2.5}$$

where the symbol $\cong$ means equivalence up to first order. Substituting Eq.(2.2.5) into Eq.(2.2.2), and taking the continuum limit for r, we get

$$\begin{aligned} Z_r(\varrho, t) \cong & \int_0^\infty dr' \frac{1}{\sqrt{\pi t}} exp\ \{ \frac{-(r-r')^2}{t} \} Z_{r'}(\varrho, 0) \\ & + \int_0^\infty dr' \frac{1}{\sqrt{\pi t}} exp\ \{ \frac{-(r+r')^2}{t} \} [2 - Z_{r'}(\varrho, 0)] \\ = & 1 - r \frac{2}{\sqrt{\pi t}} \int_0^\infty dr' \frac{2r'}{t} exp\ \{ - \frac{r'^2}{t} \} [1 - Z_{r'}(\varrho, 0)] \quad , \end{aligned} \tag{2.2.6}$$

where we have expanded the exponential function to first order in $r/\sqrt{t}$.

Let us solve the decay of the particles number with the initial condition that every site is occupied by a particle having a unit charge. The initial condition is given by $Z_r(\varrho, 0) = e^{i\varrho r}$. The

evolution of the charge distribution is obtained by Fourier inversion of Eq.(2.2.6),

$$p_r(m,t) = \frac{1}{2\pi}\int d\varrho\, e^{-i\varrho m} Z_r(\varrho,t)$$

$$\cong \left(1-\frac{2r}{\sqrt{\pi t}}\right)\delta(m) + \frac{2r}{\sqrt{\pi t}}\frac{2m}{t}e^{-m^2/t} \quad . \tag{2.2.7}$$

Here $p_r(m,t)$ denotes the probability that the sum of the charges on the r successive sites is m, at time step t. From Eq.(2.2.7) we know that the charge distribution for large m decays following a Gaussian function and that the particles number decreases for large t as

$$N \cdot p\,(m \neq 0, t) \propto \frac{2N}{\sqrt{\pi t}}, \qquad t \to \infty \quad , \tag{2.2.8}$$

where the symbol $\propto$ means proportional up to first order. This result is consistent with *J. T. Spouge* (1988), *C. R. Doering and D. ben-Avraham* (1988) where the same problem is treated by different methods.

2.2.2 In the mean-field system

Next, we consider the mean-field case(B). For large t we can assume that $Z_1(\varrho,t) \approx 1$ because the existence probability for particles should vanish as $t \to \infty$. From Eq.(2.1.15), with $\Phi(\varrho) = 1$ we have the following evolution equation:

$$Z_1(\varrho, t+1) - Z_1(\varrho, t) = \frac{1}{2}[Z_1(\varrho, t) - 1]^2 + \cdots \quad . \qquad (2.2.9)$$

By taking the continuum limit with respect to t, we obtain $Z_1(\varrho, t)$,

$$Z_1(\varrho, t) \cong 1 - \frac{2[1 - Z_1(\varrho, 0)]}{t\,[1 - Z_1(\varrho, 0)] + 2} \quad . \qquad (2.2.10)$$

The decay in the particle number can be calculated in the same way and we get

$$p\,(m \neq 0, t) \propto \frac{1}{t} \quad , \qquad t \to \infty \quad , \qquad (2.2.11)$$

for the same initial conditions as in the one-dimensional case. Notice that in one-dimensional case, Eq.(2.2.8), the decay is slower than in the mean-field case, Eq.(2.2.11), due to the effect of spatial restriction.

2.3 The steady state charge distribution in the presence of injection

In this section we study the steady state charge distribution realized by three different types of continuous and statistically homogeneous injection; random positive and negative injection, pair-creation injection, and fractal input. Throughout the whole section the system size N is assumed to be infinite [*H. Takayasu, M. Takayasu, A. Provata, and G. Huber* (1991)].

2.3.1 Solutions for one-dimension with random positive and negative injection

Let us discuss the case of basic model that every site has exactly $I=1$ injection at every time step. We will find it to be convenient to redefine the characteristic function by Laplacian transformation of distribution function instead of Fourier transformation;

$$Z_r(\varrho, t) = \langle exp\ [\ -\varrho \sum_{j=1}^{r} m\ (j, t)\ ] \rangle \quad , \tag{2.3.1}$$

$$\Phi(\varrho) = \langle exp\ [\ -\varrho I\ (j, t)\ ] \rangle$$

$$= 1 - \langle I \rangle \varrho + \langle I^2 \rangle \varrho^2/2 - \cdots \quad . \tag{2.3.2}$$

Notwithstanding the redifinitions, the basic equations for evolution introduced in the previous sections still hold without any change in their appearence.

The charge distribution in the one-dimensional case with random positive and negative injection can be obtained from the steady state solution of Eq.(2.1.5). We have the following set of linear equations for $Z_r(\varrho)$, r =1, 2, 3, ... , with the boundary condition Eq.(2.1.7):

$$Z_{r+1}(\varrho) + [2 - 4\Phi(\varrho)^{-r}]Z_r(\varrho) + Z_{r-1}(\varrho) = 0 \quad . \tag{2.3.3}$$

Dividing both sides of Eq.(2.3.3) by $Z_r(\varrho)$, we get a recurrence relation for $Z_r(\varrho)/Z_{r-1}(\varrho)$,

$$\frac{Z_r(\varrho)}{Z_{r-1}(\varrho)} = \frac{1}{4\Phi(\varrho)^{-r} - 2 - Z_{r+1}(\varrho)/Z_r(\varrho)} \quad . \tag{2.3.4}$$

Therefore, $Z_1(\varrho)$ is given by the following continued fraction:

$$Z_1(\varrho) = \cfrac{1}{4\Phi(\varrho)^{-1} - 2 - \cfrac{1}{4\Phi(\varrho)^{-2} - 2 - \cfrac{1}{4\Phi(\varrho)^{-3} - 2 - \cdots}}} \quad . \tag{2.3.5}$$

Since we are thinking of the special case that every site has unit mass injection at every time step, $\Phi(\varrho)$ can be expressed exactly in the form $\Phi(\varrho) = exp(-\varrho)$. Then Eq.(2.3.5) can be written as

$$Z_1(\varrho) = \cfrac{1}{4e^{\varrho} - 2 - \cfrac{1}{4e^{2\varrho} - 2 - \cfrac{1}{4e^{3\varrho} - 2 - \cdots}}} \quad . \tag{2.3.5'}$$

Rough estimate of Eq.(2.3.5') is easily obtained by using the theory of continued fraction CAM as we show in Appendix (2). The rigorous discussion is as follows [*G. Huber* (1991)]: As a first step in expanding $Z_1(\varrho)$, we linearize the individual terms in Eq.(2.3.5') around $\varrho = 0$,

$$\bar{Z}_1(\varrho) = \cfrac{1}{2 + 4\varrho - \cfrac{1}{2 + 8\varrho - \cfrac{1}{2 + 12\varrho - \cdots}}} \quad . \tag{2.3.6}$$

Bessel function (of real order) can likewise be expanded in linearly increasing terms[#1], making possible the closed-form solution

$$\bar{Z}_1(\varrho) = \frac{J_{1+1/2\varrho}(1/2\varrho)}{J_{1/2\varrho}(1/2\varrho)} \quad . \tag{2.3.7}$$

Since the limit of large mass $m \to \infty$ is equivalent to the limit $\varrho \to 0$, we are interested in the asymptotics of $J_{1+x}(x)/J_x(x)$ as $x \to \infty$. One of the Lommel recurrences [*G. N. Watson* (1944)] states

$$\frac{J_{1+x}(x)}{J_x(x)} = 1 - \frac{J'_x(x)}{J_x(x)} \quad , \tag{2.3.8}$$

and the method of stationary phase [*N. Bleistein and R. A. Handelsman* (1986)] allows a formal expansion of the right-hand side[#2] ,

---

[#1] This is due to the exact correspondence between the Bessel-function recurrence relation, $J_{n+1}(x) - (2n/x)J_n(x) + J_{n-1}(x) = 0$, and Eq.(2.3.3).

[#2] Asymptotic expansions of $J_x(x)$ and $J'_x(x)$ were first discovered by Cauchy and Meissel [*G. N. Watson* (1944)].

$$\bar{Z}_1(\varrho) = 1 - 2\pi \frac{(16/3)^{1/6}}{\Gamma(1/3)^2} \varrho^{1/3} - \frac{2}{5}\varrho + O(\varrho^{5/3}) \quad . \tag{2.3.9}$$

For small ϱ , one can show that $\bar{Z}_1(\varrho) > Z_1(\varrho)$. Alternatively, $Z_1(\varrho)$ can be written as

$$Z_1(\varrho) = \cfrac{(4e^{\varrho} - 2)^{-1}}{1 - \cfrac{(4e^{\varrho} - 2)^{-1}(4e^{2\varrho} - 2)^{-1}}{1 - \cfrac{(4e^{2\varrho} - 2)^{-1}(4e^{3\varrho} - 2)^{-1}}{1 - \cdots}}} \quad . \tag{2.3.10}$$

Now we "linearize" this form, as before,

$$\hat{Z}_1(\varrho) = \cfrac{1 - 2\varrho}{2 - \cfrac{1 - 6\varrho}{2 - \cfrac{1 - 10\varrho}{2 - \cdots}}} \quad , \tag{2.3.11}$$

and expand around $\varrho = 0$,

$$\hat{Z}_1(\varrho) = 1 - 2\pi \frac{(16/3)^{1/6}}{\Gamma(1/3)^2} \varrho^{1/3} - \varrho + O(\varrho^{5/3}) \quad . \tag{2.3.12}$$

Despite differences in second-order coefficient, the expansion agrees with Eq.(2.3.9) to first order. In this case, we can show $\hat{Z}_1(\varrho) < Z_1(\varrho)$. Then we have

$$\hat{Z}_1(\varrho) < Z_1(\varrho) < \bar{Z}_1(\varrho), \tag{2.3.13}$$

and thus

$$Z_1(\varrho) = 1 - c_1 \varrho^{1/3} - c_2 \varrho + O(\varrho^{5/3}) \tag{2.3.14}$$

where $c_1 = 2\pi(16/3)^{1/6}/\Gamma(1/3)^2$ and $0.4 < c_2 < 1$.

We can generalize the above particular type of injection to general positive and negative random injection case. Since we know from the previous results that, to leading order, the asymptotic behavior of Eq.(2.3.5) is identical to that of $J_{1+x}(x)/J_x(x)$ in the limit $x \to \infty$, so that for $|\varrho| \ll 1$,

$$Z_1(\varrho) \cong \frac{J_{1+x}(x)}{J_x(x)} , \tag{2.3.15}$$

where $x = 1/\{-2i\langle I\rangle\varrho + \langle I^2\rangle\varrho^2\}$. Then, instead of Eq.(2.3.14), $Z_1(\varrho)$ in the vicinity of $\varrho = 0$ is finally given by

$$Z_1(\varrho) = 1 - c_1\langle I\rangle^{1/3} i^{-1/3} |\varrho|^{1/3} - \cdots \quad for\ \langle I\rangle \neq 0 , \tag{2.3.16a}$$

$$Z_1(\varrho) = 1 - c_1\langle I^2\rangle^{1/3} 2^{-1/3} |\varrho|^{2/3} - \cdots \quad for\ \langle I\rangle = 0 , \tag{2.3.16b}$$

where c_1 is the same constant value as in Eq.(2.3.14). (The same leading order for $Z_1(\varrho)$ can be obtained in the continuum limit of Eq.(2.3.3).)

Since the characteristic function is the Fourier transform of the probability density $p(m)$, we obtain the charge distribution by inversion. In the case of $\langle I\rangle > 0$ (or $\langle I\rangle < 0$), we have

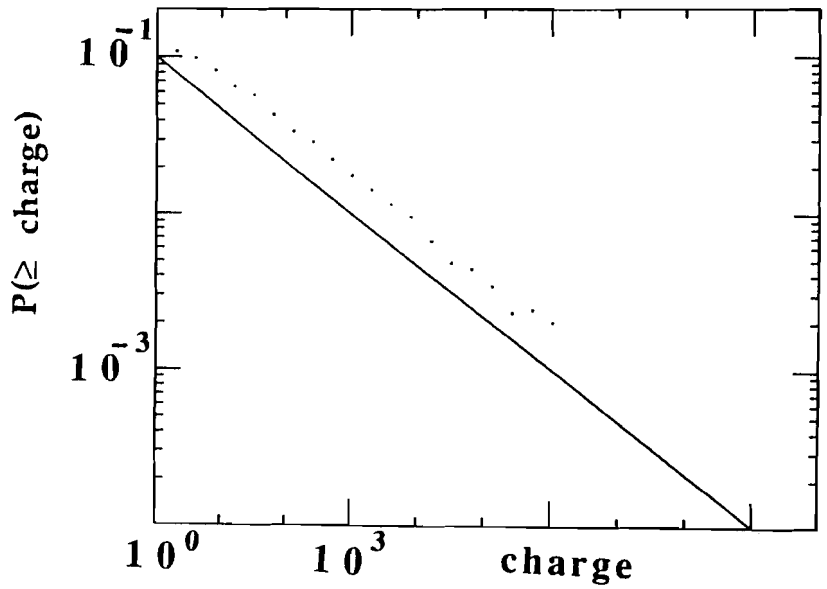

Fig.2.5 The steady-state cumulative charge distribution in one dimension in the case of $\langle I \rangle \neq 0$. The straight line shows the theoretical slope -1/3. (The slope of cumulative distribution is the slope of the original distribution, $p(m)$, increased by +1.)

$$p(m) \propto m^{-4/3} \quad for \quad m >> \langle I \rangle \ (or \ m << \langle I \rangle) \ , \qquad (2.3.17a)$$

while in the case of $\langle I \rangle = 0$, we have

$$p(m) \propto m^{-5/3} \quad for \quad m >> \langle I^2 \rangle^{1/2} . \qquad (2.3.17b)$$

The solution Eq.(2.3.17a) shows a one-sided power-law with the same exponent as for the constant injection. Eq.(2.3.17b) gives a symmetric power law. In Fig.2.5 and Fig.2.6, we show the results of

numerical simulations for the cases $\langle I \rangle > 0$ and $\langle I \rangle = 0$ which support our exact solutions.

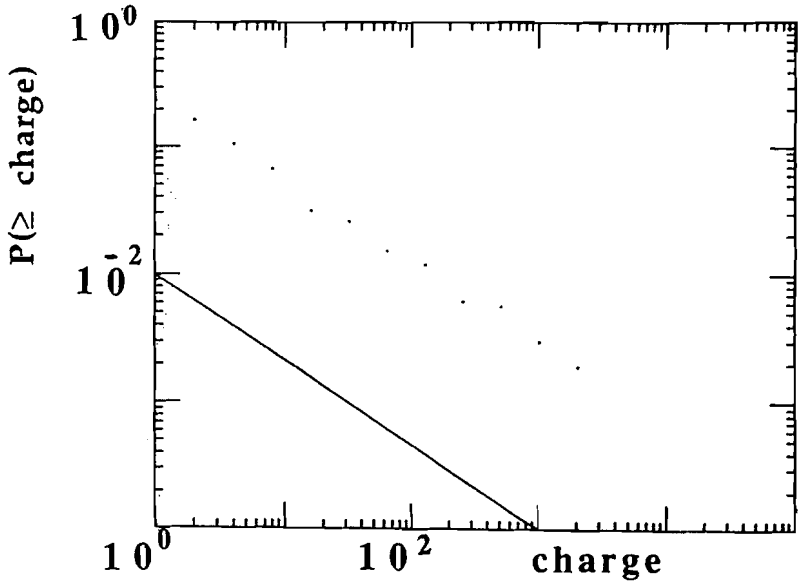

Fig.2.6 The steady-state cumulative charge distribution in one-dimension in the case of $\langle I \rangle = 0$. The straight line shows the theoretical slope -2/3.

2.3.2 Solution for one-dimension with pair-creation injection

Next we consider the pair-creation injection case. At the steady state we have the following set of linear equations for $Z_r(\varrho)$, r =1, 2, 3, ... , with the boundary condition Eq.(2.7):

$$Z_{r+1}(\varrho) + [2 - 4\Phi(\varrho)^{-2}]Z_r(\varrho) + Z_{r-1}(\varrho) = 0 \quad . \qquad (2.3.18)$$

As we repeat the same process that we did for random injection, we divide both sides of Eq.(2.3.18) by $Z_r(\varrho)$. Then we get a recurrence relation for $Z_r(\varrho)/Z_{r-1}(\varrho)$,

$$\frac{Z_r(\varrho)}{Z_{r-1}(\varrho)} = \frac{1}{4\Phi(\varrho)^{-2} - 2 - Z_{r+1}(\varrho)/Z_r(\varrho)} \quad . \tag{2.3.19}$$

It is easy to show that $Z_1(\varrho)$ is given by the following continued fraction:

$$Z_1(\varrho) = \cfrac{1}{4\Phi(\varrho)^{-2} - 2 - \cfrac{1}{4\Phi(\varrho)^{-2} - 2 - \cfrac{1}{4\Phi(\varrho)^{-2} - 2 - \cdots}}} \quad . \tag{2.3.20}$$

Eq.(2.3.20) can be transformed to

$$Z_1(\varrho) = \frac{1}{4\Phi(\varrho)^{-2} - 2 - Z_1(\varrho)} \quad , \tag{2.3.21}$$

which is a quadratic equation for $Z_1(\varrho)$. Solving Eq.(2.3.21), we get

$$Z_1(\varrho) = 1 - 2\langle I^2\rangle^{1/2} |\varrho| + \cdots \quad . \tag{2.3.22}$$

The corresponding charge distribution is

$$p(m) \propto m^{-2} \quad for \quad m >> \langle I^2\rangle^{1/2} \quad . \tag{2.3.23}$$

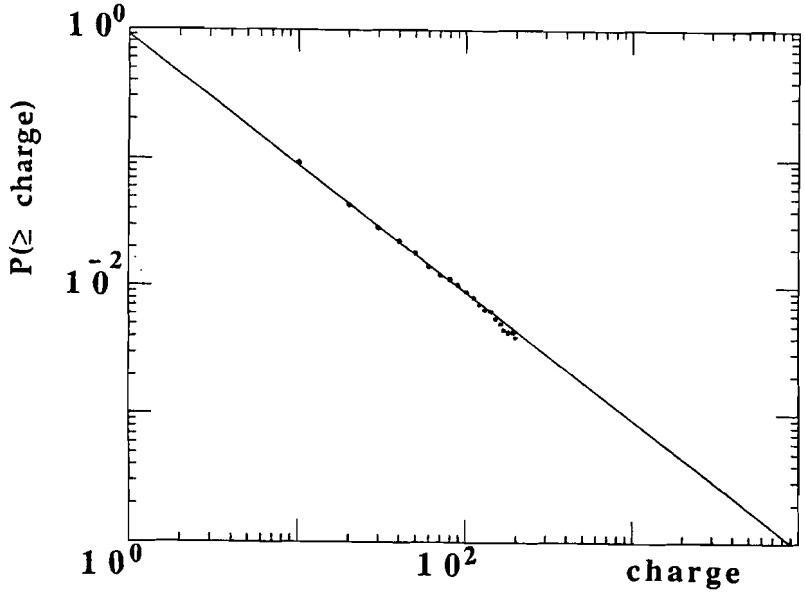

Fig.2.7 The steady-state charge distribution in one-dimension in the case of pair-creation injection. The straight line shows the theoretical slope, -1.

This probability density is symmetric and the exponent is the same as that of a Lorentzian. In Fig.2.7, we show the numerical result for pair-creation injection. Comparing the result with the mean-field case which we solve in the following section, we will find that the exponent in Eq.(2.3.23) is the same as the one for the mean-field case. This is not against intuition, since from Eqs.(2.3.19) and (2.3.21) it can be shown that the basic equation Eq.(2.3.18) satisfies a mean-field-like relation; $Z_2(\varrho)=Z_1(\varrho)^2$.

2.3.3 Solution for one-dimension with fractal injection

The equation which describes the steady state for fractal input is (from Eq.(2.1.10)) [*A. Provata, M. Takayasu, and H. Takayasu* (1992)]:

$$Z_{r+1}(\varrho) + \{2 - \Phi(\varrho)^{-cr^{d_f}}\} Z_r(\varrho) + Z_{r-1}(\varrho) = 0 \quad , \tag{2.3.24}$$

with the boundary condition $\Phi(\varrho) = \langle exp\{i\varrho 0\}\rangle = 1$. The quantity $Z_1(\varrho)/Z_0(\varrho)$ must be finite for all values of ϱ, including $\varrho = 0$. In the continuum limit, Eq. (2.3.24) can be written as

$$\frac{\partial^2 Z_r(\varrho)}{\partial r^2} - 2cr^{d_f} |\varrho|^{\beta} Z_r(\varrho) = 0 \quad , \tag{2.3.25}$$

where we have used the expansion given by Eq.(2.1.12) for $\Phi(\varrho)$. To obtain the solution of Eq.(2.3.25) with the specified boundary condition we do the following two transformations:

$$q = r\,\varrho^{\beta/(d_f+2)} \quad , \tag{2.3.26a}$$

$$W_r(\varrho) = r^{-2} Z_r(\varrho) \quad . \tag{2.3.26b}$$

Under the transformations Eqs.(2.3.26a,b), Eq.(2.3.25) is transformed into

$$q^2 \frac{\partial^2 W(q)}{\partial q^2} - 4q \frac{\partial W(q)}{\partial q} + (2 - c\,q^{d_f+2}) W(q) = 0 \quad , \tag{2.3.27}$$

with the boundary condition $W(0) = \infty$ from Eq.(2.3.26b). Note that with this new definition of variables, $W(q)$ depends explicitly only on q, and not on ϱ and r . The solution of Eq.(2.3.27) can be given in terms of the modified Bessel Functions [*G. N. Watson*(1944), *M. Abramowitz and I. Stegun* (1965)]. The appropriate solution (the one which satisfies the boundary condition given above) is

$$W(q) = q^{-3/2} K_{1/(d_f+2)}(q) . \qquad (2.3.28)$$

For small values of q (*i.e.* small values of ϱ), Eq.(2.3.28) is approximated by

$$W(q) \approx q^2(1 - q) , \quad q << 1 . \qquad (2.3.29)$$

The r -body characteristic function in the same limit takes the form

$$Z_r(\varrho) \approx 1 - c\, r\, |\varrho|^{\beta/(d_f+2)} , \quad \varrho << 1 . \qquad (2.3.30)$$

The validity of Eq.(2.3.30) as a solution of Eq.(2.3.25) can be verified by directly inserting Eq.(2.3.30) into the left-hand side of Eq.(2.3.25) and showing that the right hand side is of higher order of ϱ.

To confirm further our analytical estimation of Eq.(2.3.25), we also solved directly Eq.(2.3.24), numerically. In Fig.2.8 we plot the values of $\{1 - Z_r(\varrho)\}$ as a function of ϱ for parameter values β=1.9 and d_f=0.1. On a double logarithmic scale the points fall nicely on a straight line with a slope of 0.91±0.01. This result agrees with the theoretical result $\beta/(d_f+2)$=0.905. For parameter values β=0.5 and

d_f=0.1, the numerical solution gave an exponent 0.23±0.01 whereas the analytical solution gives $\beta/(d_f+2)$=0.24. For parameter values β=0.1 and d_f=0.5, the numerical solution gave an exponent 0.032±0.005 whereas the analytical solution gives $\beta/(d_f+2)$=0.036. In any case the result of the numerical solution approaches the analytic solution for smaller and smaller values of ϱ ($\varrho \to 0$). Other cases were also checked and the analytical results agree always with the numerical solution.

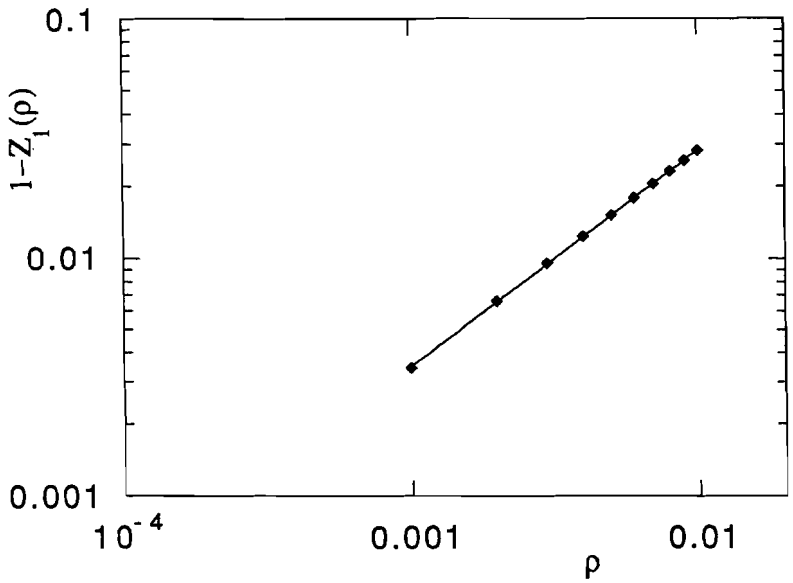

Fig.2.8 Numerical solution of Eq.(2.3.24) with parameter values β = 1.9 and d_f = 0.5. In a double logarithmic scale the value of $(1 - Z_1(\varrho))$ as a function of ϱ fall on a straight line which has slope 0.91 ± 0.01.

By taking Fourier inverse of $Z_1(\varrho)$ we find the form of the charge probability distribution

$$p(m) \propto |m|^{-1-\beta/(d_f+2)} \quad for \quad m >> 1 \ . \tag{2.3.31}$$

This is a general result for the steady state distribution for one-dimensional aggregation with both weighted (power-law) and fractal input.

In particular, when the input takes place over all space (for the 1-dimensional case $d_f=1$), the result for the charge probability distribution function is

$$p(m) \propto |m|^{-1-\beta/3} \quad for \quad m >> 1, \ 0<\beta \leq 1 \ . \tag{2.3.32}$$

The case of $\beta=1$ gives the case for random positive and negative injection with $<I>>0$ and the case of $\beta=2$ gives the case for random positive and negative injection with $<I>=0$ both of which have been rigorously solved in Eq.(2.3.17a,b).

2.3.4 Solutions for the mean-field case

For the mean-field case, the time-independent solution of Eq.(2.1.15) satisfies,

$$Z_1(\varrho) = \Phi(\varrho)\, e^{Z_1(\varrho)-1} \ . \tag{2.3.33}$$

In the vicinity of $\varrho \to 0$ we can expand $Z_1(\varrho)$ around 1. Neglecting the higher-order terms of ϱ, we get the following solutions,

$$Z_1(\varrho) = 1 - \sqrt{2}\langle I \rangle^{1/2} i^{-1/2} |\varrho|^{1/2} + \cdots \quad for \quad \langle I \rangle \neq 0 , \tag{2.3.34a}$$

$$Z_1(\varrho) = 1 - \langle I^2 \rangle^{1/2} |\varrho| + \cdots \quad for \quad \langle I \rangle = 0 , \tag{2.3.34b}$$

$$Z_1(\varrho) = 1 - const \cdot |\varrho|^{\beta/2} + \cdots \quad for\ fractal\ injection . \tag{2.3.34c}$$

The corresponding steady-state charge distribution in the case of $\langle I \rangle > 0$ (or $\langle I \rangle < 0$) becomes

$$p(m) \propto m^{-3/2} \quad for \quad m >> |\langle I \rangle| , \tag{2.3.35a}$$

and in the case of $\langle I \rangle = 0$,

$$p(m) \propto m^{-2} \quad for \quad m >> \langle I^2 \rangle^{1/2} , \tag{2.3.35b}$$

and in the case of fractal injection,

$$p(m) \propto |m|^{-1-\beta/2} \quad for \quad m >> 1 . \tag{2.3.35c}$$

Again, we have a one-sided power law in the case of $\langle I \rangle \neq 0$, and a symmetric one in the case of $\langle I \rangle = 0$.

2.4 Intuitive prospects and other approaches

2.4.1 Geometrical approach

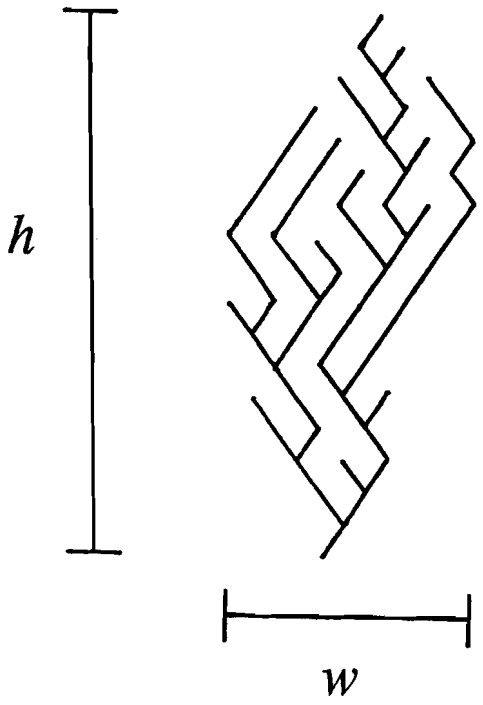

Fig.2.9 An example of the space-time trajectory of a particle. The width and height are given by w and h, respectively.

The results can be understood intuitively by contemplating the random walk process. As it was mentioned in Section 2.1, in one-dimensional case the charge of a particle is equal to the sum of the charges of the particles injected over the corresponding river basin. It is obvious from the evolution rule that the basin's left and right boundaries are formed by simple random walks (see Fig.2.9)

Therefore, the area of the basin is roughly given by $S=hw$, where h and w denote the basin's height and width. Since the boundaries of the basin are random walks, w is proportional to $h^{1/2}$ and the distribution of the height h is identical to the distribution of a Brownian particle's recurrence time [*W. Feller* (1966)],

$$p(h) \propto h^{-3/2} \quad . \tag{2.4.1}$$

Hence, the distribution function for the area of the basin, $S = h \cdot w \propto h^{3/2}$, is given by

$$p(S) = p(h) \frac{\partial h}{\partial S} \propto S^{-4/3} \quad . \tag{2.4.2}$$

By definition, the charge of a particle having a basin of size S is given by the sum of S independent random variables $\{I_j\}$. In the case of $\langle I \rangle \neq 0$ the charge m is obviously proportional to S, hence we have $p(m) \propto m^{-4/3}$. When the average value of I is zero, m becomes proportional to the variance $(\langle I^2 \rangle S)^{1/2}$. Substituting the relation $m \propto S^{-1/2}$ into Eq.(2.4.2) we get $p(m) \propto m^{-5/3}$. In the case of pair-creation injection, a pair-creation in the area does not contribute to the charge m, because positive and negative charges cancel. The contribution to m comes only from the boundaries, namely, m is given by the sum of $2h$ random variables I_j. The mean value of I_j is automatically zero, so that, m is proportional to $(2h)^{1/2}$. Substituting this relation into Eq.(2.4.1), we obtain the charge distribution $p(m) \propto m^{-2}$. These intuitive results agree perfectly with the analytic results of Eqs.(2.3.17a), (2.3.17b) and (2.3.23).

In the case of the fractal input, we are adding particles with mass following a power-law only on the subspace of dimension d_f. In such a case, the number of sites in the same river will be proportional to $S \propto h \cdot w^{d_f}$. Though the boundaries of the basin are the ordinary

random walks we have the relation $w \propto h^{1/2}$. So the number of injected particles $\{I_j\}$ that drain into the basin is

$$S \propto h \cdot w^{d_f} = h^{1+d_f/2}. \tag{2.4.3}$$

Since the distribution of h follows a power-law (equivalent to the distribution of recurrence time of two random walks), as we have shown in Eq.(2.4.2), we have

$$p(S) = p(h) \frac{\partial h}{\partial S} \propto S^{-1-1/(d_f+2)}. \tag{2.4.4}$$

The characteristic function for m is then given as

$$Z_r(\varrho) = \sum_{S=1}^{\infty} p(S)\{\Phi(\varrho)\}^S \propto \sum_{S=1}^{\infty} S^{-1-1/(d_f+2)} exp\left(-\frac{c}{2}|\varrho|^{\beta} S\right)$$

$$= exp\left(-\frac{c}{2}|\varrho|^{\beta/(d_f+2)}\right). \tag{2.4.5}$$

Here we have approximated the summation over S by an integral $\int_0^{\infty} dS$. In the neighborhood of $\varrho = 0$, Eq.(2.4.5) shows the same singularity as in Eq.(2.3.30), namely $|\varrho|^{\beta/(d_f+2)}$, which means that the distribution of m has a power-law tail, Eq.(2.3.31), namely $m^{-1-\beta/(d_f+2)}$.

2.4.2 Branching process and phase transition

The time reversed process (the process that the time to flow backward) of Scheidegger's river model can be regarded as a branching process. Let us recollect the space-time trajectory given in Fig 2.3. Every site can be regarded as having its origin (or ancestor) at the time zero layer, which is located at the top of the figure. Reversing the time, we can say that a branching process starting from a bottom site has on average one offspring in order to conserve the number of sites at every reversed time step . To be precise, a branch has two offsprings with probability 1/4, one offspring with probability 1/2, and non with probability 1/4 in one reversed time step.

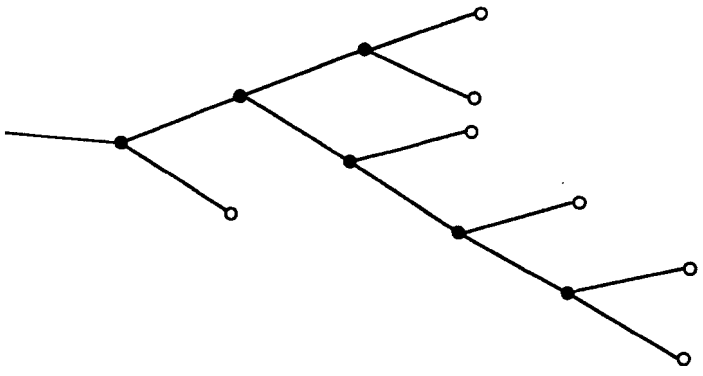

Fig.2.10 An example of a branching tree.

Now, let us consider a general simple branching process as shown in Fig.2.10. A branch has two offsprings with probability p and no offspring with probability $1-p$. For the particular branch shown in

Fig.2.10, the probability of existence becomes $p^6(1-p)^7$. In the general case of the probability of existing a branch of size s ; $N(s)$, it is difficult to count probabilities for all possible shapes. But fortunately, we do not need to fulfill such a troublesome task since we know that $N(s)$ satisfies the following relation:

$$N(s+1) = p \sum_{s'=1}^{s} N(s')N(s-s') \quad . \tag{2.4.6}$$

Here we sum up the probabilities that two offsprings separated from a same site at a time step become matured branches of size s and size s-s' after a sufficiently long time. By using generating function;

$$W(x) = \sum_{s=0}^{\infty} x^s W(s) \quad , \tag{2.4.7}$$

we obtain from Eq.(2.4.6) the following result:

$$N(s) \propto s^{-3/2} e^{-a \cdot s}, \quad a = \log 4p(1-p). \tag{2.4.8}$$

As we can see, for $p < 1/2$ the exponential factor in Eq.(2.4.8) becomes dominant, so that $N(s)$ shows an exponential decay and all branches die out in a finite time steps. For $p = 1/2$, the constant value a become zero and $N(s)$ follows a power-law with an exponent equal to -3/2. For $p > 1/2$, the exponential factor dominates again and $N(s)$ shows an exponential decay but in this case there exists a finite value of $N(\infty)$. This picture can be interpreted in terms of the

second order phase transition like in the percolation problem. In such a view, $N(\infty)$ is an order parameter and p is a control parameter and at the threshold, $p_c = 1/2$, a power-law distribution is observed.

Let us now discuss the critical point in some detail. The mean number of offsprings is $2p$ because a branch has two offsprings with probability p and it dies out with probability $1\text{-}p$. If p is smaller than 1/2 the mean number of offsprings become smaller than 1 so that the number of branches decays exponentially and all of them die out in a finite time. In the opposite case that p is larger than 1/2 the mean number of offsprings become larger than 1 and the number of branches grows exponentially. From this point of view, $p = 1/2$ is the only case when the number of branches is constant, namely, the critical point is the case when the mean number of offsprings in a time step becomes 1. This corresponds to the case of Scheidegger's river model which has one offspring on average in a reversed time step. And the critical exponent, -3/2, is equal to the exponent of size distribution for mean-field case with non zero mean injection. This correspondence is due to the fact that in the model of the branching process we did not take into account the interaction of neighboring branches, in other words, we neglected the lattice structure effects.

Thus, we can regard the state of Scheidegger's river model being at a critical condition, and the stochastic process of model itself realizes a criticality. Namely, Scheidegger's river model is a self-organizing model that realizes a critical point without any tuning.

2.4.3 View from stable distributions

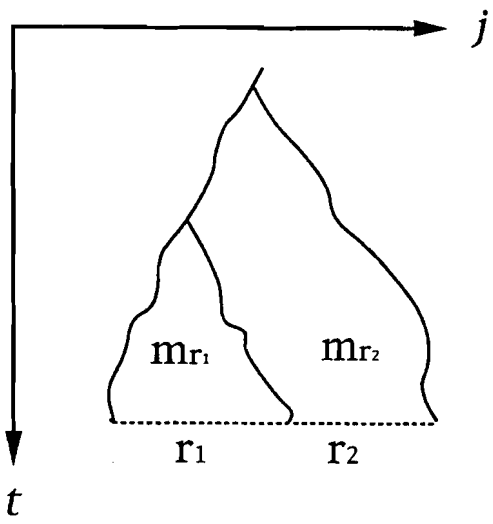

Fig.2.11 The ridges of river basins for two sections which consist of r_1 and r_2 numbers of successive sites.

Starting from the beginning of this chapter we were once and again focusing on the properties of "the sum of a random number of random variables; $m = \sum_{<j,t>} I(j, t)$". From the mathematical point of view, for "the sum of a fixed number of random variables" the central limit theorem can be applied and we have a Gaussian distribution if "the fixed number" is sufficiently large.

However, when the number of variables is not fixed but follows a power law distribution, as in Eqs.(2.4.2) and (2.4.4), the central limit theorem does not hold. Instead, the sum converges to a power-law distribution [Eqs.(2.3.17ab), (2.3.23), (2.3.31) and (2.3.35ab) belong to so called stable distributions (see Appendix (3))].

Let us consider two sections(section1 and section2) consisting of r_1 and r_2 numbers of successive particles at time step t. Fig.2.11 shows the ridges of river basins which flow into section1 and section2 at time step t. For convenience, let us call the areas of the

river basins which contribute to form the total charge of section1 and section2 as area1 and area2 respectively. All injection falling into the area1 and area2, partitioned by the ridges, flow into section1 and section2 at time step t. Let the total charge of r successive sites be m_r. If we assume that m_r is a variable following a stable distribution, we have the relation;

$$m_{r_1+r_2} \stackrel{d}{=} m_{r_1} + m_{r_2} \quad , \tag{2.4.9}$$

where $\stackrel{d}{=}$ denotes that variables on both sides obey the same distribution function. Also, the distributions for the charge of r-body and 1-body are easily shown to satisfy the following relations by using the same arguments of random walk trajectories as we discussed in section 2.4.1.

$$m_r \stackrel{d}{=} r^3 m_1 \ , \quad for \ \langle I \rangle \neq 0 \ random \ injection \ . \tag{2.4.10a}$$

$$m_r \stackrel{d}{=} (r^3)^{1/2} m_1 \ , \quad for \ \langle I \rangle = 0 \ random \ injection \ . \tag{2.4.10b}$$

$$m_r \stackrel{d}{=} (r^2)^{1/2} m_1 \ , \quad for \ pair\text{-}creation \ injection \ . \tag{2.4.10c}$$

$$m_r \stackrel{d}{=} r^{2+d_f} m_1 \ , \quad for \ fractal \ injection \ . \tag{2.4.10d}$$

From the properties of stable distribution, we know that a variable, m, satisfying both Eqs.(2.4.9) and (2.4.10a) follows a stable distribution with a characteristic exponent equal to 1/3. In that sense we know that the cumulative charge distribution for $\langle I \rangle \neq 0$

random injection has a power-law tail with an exponent equal to $-1/3$ for large m. In a similar way, we can uniquely determine the charge distribution for each of the cases; a both-sided stable distribution with the characteristic exponent equal to 2/3 for the random injection case with $<I>=0$, a both-sided stable distribution with the characteristic exponent equal to 1 for the pair-creation injection case, and a one-sided stable distribution with the characteristic exponent equal to $1/(d_f+2)$ for the fractal injection case. (see Fig.A2 in Appendix(3)).

2.5 Uniqueness and Stability

In the preceding section we have seen that there exists a statistically invariant steady-state which is realized by injection. Here we show that the steady-state is uniquely determined for a given type of injection, independent of the initial conditions [*H. Takayasu, A. Provata, M. Takayasu* (1990)]. Let us introduce a perturbation $\tilde{Z}_r(\varrho, t)$ around the steady-state $Z_r(\varrho)$:

$$Z_r(\varrho, t) = Z_r(\varrho) + \tilde{Z}_r(\varrho, t) \quad . \tag{2.5.1}$$

Due to the linearity of Eqs.(2.1.5), (2.1.9), (2.1.10) the equation for the perturbation $\tilde{Z}_r(\varrho, t)$ in the one-dimensional case is given by

$$\tilde{Z}_r(\varrho, t+1) = \frac{1}{4} \Phi(\varrho)^{\mu} [\tilde{Z}_{r+1}(\varrho, t) + 2\tilde{Z}_r(\varrho, t) + \tilde{Z}_{r-1}(\varrho, t)] \quad , \tag{2.5.2}$$

where $\mu=r$ is for random positive and negative injection, $\mu=2$ is for pair-creation injection, and $\mu=cr^{d_f}$ is for fractal injection. The boundary conditions are $\tilde{Z}_o(\varrho, t) = 0$ and $\tilde{Z}_r(0, t) = 0$.

Taking the absolute value of both sides of Eq.(2.5.2) and replacing the right hand side by the maximum of $\{|\tilde{Z}_{r'}(\varrho, t)|\ ;\ r' = r-1, 0, r+1\}$, we obtain the following relation :

$$|\tilde{Z}_r(\varrho, t)| = |\Phi(\varrho)^{\mu}| \cdot max\ \{\ |\tilde{Z}_{r'}(\varrho, t-1)|\ ;\ r' = r-1, 0, r+1\} \quad . \tag{2.5.3}$$

Iterating Eq.(2.5.3) t times and using the inequality $|\Phi(\varrho)| \leq 1$, which is valid for any characteristic function, we get for $r \neq 0$

$$|\tilde{Z}_r(\varrho, t)| \leq |\Phi(\varrho)^{\mu}|^t \cdot max \{ |\tilde{Z}_{r'}(\varrho, 0)| ; r' = 1, 2, \cdots \}. \qquad (2.5.4)$$

Therefore, for any ϱ which satisfies $|\Phi(\varrho)| < 1$ the perturbation goes to zero exponentially with time. This is true for any initial condition and it means that the steady state is unique and stable. The stability for the case $|\Phi(\varrho)| = 1$ is not trivial, but as we show in Appendix (4), even in this case the system relaxes to a unique steady state for any initial perturbation.

In the mean-field case the equation for the perturbation is derived by subtracting Eq.(2.3.33) from Eq.(2.1.15), namely:

$$\tilde{Z}_1(\varrho, t+1) = \frac{\Phi(\varrho)}{e} [e^{Z_1(\varrho) + \tilde{Z}_1(\varrho, t)} - e^{Z_1(\varrho)}]. \qquad (2.5.5)$$

Taking the absolute values on both sides of Eq.(2.5.3) and using the general inequality

$$|e^x - e^y| \leq e |x - y| \quad for \quad |x|, |y| \leq 1, \qquad (2.5.6)$$

we find that

$$|\tilde{Z}_1(\varrho, t)| < |\Phi(\varrho)|^t \cdot |\tilde{Z}_1(\varrho, 0)|. \qquad (2.5.7)$$

Again, for $|\Phi(\varrho)|<1$ it is trivial that the perturbation vanishes as $t\to\infty$, so that the steady-state solution $Z_1(\varrho)$ is unique and stable. Discussion in Appendix (4) is also applicable to this case, therefore uniqueness and stability hold for any type of injection.

2.6 Relaxation

In the preceding section, we have seen that the steady state, realized by injection, is unique and stable. In the current section we shall analyze the relaxation to the steady state [*H. Takayasu, A. Provata, and M. Takayasu* (1990)].

2.6.1 Relaxation in one-dimension with positive and negative random injection

In the continuum space and time limit (for small ϱ), the evolution equation for the perturbation in the case of independent random injection in one-dimension (Eq.(2.5.2) with $\mu=r$), takes the form of the following partial-differential equation:

$$\frac{\partial \tilde{Z}_r(\varrho,t)}{\partial t} = D\frac{\partial^2 \tilde{Z}_r(\varrho,t)}{\partial r^2} - Rr\,\tilde{Z}_r(\varrho,t), \quad \varrho \to 0 \qquad (2.6.1)$$

Here $D = 1/(4\Delta t)$, and $R = (-i\langle I\rangle + \langle I^2\rangle \varrho^2/2)/\Delta t$ where Δt denotes the time step. By performing Fourier transformation with respect to t (and using the boundary conditions $\tilde{Z}_0(\varrho,t) = 0$ and $\tilde{Z}_\infty(\varrho,t) = 0$), Eq.(2.6.1) can be solved in terms of Airy functions, $A_i(x)$, as:

$$\tilde{Z}_r(\varrho,t) = \sum_{k=1}^{\infty} e^{-\lambda_k t} E_k(r) \qquad (2.6.2)$$

where

$$\lambda_k = |a_k|\,(2DR^2)^{1/3},$$

and

$$E_k(r) = A_i((R/2D)^{1/3} + a_k) \quad ,$$

and a_k denotes the k-th zero of Airy function, a_1=-2.33$\cdots$, a_2=-4.08$\cdots$, *etc*.. Since λ_1 is the smallest of $\{\lambda_k\}$, we have the following time dependence for $t \to \infty$ in the case of $\langle I \rangle \neq 0$:

$$\tilde{Z}_1(\varrho, t) = f_1(\varrho) exp\ \{- b_1 \langle I \rangle^{2/3} exp\ (-\pi i/3)\ \varrho^{2/3} t\ )\} \quad , \qquad (2.6.3)$$

where $b_1 = |a_1|2^{-2/3}/\Delta t$, and $f_1(\varrho)$ is independent of t. In this type of process the relaxation is faster for larger values of ϱ and slower for smaller values of ϱ. The relaxation form of the corresponding mass distribution function can be obtained by performing reverse Fourier transformation of Eq.(2.6.3). Analytical expression of the reverse Fourier transformation can be obtained by applying the theory of stable distributions. [Note that the time-dependent factor on the right-hand side of Eq.(2.6.3) has the same form as the characteristic function of the stable distribution, $p\ (x, 2/3, -2/3\ )$ (see the notation in Appendix (4))]. The time evolution of the perturbation is described by the following form:

$$\tilde{p}\ (m, t) = \int dm'\ \tilde{p}\ (m - m', 0) g\ (m', t) \quad . \qquad (2.6.4)$$

Here the Green function $g\ (m, t)$ is given by

$$g\ (m, t) \propto \frac{1}{x} e^{-16/(27x^2)} W_{1/2,\ 1/6}\left(\frac{32}{27x^2}\right) \quad , \qquad (2.6.5)$$

where $x = b_1 |<I>/m|^{2/3} t$ and $W_{\mu,\nu}$ is the Whittaker function. The asymptotic behavior of Eq.(2.6.5) is estimated as

$$g(m,t) \propto exp\left(- \frac{b_1 |<I>|^2 t^3}{m^2} \right). \qquad (2.6.6)$$

This decay is faster than Gaussian and its characteristic time is proportional to $m^{2/3} |<I>|^{2/3}$.

In the case of $<I> = 0$, Eq.(2.6.3) for $\varrho \to 0$ is replaced by

$$\tilde{Z}_1(\varrho, t) = f_2(\varrho) exp\ \{ - b_2 <I^2>^{2/3} \varrho^{4/3} t \}, \quad t \to \infty, \qquad (2.6.7)$$

where $b_2 = |a_2| 2^{-4/3} / \Delta t$, and $f_2(\varrho)$ is independent of t. The Fourier inversion of Eq.(2.6.7) has the form of Eq.(2.6.4) where the Green function is given by a symmetric stable distribution with the characteristic exponent 4/3. For large $|m|$ the asymptotic behavior is estimated as

$$g(m,t) \propto <I^2>^{-1/2} t^{-3/4} \quad for \quad t >> m^{4/3} <I^2>^{-2/3}. \qquad (2.6.8)$$

This power-law decay is slow enough to be confirmed numerically as shown in Fig.2.12. The points scatter at large t but they are in good agreement with the theoretical slope.

The reason for these two different types of decay, Eq.(2.6.6) and Eq.(2.6.8), will be discussed at the end of this section.

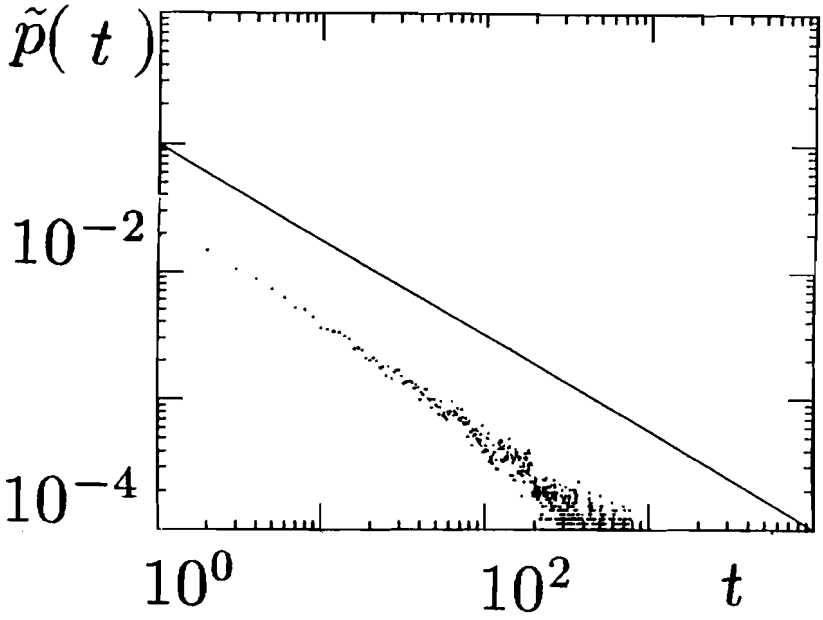

Fig.2.12 The relaxation function in the case of $<I>=0$ plotted on a log-log scale. The straight line shows the theoretical slope, -3/4.

2.6.2 Relaxation in one-dimension with pair-creation injection

In the case of pair-creation injection, the perturbation equation in the continuum limit is derived from Eq.(2.1.9) in the vicinity of $\varrho \to 0$:

$$\frac{\partial \tilde{Z}_r(\varrho, t)}{\partial t} = \frac{1}{4\Delta t} \frac{\partial^2 \tilde{Z}_r(\varrho, t)}{\partial r^2} - b_3 \varrho^2 \tilde{Z}_r(\varrho, t) = 0 \quad , \tag{2.6.9}$$

where $b_3 = \langle I^2 \rangle / \Delta t$. The solution of Eq.(2.6.9) is given by

$$\tilde{Z}_r(\varrho, t) = \frac{exp\ (-b_3\, \varrho^2 t)}{(\pi t / \Delta t)^{1/2}} \int dr'\, \tilde{Z}_{r'}(\varrho, 0)$$

$$\times \left\{ exp\left(- \frac{(r - r')^2}{t / \Delta t} \right) - exp\left(- \frac{(r + r')^2}{t / \Delta t} \right) \right\} . \qquad (2.6.10)$$

Reverse Fourier transformation of Eq.(2.6.10) can be put into the form of Eq.(2.6.4), and the corresponding Green function is shown to have the following long-time behavior

$$g(m, t) \propto \langle I^2 \rangle^{-1/2} t^{-1} \quad for \quad t >> m^2 \langle I^2 \rangle^{-1} . \qquad (2.6.11)$$

In this case, we again have a power-law decay but with a different exponent than in the case of random positive and negative injection with $\langle I \rangle = 0$.

2.6.3 Relaxation in one-dimension with fractal injection

In the case of fractal injection [*A. Provata, M. Takayasu, and H. Takayasu* (1992)] , the perturbation equation in the continuum limit is written as

$$\frac{\partial \tilde{Z}_r(\varrho, t)}{\partial t} = D \frac{\partial^2 \tilde{Z}_r(\varrho, t)}{\partial r^2} - 2\pi r^{d_f} |\varrho|^{\beta} \tilde{Z}_r(\varrho, t) , \qquad (2.6.12)$$

where $\varkappa$ is a constant and, again, the expansion Eq.(2.1.12) was used for $\Phi(\varrho)$, and $D = (\Delta x)^2/(4\Delta t)$ is a constant. This is the well-known problem of the time-dependent Schrödinger's equation for a particle moving in a potential of the form $V(r) \propto r^{d_f}$. By separation of variables, $\tilde{Z}_r(\varrho, t) = \tilde{Z}_r(\varrho) T(t)$, the time-dependent part of Eq.(2.6.12) can be shown to satisfy

$$T(t) \propto e^{-\Lambda(\varrho)t} , \tag{2.6.13a}$$

and the time-independent part satisfies

$$D \frac{\partial^2 \tilde{Z}_r(\varrho)}{\partial r^2} - \{2\varkappa r^{d_f} |\varrho|^{\beta} - \Lambda(\varrho)\} \tilde{Z}_r(\varrho) = 0 , \tag{2.6.13b}$$

where $\Lambda(\varrho)$ can only be a function of ϱ.

With the change of variables as in Eq.(2.3.26a), Eq.(2.3.26b) reads

$$\frac{\partial^2 \tilde{Z}(\varrho, q)}{\partial q^2} - \{2\varkappa q^{d_f} |\varrho|^{\beta} - \Lambda(\varrho)\varrho^{-2\beta/(d_f+2)}\} \tilde{Z}(\varrho, q) = 0 . \tag{2.6.14}$$

Note that the above equation can be interpreted as the time-independent Schrödinger problem for a particle which moves in a potential $V(q) \propto 2\varkappa |\varrho|^{\beta} q^{d_f}$ and has energy $E(\varrho) = \Lambda(\varrho)\varrho^{-2\beta/(d_f+2)}$. Using such quantum mechanical picture of particle's motion, we can obtain [*A. Provata, M. Takayasu, and H. Takayasu* (1992)];

$$\tilde{Z}_1(\varrho, t) \propto exp\ \{- const \cdot |\varrho|^{2\beta/(d_f+2)} t\} , \quad \varrho << 1 . \tag{2.6.15}$$

Finally to find the behavior of the perturbation of the charge probability distribution with time, we just need to perform Fourier reverse transformation of Eq.(2.6.15),

$$g(m,t) \propto t^{-(d_f+2)/2\beta}, \quad t>>1 . \tag{2.6.16}$$

So in the case of power-law and fractal input, as expected, perturbations of the power-law steady state decay following a power-law in time, with an exponent that depends both on the power exponent of the input and on the fractal dimension of the input subspace. In the special case of $\beta = 2$ and $d_f = 1$, which corresponds to the case of positive and negative random injection with $<I> = 0$, the exponent 3/4 given by Eq.(2.6.16) agrees with the result given by Eq.(2.6.8). Thus, we can confirm that Eq.(2.6.16) is a natural extension of the previous results.

2.6.4 Relaxation in the mean-field case

In the mean-field case, the equation for small perturbations is given by a linearized version of Eq.(2.5.5):

$$\tilde{Z}_1(\varrho, t+1) = \Phi(\varrho) e^{Z_1(\varrho)-1} \tilde{Z}_1(\varrho, t) . \tag{2.6.17}$$

Substituting the steady-state solutions, Eqs.(2.3.34a), (2,3,34b) and (2.3.34c), into Eq.(2.6.17), we have the following solutions for small ϱ :

In the case of $<I> \neq 0$,

$$\tilde{Z}_1(\varrho, t) \equiv \tilde{Z}_1(\varrho, 0)\ exp\ \{ -\sqrt{2}\ <I>^{-1/2} i^{-1/2} |\varrho|^{1/2}\ t \}\ . \qquad (2.6.18a)$$

In the case of $<I> = 0$,

$$\tilde{Z}_1(\varrho, t) \equiv \tilde{Z}_1(\varrho, 0)\ exp\ \{ -<I^2>^{-1/2} |\varrho|\ t \}\ . \qquad (2.6.18b)$$

In the case of fractal injection,

$$\tilde{Z}_1(\varrho, t) \equiv \tilde{Z}_1(\varrho, 0)\ exp\ \{ -const \cdot |\varrho|^{-\beta/2} t \}\ . \qquad (2.6.18c)$$

Corresponding temporal behaviors of the distribution functions are also given in the form of Eq.(2.6.4). The asymptotic behavior of the corresponding Green functions in the continuum limit are obtained as:

In the case of $<I> \neq 0$,

$$g\ (m, t) \propto exp\ \left(-\frac{|<I>|\ t^2}{2m} \right), \qquad t \to \infty\ . \qquad (2.6.19a)$$

In the case of $<I> = 0$,

$$g\ (m, t) \propto <I^2>^{-1/2} t^{-1}\ , \qquad t >> m\ <I^2>^{-1/2}\ . \qquad (2.6.19b)$$

In the case of fractal injection,

$$g\ (m, t) \propto t^{-2/\beta}\ , \qquad t >> |m|^{-\beta/2}\ . \qquad (2.6.19c)$$

We again have a fast decay (Gaussian decay) in the case of biased injection and a slow decay in the case of zero-mean injection. For fractal input, we have power-law long time decay with an exponent depending on β.

2.6.5 Summary

The results are summarized in Table 2.I together with the corresponding steady-state distributions.

Table 2.I Summary of the size distributions, p(m), and the form of relaxation, g(m, t) for one-dimensional case(1D) and the mean-field case(MF).

	$p(m)$	$g(m,t)$
$1D, \langle I \rangle \neq 0$	$m^{-4/3}$	$exp(-t^3)$
$1D, \langle I \rangle = 0$	$m^{-5/3}$	$t^{-3/4}$
$1D$, *pair creation*	m^{-2}	t^{-1}
$1D$, *Fractal input*	$m^{-1-\beta/(d_f+2)}$	$t^{-(d_f+2)/2\beta}$
$MF, \langle I \rangle \neq 0$	$m^{-3/2}$	$exp(-t^2)$
$MF, \langle I \rangle = 0$	m^{-2}	t^{-1}
MF, pair creation		
MF, Fractal input	$m^{-1-\beta/2}$	$t^{-2/\beta}$

The reason for the rapid decay in the biased injection cases, $\langle I \rangle \neq 0$, can be understood intuitively as follows. Assume that we have perturbed the steady-state distribution by introducing a sharp peak in the charge distribution around m_0. The number of particles

of charge m_0 decreases by aggregation or by injection. Aggregation of two particles with charges m_0 and m creates a particle of charge m_0+m. Consequently the aggregation process scatters the distribution around m_0 continuously. On the other hand, injection shifts the charge of the particle from m_0 to m_0+I. In the case of positive-mean injection, for example, the injection causes the peak of the charge distribution to drift continuously towards larger m, and aggregation also scatters m_0 to larger values. Thus the relaxation observed at a fixed charge m_0 is very fast. On the other hand, in the cases of $<I>=0$ (including pair-creation injection) and symmetric fractal input, the perturbation diffuses slowly around m_0 due to the injection and scatters nearly symmetrically by aggregation. The peak of the perturbation does not move on average, and so the decay is much slower than in the biased-injection case.

2.7 Critical dimensions of the model

In Sections 2.1, 2.3 and 2.6 we have addressed the question of critical dimension. It is an open problem to analyze our model in dimensions greater than 1. Above the critical dimension, the mean-field model gives the correct exponents for both the steady state and for the relaxation. It should be noted that in the case of pair-creation, the exponents for 1 dimension coincide with those for mean field. This result seems to suggest that the critical dimension is 1 in the case of pair-creation injection. On the other hand for random injection (both for $<I> \neq 0$ and for $<I> = 0$), the exponents for one-dimension are different from the mean-field values, which indicates that the critical dimension is greater than 1. The result from simulations on a lattice with random positive injection shows that the critical dimension for charge distribution is equal to 4. From the analysis using the statistical properties of random walk trajectories, we can show that the variance of charge depends on the spatial dimension up to $d < 2$, for $d \geq 2$ the variance becomes function of only t and does not depends on spatial dimension. In such sense, we can say that the critical dimension is 2. *D. Dhar and R. Ramaswamy* (1989) show that the critical dimension is 2 for the relation between charge m and its corresponding basin's height h shown in Eq.(2.4.3), by relating the basic Scheidegger's model to self organized criticality problems. It is, therefore, likely that the critical dimension is not universal, but depends on the type of injection and on observed values. *S. P. Obukhov* (1989) claimed that the critical dimension is

not universal but depends on the order of the moment we are observing.

2.8 Discussion

In this chapter we analyzed the statistical properties of an aggregation system, for one-dimensional and mean-field cases using the equation for the many-body characteristic function. In the case of no-injection, the particle number decays following a power law. But there appears a non-trivial statistically-invariant steady state if we supply particles at a constant rate. The most interesting point here is that the system converges to a steady state even in the absence of a sink or particle breakup. It is easy to confirm from Eqs.(2.1.5) and (2.1.15) that the variance of particle charge increases linearly with time, namely, it diverges in the limit of $t \to \infty$. Usually such divergence means that the system does not have a stationary state, but in this case the charge distribution converges to a power-law distribution in which the mean value and the variance diverge. Thus, we call this quasi-steady state as "statistically steady state".

According to the theory of stable distributions, the divergence of the variance is essential to power law distributions. The central limit theorem, though, can be generalized to include independent random variables with divergent variances. The limiting distribution of the sum of such variables is, if exists, a non-Gaussian stable distribution with a power-law tail as we mentioned in section 2.4.3. In our model, the variance is divergent in the statistically steady state, and a particle's charge is given by a sum of random aggregating variables, $I(j, t)$, of each time step. We can not directly apply the generalized central-limit theorem because we know that there exists a weak spatial correlation among the random variables. However, it seems

likely that the charge distribution here belongs to the domain of attraction of a non-Gaussian stable distribution and thus has a power-law tail.

Our aggregation model does not have any control parameter and automatically realizes a power-law distribution, typically a sign of critical behavior. In order to see the criticality from the point of view of a branching model one just needs to invert the time axis. As a branching model the system can be described by the values of the branching probability(see section 2.4.2). For high branching probability the number of particles increases exponentially and for low branching probability it decreases exponentially. There exists a critical value of the branching probability at which the particle number becomes constant on average. This model is equivalent to the stochastic cellular automata analyzed by *E. Domany and W. Kinzel* (1984), and it is known that phase transitions of this type are similar to the one in directed percolation. In our aggregation model, the number of particles is kept constant by injection, therefore, the corresponding branching probability must be equal to the critical value to keep the particle number constant.

As we show in Section 2.5, the steady-state power-law distribution is very robust. It is uniquely determined by the type of injection and is independent of specific details of injection or initial conditions. The functional form of the relaxation to the steady state is also determined by the type of injection.

The voter model [*T. M. Liggett* (1985), *R. Durrett* (1988)] is known to be equivalent to Scheidegger's river model, though the process proceeds reversely in time. Namely, the voter model is a time-

reversed version of Scheidegger's river model. In the voter model the sites of a one-dimensional lattice are occupied by persons who are either in favor of or opposed to some issue. The voters are simple minded, and change their opinions very easily by being spoken to by their neighbors and speak frankly about their opinions to the neighbors. This is equivalent to a particle system in which a particle at a certain time changes its state to one of the neighboring particle's state stochastically. After a long time, the particles having the same state start forming clusters in one-dimensional lattice, and finally all particles take the same state. Fig.2.13 shows a space-time pattern of voter model which shows who is influenced by whom as time goes. From this pattern, it is clear that the model is a time reversed version of Scheidegger's model. The clustering process has been analyzed mathematically [*T. M. Liggett* (1985), *R. Durrett* (1988)].

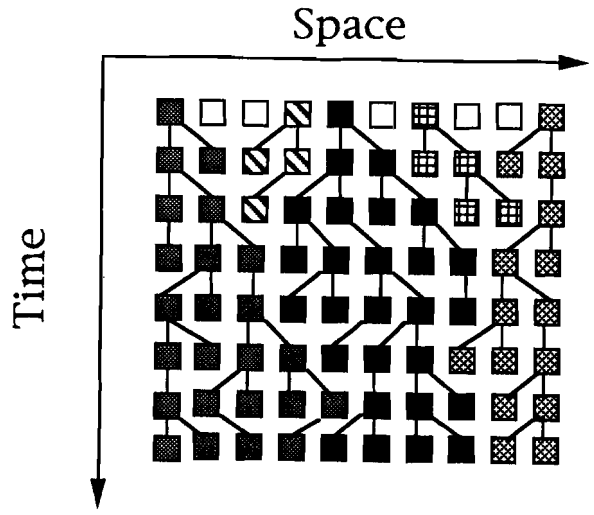

Fig.2.13 A space-time configuration of voter model.

The potential applicability of our model is expected to be very wide since our model describes very basic process of non-equilibrium systems. By regarding $m(j, t)$ as the height differences of a dislocation at site j in one-dimension [*M. Karder, G. Parisi, and Y.-C. Zhang* (1986)], the aggregation process corresponds to a coalesce of two dislocations in order to form a bigger dislocation, and the injection corresponds to a process of creating a new dislocation or bump (pair creation) on the surface. The steady state of this case can be regarded as a situation of balancing smoothing and roughening process of the surface.

Another potential field of application may be turbulence. It is well known that one-dimensional turbulence governed by Burgers equation is described by a set of shock waves which behave just like sticky particles in low viscosity limit [*J. M. Burger* (1974)]. If we regard the difference of velocities in two nearest sites as $m(j, t)$, we can observe the process of aggregating $m(j, t)$ with momentum conserved. When we apply external forces then the system converges to a statistically steady state with power-law distribution. The exponent is equal to the one in the case of one-dimensional random injection, which is 1/3 in cumulative distribution [*H. Hayakawa, et.al.* (1987)].

Other extended versions of our model are introduced in the next chapter.

Chapter 3

Extended versions of the model

3.1 Aggregation of exponentially growing particles

Let us consider the situation when the basic Scheidegger's model which we introduced in the previous chapter has dissipation proportional to mass(charge) at each time step in addition to the uniform injection. In such a case the mass distribution holds the same power-law as the case of nondissipated system and an exponential decay is observed at large mass due to the dissipation. For smaller dissipation the exponential decay becomes more gentle, and for very small dissipation the distribution looks practically the same as in the case of nondissipated system. What will happen to the charge distribution when the system has an effect opposite to dissipation? Namely, we consider a mass growing effect, *i.e.*, the particle grows proportional to its own mass at each time step. Does a stationary state still exist? In this section, we discuss the fact that a steady state exists even in such mass self-growing systems. Now, let us introduce the details of the model in the case of one-dimension [*M. Takayasu* (1992)].

We consider an aggregation process in one-dimensional discretized space-time with a periodic boundary. In one time step each particle jumps randomly either to the right or to the left neighbor. If two particles happen to jump on to the same site simultaneously, they immediately coalesce into a single particle with mass equal to the sum of the masses of the incident particles. Then we inject a unit mass particle onto each site. Up to this part of operation, all processes are the same as in the basic Scheidegger's model. But, in addition, at the end of each time step, we multiply the total mass of each site by $1 + \lambda$ ($\lambda > 1$).

The space-time configuration of particles' trajectories is exactly the same as in the basic Scheidegger's model (Fig.2.3) under the same random evolutions since the space-time pattern depends only on random walk process. But both the structure of the branches and the mass self-growing process contribute to the mass of each particle.

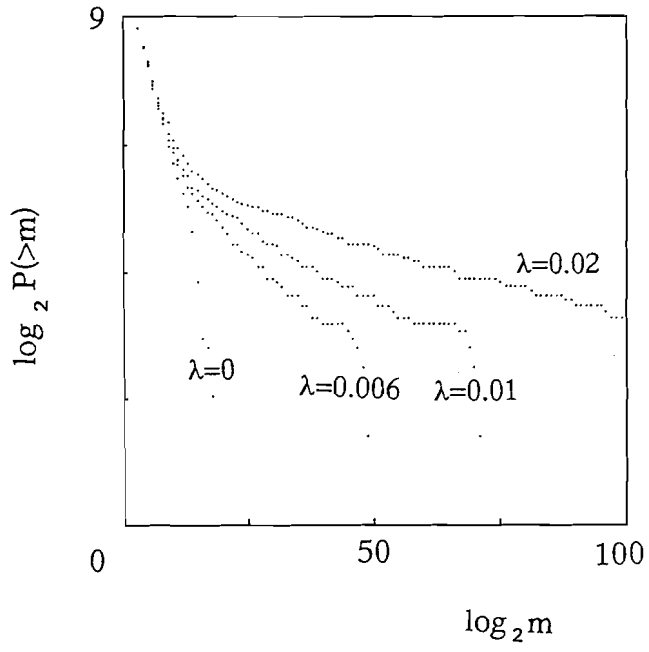

Fig.3.1 Numerical results of the cumulative mass distribution for different λ's.

Fig.3.1 shows the cumulative mass distributions for four different values of λ obtained by numerical simulations using the same random numbers, on 1000 sites for 4000 time steps. The distribution has two characteristic ranges. In the small mass range $0 < m < 2^{10}$, the random aggregation process dominates over the mass self-growing effect and a power-law distribution $p\ (>m) \propto m^{-1/3}$, which is the same distribution as in the random

positive and negative injection case (see section 2.3.1), appears to be independent of λ. In the large mass range $2^{10} < m$, the mass self-growing effect rules over the system and the distributions clearly depend on λ. Note that the tail of this range is extraordinarily long (about 10^{18} for $\lambda = 0.01$), and exponential decays caused by finite-size-effect are observed only at the very end of the tails.

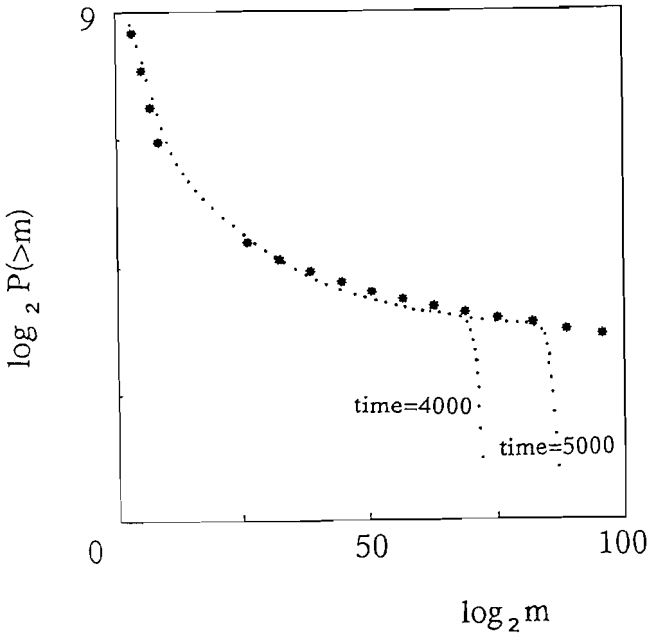

Fig.3.2 Numerical results of the finite-time-step effect observed in the cumulative mass distribution in the case of λ=0.01. The large dots are the theoretical results for the steady state plotted as a comparison.

The dotted line in Fig.3.2 shows the numerical result for the mass distribution with $\lambda = 0.01$. The data are obtained by taking average over 10 realizations. It is clear that the functional form of the distribution does not depend on the number of time steps. In this figure, we have more manifest appearance of the large mass

range. If we observe mass in relatively short scale then it may be regarded as a part of a power-law. However, we can tell that the tail does not fall on a straight line on the log-log plot, *i.e.*, the tail does not follow a rigorous power-law.

The theoretical explanation for this tail is given as follows. Let us estimate the mass of a particle whose trajectory at time t is characterized by the height (or lifetime), h , and width of the river basin, $w\ (t\ )$, as shown in Fig.2.9 (see section 2.4). The mass m of the particle is given by

$$m = \sum_{t=0}^{h} w\ (t\ )(1 + \lambda\ )^{t} = \sum_{t=0}^{h} w\ (t\ )e^{\,t\ ln\ (1+\lambda\ )} \quad . \tag{3.1.1}$$

When $h >> 1/\lambda >> 1$, Eq.(3.1.1) can be approximated as

$$m \equiv e^{\,\lambda\ h} \sum_{t=0}^{h} w\ (t\ )e^{\,-\lambda\ t} \quad . \tag{3.1.2}$$

As the summation can be proved to remain finite the mass is estimated as

$$m \propto e^{\,\lambda\ h}, \qquad h >> 1/\lambda \quad . \tag{3.1.3}$$

This implies that the mass self-growing effect becomes prominent for the particles having height h longer than $1/\lambda$.

As for the particles satisfying $h << 1/\lambda$, we can treat the system simply as the case of the random aggregating particles with injection in one-dimension, so that the discussion we made in section 2.4 can be applied (see section 2.4). Let us give a little

summary: In such a case, the mass is given by the summation of $w(t)$, which equals to the area of the branches in the space-time in Fig.2.9. The relation between m and h is known from the problems of random walk. Thinking of the first encounter of the two random walkers starting from the same point, the area surrounded by the two trajectories in the space-time gives the area of the branches because the edges of the branches can be regarded as random walkers' trajectories. As the width, $w(t)$, of the branches is nearly proportional to $h^{1/2}$, the mass for a particle with $h \leq 1/\lambda$ is related to h as

$$m \propto h^{3/2}, \qquad h \leq 1/\lambda . \tag{3.1.4}$$

The inequality $h \leq 1/\lambda$ corresponds to the small mass range in Fig.3.2 and $h >> 1/\lambda$ corresponds to the large mass range. Namely, $h = 1/\lambda$ gives the threshold of these two characteristic ranges.

Fig.3.3 shows the relation between m and h for numerical data of $\lambda = 0.01$ simulated on 1000 sites with 4000 time steps. We can confirm the validity of Eq.(3.1.3) for $h >> 1/\lambda = 100$. The maximum value of h in the figure is 4000 which is restricted by the maximum number of time steps in the simulation. 10 realizations are plotted on the figure, yet we have practically no fluctuations. For $h \leq 1/\lambda = 100$, evidently the exponential relation between m and h is broken, which is consistent with our previous discussions. By plotting the same data in log-log scale, Eq.(3.1.4) has also been confirmed for small h.

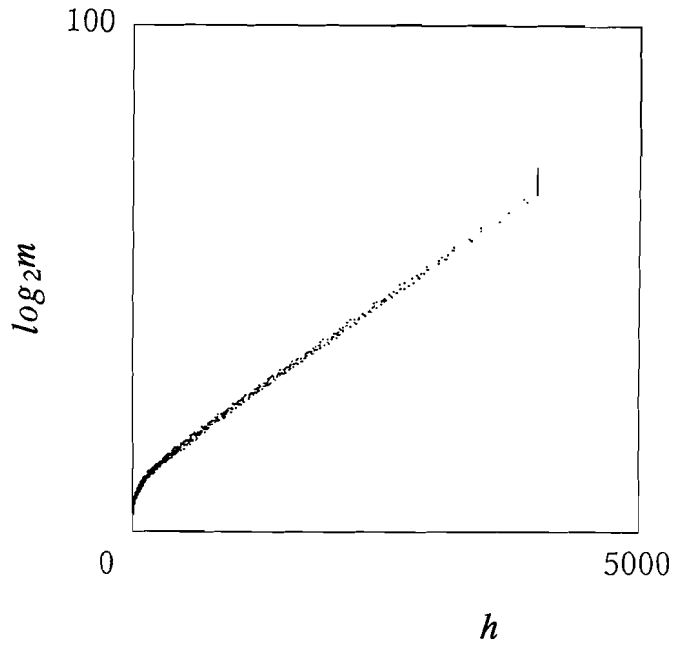

Fig.3.3 Mass m vs. height h in semilogarithmic scale for one-dimensional case. The slope for large h fits nicely on the theoretical estimation $\lambda/\ln 2$ (λ=0.01).

Let us consider the size distribution of h. This distribution is equivalent to the distribution of two random walkers' first encounter time and is known to be given as

$$p\ (>h) \propto h^{-1/2} \quad . \tag{3.1.5}$$

Note that the patterns of branching trees are not effected by the exponential growth, therefore, h is independent of λ. Eq.(3.1.5) is confirmed numerically in Fig.3.4, which is obtained for the same situation as Fig.3.3. It shows that Eq.(3.1.5) holds in the range $10 < \lambda \leq 4000$.

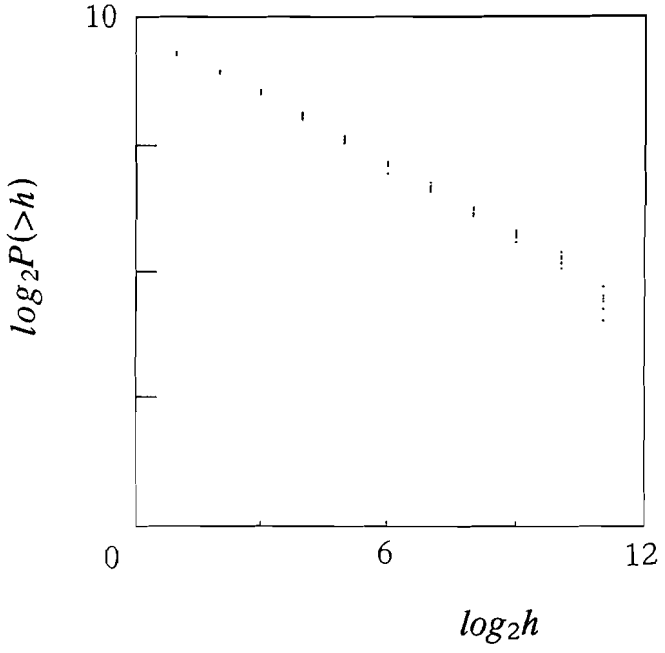

Fig.3.4 The cumulative size distribution of h for one-dimensional case. The slope is close to the theoretical value -1/2.

The distribution of m is obtained as follows by assuming that h is uniquely determined for a given m by a monotonous function, $h\ (m\ )$. Then we have the following relation:

$$p\ (>m) = p\ [>h\ (m\ )]\ . \tag{3.1.6}$$

From Eqs.(3.1.3),(3.1.5) and (3.1.6), and Eqs.(3.1.4),(3.1.5) and (3.1.6), we get, respectively,

$$p\ (>m) \propto \lambda^{1/2}\ (ln\ m\ )^{-1/2}, \qquad h >> 1/\lambda\ , \tag{3.1.7}$$

$$p\ (>m) \propto\ m^{-1/2}, \qquad h \leq 1/\lambda\ . \tag{3.1.8}$$

Differentiating Eqs.(3.1.7) and (3.1.8) with respect to m, we obtain

$$p(m) \propto \frac{1}{m}(\ln m)^{-3/2}\lambda^{1/2}, \qquad h >> 1/\lambda , \tag{3.1.9}$$

$$p(m) \propto m^{-4/3}, \qquad h \leq 1/\lambda . \tag{3.1.10}$$

In the limit of $m \to \infty$, Eq.(3.1.9) behaves as $p(m) \propto 1/m$, which is often called a Zipf's law.

The large dots plotted in Fig.3.2 are the theoretical values obtained from Eqs.(3.1.7) and (3.1.8) with an appropriate choice of the proportional constants. It shows a good fit with numerical results.

Now, we discuss the case of mean-field. Let us figure the system with all sites connected to each other directly so that a particle on an arbitrary site can jump to any site, even to itself, in one time step. As in the case of one-dimension, merged particles and injected unit particle falling on the same site are combined to form a new particle with mass conserved at every time step. In the case without the mass self-growing process, the mass distribution is known to form a stable power-law, $p(>m) \propto m^{-1/2}$, like in the case of one-dimension but with a different exponent (see section 2.3.4). Then, let us take into account the mass self-growing effect. Eq.(3.1.3) holds again as we have seen in Fig.3.5. The numerical results shown in Fig.3.5 are obtained for the same condition as in Fig.3.3; system size=1000, maximum number of time steps=4000, $\lambda = 0.01$, and ten realizations are plotted without taking an average.

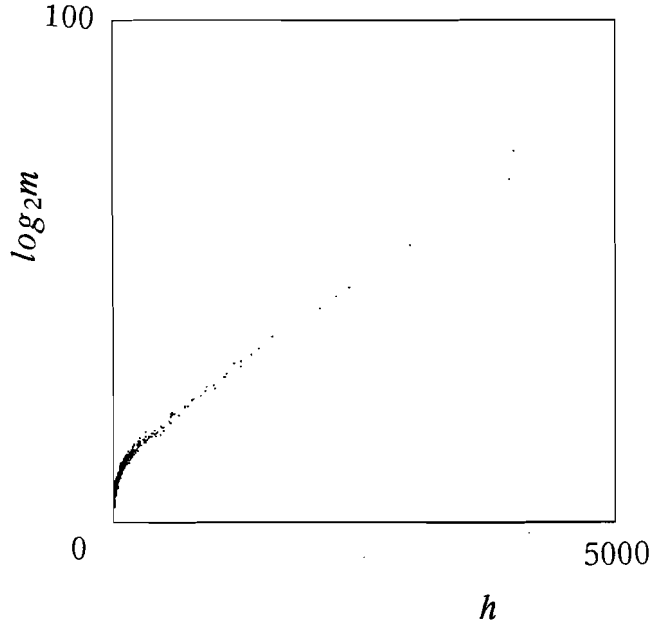

Fig.3.5 Mass m vs. height h in the semilogarithmic scale for the mean-field case.

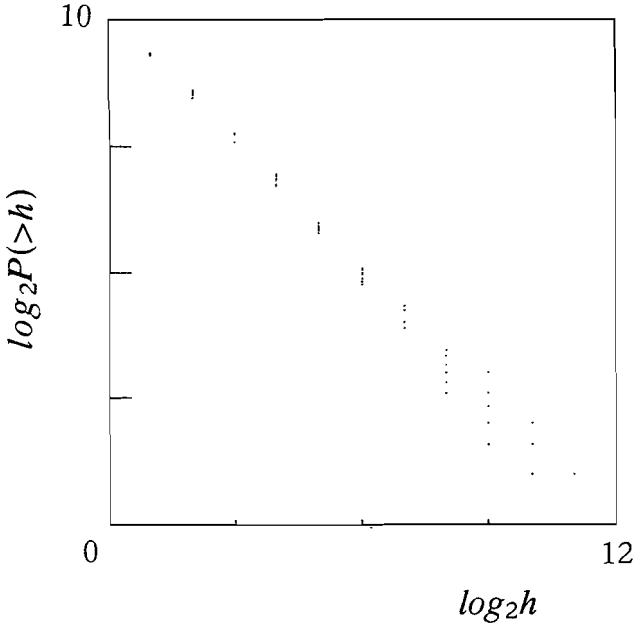

Fig.3.6 The cumulative size distribution of h for the mean-field case. The slope is -1 as is estimated theoretically.

In the mean-field case we cannot apply the results from the random walk problem but we can directly derive an equation for $p\,(>h)$ (see Fig.3.6). The followings are the processes contributing to the probability of having a particle with a lifetime longer than h, $p\,(>h)$, at time step t. Consider a particle having a lifetime longer than $h-1$ at step $t-1$. Both in the case when it aggregates with particles having lifetimes smaller than $h-1$ and when it is not involved in any aggregation, it produces a particle with lifetime longer than h in the next time step. But if two or more particles having the lifetime longer than $h-1$ at time $t-1$ combine together to form a heavy particle at time t, then the probability $p\,(>h, t)$ decreases. Therefore, the equation for the probability $p\,(>h, t)$ is given as

$$p\,(>h, t) \cong p\,(>h-1, t-1) - p\,(>h-1, t-1)^2 , \qquad (3.1.11)$$

where higher-order terms are neglected. The stationary solution of Eq.(3.1.11) is obtained by taking continuum limit with respect to h as

$$p\,(>h) \propto h^{-1}. \qquad (3.1.12)$$

From Eqs.(3.1.3), (3.1.6) and (3.1.12), we obtain the probability density as

$$p\,(m) \propto \frac{1}{m}(\ln m)^{-2}\lambda, \qquad h >> 1/\lambda , \qquad (3.1.13)$$

$$p\,(m) \propto m^{-3/2}, \qquad h \leq 1/\lambda . \qquad (3.1.14)$$

Again we have $p(m) \propto 1/m$ in the limit of $m \to \infty$.

Our results for one-dimension and for the mean-field case indicate that the asymptotic behavior of the mass distribution converging to $1/m$ may be universal in the exponentially growing particle system. The mechanism of having such a universality can be summarized as follows. Imagine an exponentially growing variable X ; $X \propto exp(\lambda Y)$, where the characterizing variable Y has a probability distribution in the form of power-law, $p(Y) \propto Y^{-\alpha}$. In the same way as we derive Eqs.(3.1.9) and (3.1.13), the probability density for X can be shown to be

$$p(X) \propto \frac{1}{X} (ln\, X)^{-\alpha} \lambda^{\alpha - 1}. \tag{3.1.15}$$

This simple mechanism can be proposed as a model for the systems having long tails satisfying Zipf's law, X^{-1}, in various fields of science. Concerning the model introduced in this section, diffusion and aggregation processes of particles are not so essential to the universality of $p(X) \propto X^{-1}$, but the exponential growth and the power-law distribution of $p(Y)$ play an important role. From the statistical point of view, it is a new result that even in the mass growing-particle system there exists a statistically stationary state.

3.2 Non-Gaussian distribution in random transport dynamics

Non-Gaussian distributions are found to be important in the study of fluid turbulence [*G. K. Batcherlor* (1953); *A. S. Monin and A. M. Yaglom* (1975)]. They are found in the fluctuation of velocity field by using the latest technique of direct observation of turbulence [*H. K. Park and W. I. Goldburg* (1992)] and numerical integration of Navier-Stokes equation [*Z-S. She, E. Jackson and S. A. Orszag* (1988); *S. Kida and Y. Murakami* (1989)]. In these results the distribution of velocity difference, $\delta v(r) \equiv v(x) - v(x+r)$, shows tails which are much longer than those of Gaussian but still much shorter than power-laws. Scalar quantities in turbulence such as temperature are also known to follow neither Gaussian nor power-laws [*E. D. Sinai and V. Yakhot* (1989); *A. Pumir, B. Shraiman, and E. D. Siggia* (1989)]. In the followings we introduce a random transport dynamics which is a stochastic model realizing non-Gaussian distributions. We will see the steady-state distribution of the model for extreme limits comparing with Scheidegger's river model.

Recently, *H. Takayasu and Y-h. Taguchi* (1993) introduced a random transport dynamics model in which a finite portion of a scalar quantity on a site is transported to its neighbor and the rest of the portion remains on the same site in a time step. Namely, we can view this model in terms of particles as a breaking up process. In such model they found both numerically and theoretically that the fluctuation of a scalar quantity("charge" or "mass" in Scheidegger's river model) is generally not Gaussian, and the tail of its distribution is between Gaussian and a power-law. Gaussian and power-law distributions appear only in extreme situations.

Let us define the model more precisely for a one-dimensional system. Consider the situation that the charge, $m(j,t)$, is distributed on a one-dimensional lattice. A portion of $m(j,t)$ is transported randomly to the neighboring sites at a time step as described by the following stochastic equation:

$$m(j, t+1)=m(j, t)-\theta(j, t)m(j, t)+\sum_k W_{j,k}(t)\theta(k, t)m(k, t) \quad , \qquad (3.2.1)$$

where $\theta(j, t)$ is a random number in the range $0\le\theta(j, t)\le 1$, $W_{j,k}(t)$ is also a random number which takes either 1 or 0, and k denotes the location of neighboring sites. $W_{j,k}(t)=1$ means that there exists transport from k to j at time step t. In order to conserve the total quantity, $\Omega\equiv\sum_j m(j, t)$, we require that $W_{j,k}(t)$ equals to 1 with only one j for each k, namely, in a time step a site can distribute a portion of its charge to only one of the nearest neighbors. Here, we allow the possibility of $W_{j,j}(t)=1$, which means no transport.

Comparing Eq.(3.2.1) and Eq.(2.2.1), we notice that in the case that $\theta(j, t)=1$ Eq.(3.2.1) become the same as Eq.(2.1.1) in Scheidegger's river model with $I(j, t)=0$, no injection case, in which all particle coalesce to form a particle in the limit of $t\to\infty$. But in the later part of this section, we will find an interesting fact that the steady state distribution in the limit of $\theta(j, t)\to 1$. follows a power-law which is absolutely different from the case of $\theta(j, t)=1$.

In the limit $\theta(j, t)\to 0$, the model can be represented by the formalism of a motion of continuum in a random velocity field, $v(j, t)$, where $v(j, t)$ is expressed as follows:

$$|v(j, t)|=\frac{\theta(j, t)}{\Delta t} \quad , \qquad (3.2.2a)$$

$$\frac{\partial}{\partial t} m(j, t) + \frac{\partial}{\partial j} (v(j, t) m(j, t)) = 0 \quad . \qquad (3.2.2b)$$

where the direction of $v(j, t)$ is determined by $W_{j,k}(t)$ and its magnitude, Δt , is the time step. Then Eq.(3.2.1) can be viewed as a discretized version of the following equation for passive scalar diffusion in a random velocity field $v(j, t)$,

$$\frac{\partial}{\partial t} m(j, t) + \nabla (v(j, t) m(j, t)) = 0 \quad , \qquad (3.2.3)$$

As is well-known Eq.(3.2.3) becomes an ordinary diffusion equation if the autocorrelation of $v(j, t)$ or $W_{j,k}(t)$ vanishes quickly.

Considering the above two extreme limits, Eq.(3.2.1) generally represents both diffusion and aggregation effects for $0<\theta(j, t)<1$. In the following analysis, to avoid unessential complexity, we assume that all $\theta(j, t)$ take a constant value θ $(0<\theta<1)$, and observe how the system changes for different values of θ.

We start our study with a mean-field version of Eq.(3.2.1) to estimate theoretically the effect of the finite portion transports. We consider the situation that a site is interacting with a mean-field site and transports to or from the mean-field site occur with probability 1/2, independently. In such case the stochastic Eq.(3.2.1) becomes

$$\begin{aligned}
&m(t+\Delta t)=m(t) && \text{with probability } 1/4,\\
&m(t+\Delta t)=(1-\theta)m(t) && \text{with probability } 1/4,\\
&m(t+\Delta t)=m(t)+\theta m_{MF} && \text{with probability } 1/4,\\
&m(t+\Delta t)=(1-\theta)m(t)+\theta m_{MF} && \text{with probability } 1/4, \qquad (3.2.4)
\end{aligned}$$

where m_{MF} is the value at the mean-field site which is defined as an independent random number having the same distribution as $m(t)$. By introducing the characteristic function

$$Z(\varrho, t) \equiv \int_{-\infty}^{\infty} e^{-i\varrho m} p(m, t)\, dm$$
$$= 1 + i\varrho \langle m \rangle - \frac{\varrho^2}{2!} \langle m^2 \rangle + \cdots , \qquad (3.2.5)$$

where $p(m, t)$ is the probability density for m at time t, Eq.(3.2.4) becomes

$$Z(\varrho, t+\Delta t) = \frac{1}{4}\{Z(\varrho, t) + Z(\varrho - \theta\varrho, t)\}\{1 + Z(\theta\varrho, t)\} , \qquad (3.2.6)$$

Substituting Eq.(3.2.5) into Eq.(3.2.6), a set of equations for the moment functions $\langle m^n \rangle$ are obtained, and it can be easily shown that a non-trivial steady state exists when $\langle m \rangle \neq 0$, i.e. $\Omega \neq 0$. In the case $\langle m \rangle = 0$ we will see later that the only steady state solution is $p(m) = \delta(m)$, that is, no fluctuation remains.

The steady state solution for $\langle m \rangle \neq 0$ is shown in Fig.3.7. It shows the cumulants for orders up to 7 together with those for one-sided exponential distribution for comparison. Higher order cumulants are not zero in all cases and showing a tendency to diverge as the order goes to infinity, which clearly demonstrates that the steady state distribution is not Gaussian for which cumulants are zero for orders greater than or equal to 3.

For smaller m the cumulants are smaller, and in the limit of $\theta \to 0$ it can be shown theoretically that the normalized cumulant of order n, $\langle m^n \rangle_c / \langle m^2 \rangle_c^{n/2}$, vanishes for $n \geq 3$. Namely, the distribution

converges to a Gaussian in this limit, which agrees with the well-known fact that the distribution function satisfying the usual diffusion equation in the continuum limit is a Gaussian. This result indicates that the finiteness of θ is very important for the appearance of non-Gaussian in our random transport dynamics.

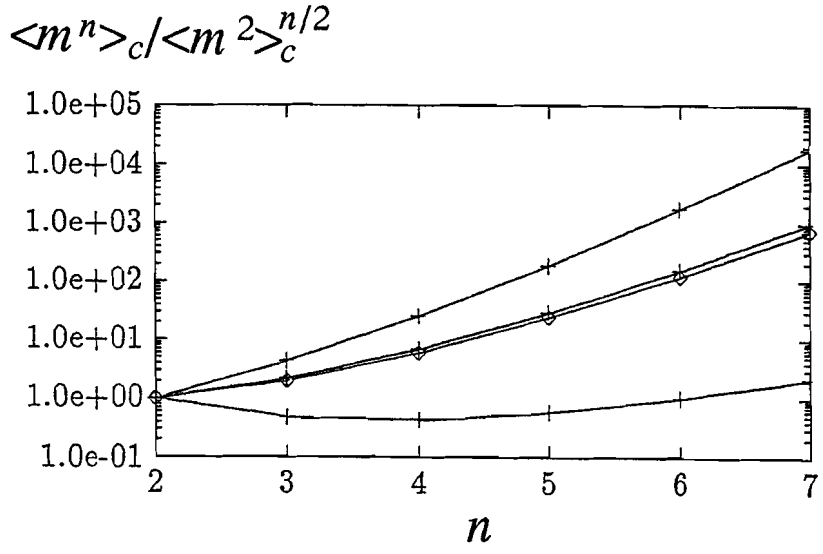

Fig.3.7 Higher order cumulants $<m^n>_c$ are plotted by crosses for the mean-field model; θ=0.1, 0.7 and 0.9 from bottom to top. The exponential distribution is plotted by squares for comparison[*H. Takayasu and Y-h. Taguchi* (1993)].

In the special case of θ=1/2, theoretical estimation for the asymptotic behaviors of the steady-state characteristic function, $Z(\varrho)$, is given as

$$Z(\varrho) \propto \varrho^{-2/3} \quad . \tag{3.2.7}$$

in the vicinity of $\varrho \to \infty$. This power law decay is very different from the case of a Gaussian distribution where the characteristic function decays faster than any power of ϱ. In the case of exponential distribution the characteristic function is given by $1/(1+i\,\varrho)$ (asymmetric case) or $1/(1+\varrho^2)$ (symmetric case), which also shows a power-law decay as $\varrho \to \infty$. In this sense the distribution is far from Gaussian, but is similar (but not identical) to the exponential distribution.

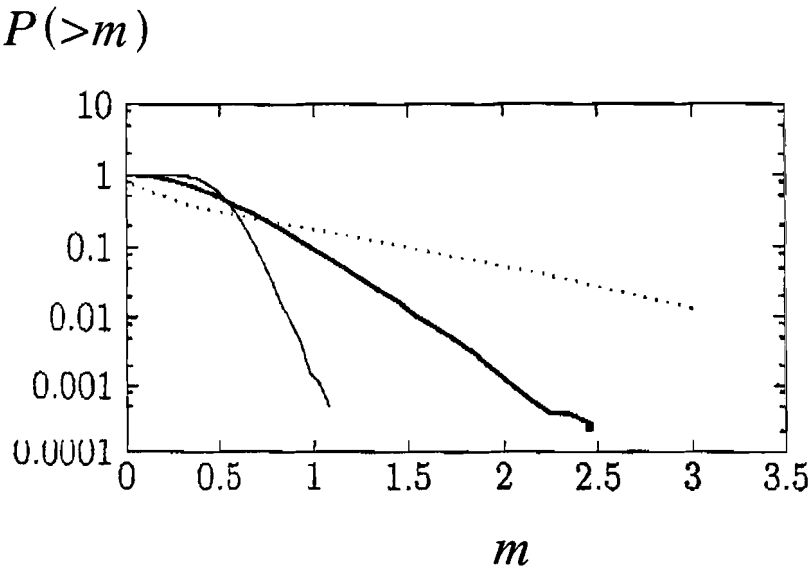

Fig.3.8 Semi-log plot of the steady state cumulative distribution, $P(>m) = \int_m^\infty P(m')\,dm'$, in one-dimension with $\langle m \rangle >> 0$. The values θ are 0.3 (thin line), 0.5 (bold line), and 0.9 (dotted line). Averages are taken over 10 realization [*H. Takayasu and Y-h. Taguchi* (1993)].

Fig.3.8 shows the results of numerical simulations on one-dimensional lattice. The steady-state cumulative distributions for θ=0.1, 0.5 and 0.9 are shown in semi-log scale. The steady-state is expected to be independent of the initial condition. For θ=0.1 the

tail of the distribution decays quickly like a Gaussian, and for larger θ the tail becomes larger as estimated by the mean-field analysis.

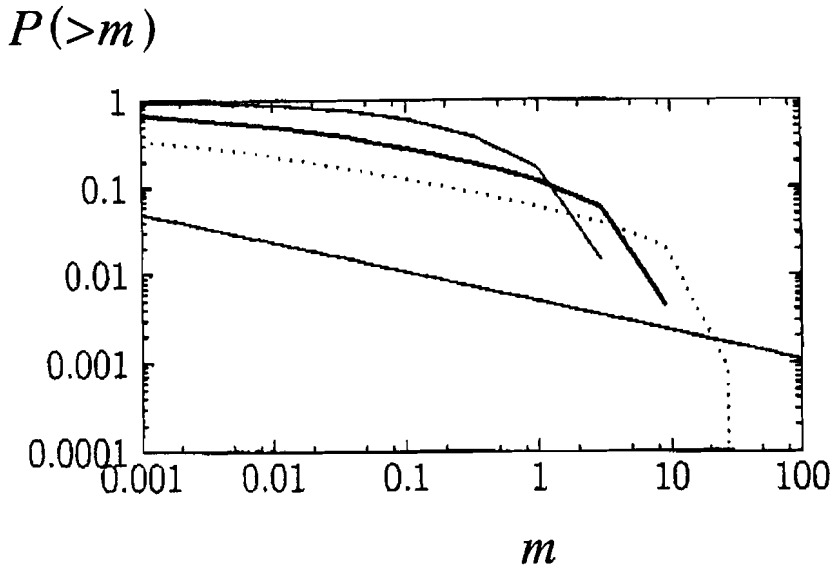

Fig.3.9 Log-log plot of the steady state cumulative distribution in one-dimension with $\langle m \rangle > 0$. The values θ are 0.9 (thin line), 0.99 (bold line), and 0.999 (dotted line). The slope of the straight line is -1/3 [*H. Takayasu and Y-h. Taguchi* (1993)].

To see the asymptotic behavior in $\theta \to 1$ we plot the cases of θ=0.9, 0.99 and 0.999 in log-log scale in Fig.3.9. The steady-state distribution gradually approaches a power-law $P(>m) \propto m^{-1/3}$, which is the same as the exact solution of one-dimensional Scheidegger's river model in the presence of positive injection (see section 2.3). In our simulation we have no injection, however, in the case θ is close to but not equal to 1, the small portion left behind at every transport, $(1-\theta)m(j,t)$, may play the role of injection while the dominant effect is the aggregation process, then

the system can realize a nearly power-law steady state. Namely, the limit of $\theta \to 1$ corresponds to the presence of positive injection since the breaking up process gives the same effect as injection of small particles.

Next, we consider the case of $<m>=0$, *i.e.* $\Omega = 0$. The second order terms of ϱ in the mean field equation, Eq.(3.2.5), give the following equation for the variance of m,

$$<m^2(t+\Delta t)> = (1 - \theta + \theta^2)<m^2(t)> \quad . \tag{3.3.8}$$

It follows immediately from this equation that the variance decays exponentially to zero for $0<\theta<1$, which shows that the only steady state is the trivial state, $P(m)=\delta(m)$, as we mentioned previously.

The system becomes non-trivial if we apply random external fluctuations. Namely, we add a new term, $I(j, t)$, in Eq.(3.2.1) or $I(t)$, in Eq.(3.2.4), which are random variables having zero mean, $<I>=0$. Accordingly a new term, $<I^2>$, is now added to Eq.(3.3.8) and the variance converges exponentially to a finite value. The same argument holds for every moment of m, $<m^n>$, so that we have a non-trivial stable steady distribution $p(m)$.

Numerical results are shown in Fig.3.10. Here the transport is long-ranged(a site is directly connected to the other sites), *i.e.*, the probability of $W_{j,k}(t)=1$ is independent of j for each k. For small θ the distribution is close to a Gaussian as shown in the case of $\theta=0.3$ in Fig.3.10. For larger θ the tails become larger as seen in the case of $\theta=0.8$, and as $\theta \to 1$ the distribution converges to Lorentzian tails, $P(m) \propto |m|^{-2}$ (see the case of $\theta=0.99$), which is the same as one obtained in Scheidegger's river model with pair-creation injection (the exact equivalence between this model in the case of $<m>=0$

with injection and Scheidegger's river model with pair-creation injection is established in the particular case $\theta=1$). Here, we confirm that the the result of $\theta \to 1$ converges to the result of $\theta=1$. This result is not like the case of $<m>\neq 0$ without injection because in such a case the results of $\theta=1$ and $\theta \to 1$ are different.

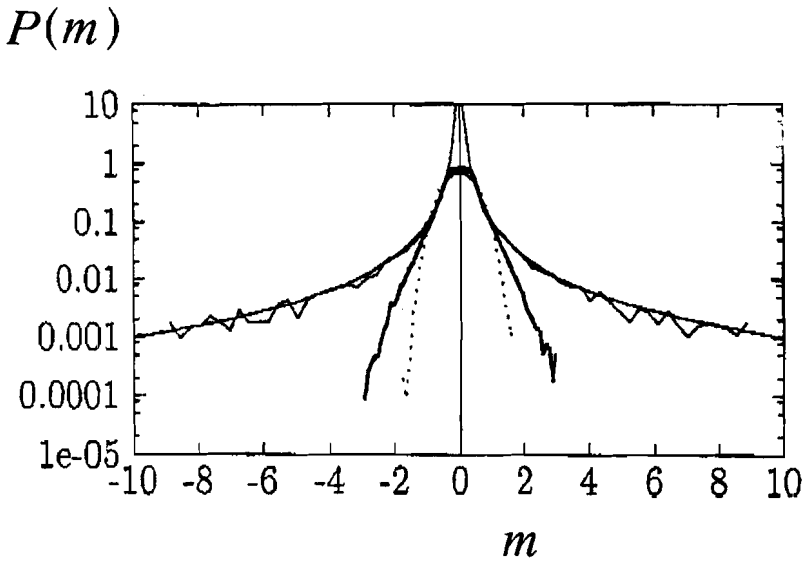

Fig.3.10 Semi-log plot of the steady-state probability density $P(m)$ in the long-ranged transport with $<m>=0$. Random perturbations in the range of [-1,1] are added constantly (the sum of perturbations are controlled to keep zero). The parameters are $\theta=0.3$ (dotted line), $\theta=0.8$ (bold line) and $\theta=0.99$ (thin line). The smooth curves show the Lorentzian tails, $P(m) \propto m^{-2}$ [*H. Takayasu and Y-h. Taguchi* (1993)].

For one-dimensional case of $<m>=0$ with no injection the variance converges quickly to zero as predicted by the mean-field analysis in Eq.(3.2.8), however, when we add injection of $<I>=0$ the variance $<m(t)^2>$ does not converge to a finite value but shows a tendency to diverge. This strange behavior may be caused by the peculiarity of one-dimension like it happens in the segregation

phenomenon [*L. W. Anacker and R. Kopelman* (1987); *K. Lindenberg, B. J. West, and R. Kopelman* (1988)], but the details are yet to be clarified.

It is confirmed numerically that in both cases, the mean-field and one-dimension, satisfying $<m>=0$, the distribution of m converges if it is normalized by the square root of the variance, $<m(t)^2>^{1/2}$. The functional form of the normalized distribution is very similar to that in Fig.3.10, namely, it is close to a Gaussian for small θ, the tails become larger for larger θ, and for θ very close to 1 the tails nearly follow power-laws.

Let us summarize the essence of the model of random transports. We observe the behavior in one-dimension with nearest neighbor transports for $<m>\neq 0$. In the limit $\theta \to 0$ Gaussian distribution is obtained. In the other limit $\theta \to 1$ a power-law tail is observed. And in the case $\theta = 1$, the model become equivalent to Scheidegger's river model with no injection. For $0<\theta<1$, neither a Gaussian nor a power-law distribution is obtained.

For the cases $<m>=0$ with $<I>=0$ injection we have no steady-state in one-dimension. But from the numerical simulations it is confirmed that it exists in the case of $<I>=0$ if we assume a long-ranged transport. The result in the limit of $\theta \to 1$ gives a distribution of m with power-law tails with exponent equivalent to that in Scheidegger's river model with pair-creation injection.

3.3 Scheidegger's model of mass-dependent random walk

Recently, *T. Nagatani* (1992) extended the basic Scheidegger's river model assuming that a heavier particle moves slower than a lighter particle. In such a system the mass distributions are obtained numerically and dynamic scaling behavior of the mass distribution is estimated.

The model is described as follows: Let a massive particle on one-dimensional lattice move to the right neighbor or left neighbor randomly with probability $p/2$, respectively, and it remains on its own site with probability $1-p$. In order to take into account that a heavy particle move slowly, we set the probability p , which can be considered as mobility, as $p = m^{-\gamma}$ ($\gamma>0$). In a time step particles move randomly following the above probabilities and merge when two or more particles encounter at the same site. Beside, a unit mass is added to each site at each time step. It is clear that $\gamma=0$ corresponds to the basic Scheidegger's river model.

The stochastic process of aggregation of this model can be expressed by the same equation as that of the basic Scheidegger's river model in Eq.(2.1.1):

$$m(j, t+1)=\sum_{k} W_{jk}(t)m(k, t) + I(j, t) \quad , \tag{3.3.1}$$

where $I(j,t)$ denotes the charge of a particle injected at the j-th site at time t, and $W_{jk}(t)$ is a random variable which is equal to 1 when the particle on the k-th site jumps on the j-th site and is equal to zero otherwise. Since one particle cannot go to two different sites in a single time step, $W_{jk}(t)$ must be normalized: $\sum_j W_{jk}(t)=1$. But

$W_{jk}(t)$ takes different weights of probabilities than in Scheidegger's river model, such as,

$W_{j,j}(t)=1$ with probability $1-p$,
$W_{j,j-1}(t)=1$ with probability $p/2$
$W_{j,j+1}(t)=1$ with probability $p/2$
$W_{jk}(t)=0$ for $k \neq j-1, j, j+1$.

The computer simulations are performed on a triangular lattice with the periodic boundary condition. Fig.3.11 shows examples of space-time trajectories obtained for $\gamma=0.5$ and 1.0. Comparing these figures with that of the basic Scheidegger's river model in Fig.2.3, we find that as γ takes larger value, trajectories of particles are apt to going straight downward.

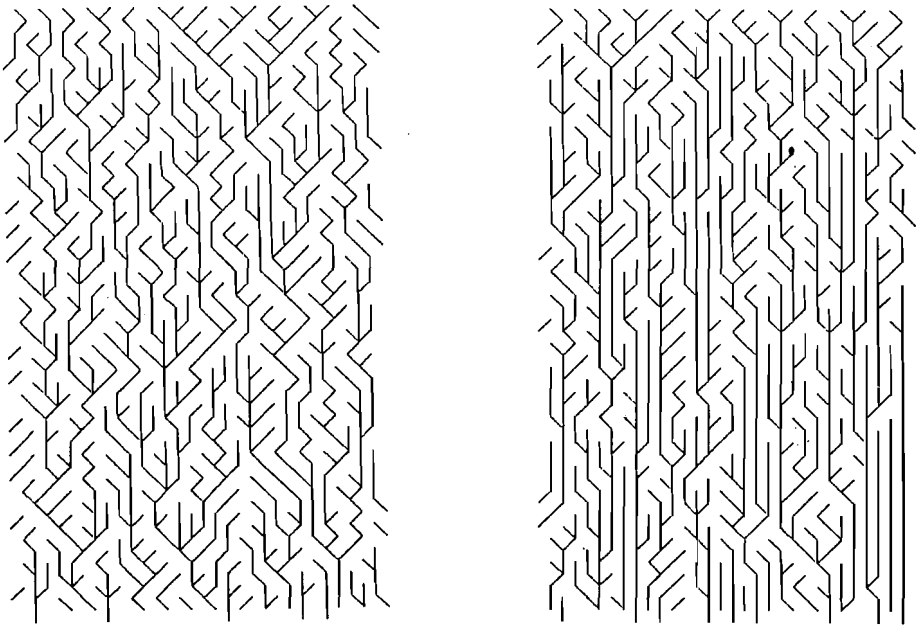

Fig.3.11 Examples of space-time trajectories for $\gamma=0.5$ on the left and $\gamma=1.0$ on the right [*T. Nagatani* (1992)].

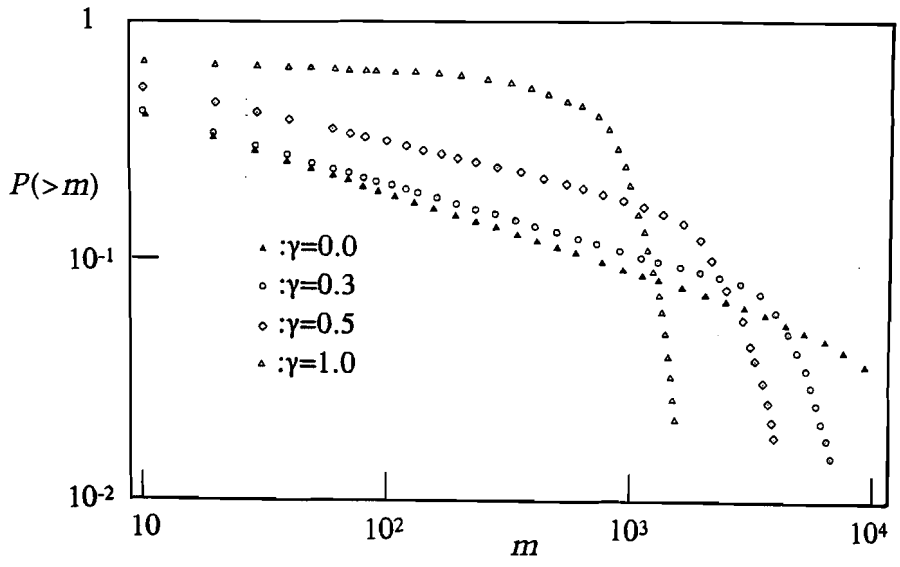

Fig.3.12 A log-log plot of the cumulative mass distribution for γ=0, 0.3, 0.5 and 1.0, and the slopes are 0.33, 0.26, 0.17, 0.04±0.02, respectively [*T. Nagatani*(1992)].

Fig.3.12 shows the cumulative mass distributions for γ=0, 0.3, 0.5 and 1.0 on log-log scale. It is clear from the figure that the mass distribution can be expressed in the form

$$P(>m) \propto m^{-\beta(\gamma)}. \tag{3.3.2}$$

In the case of γ=0 we can confirm that the slope is the same as the basic Scheidegger's model, 1/3. As the value of γ becomes greater the absolute value of the slope becomes smaller gradually converging to a slope equal to zero.

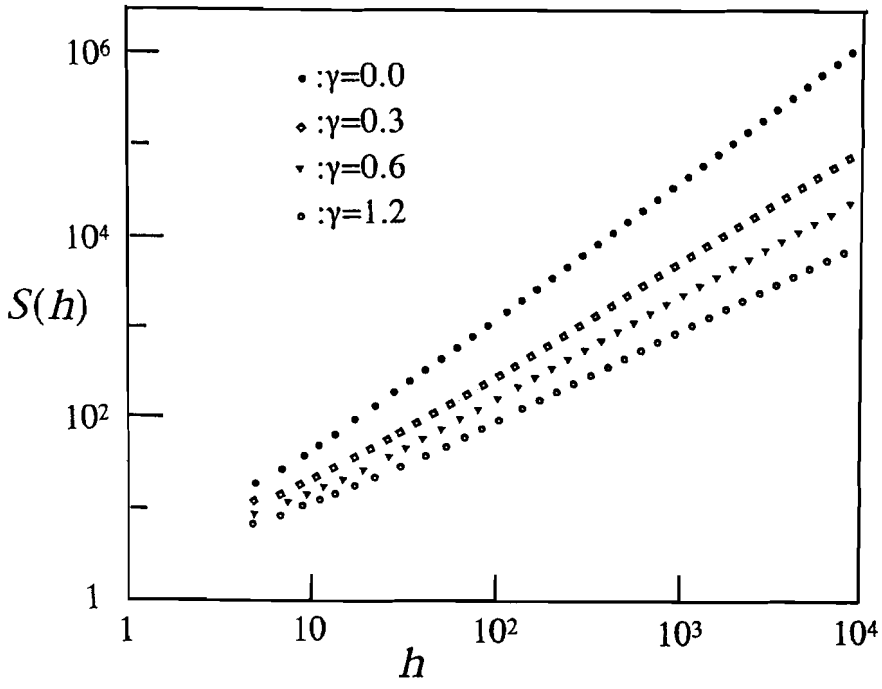

Fig.3.13 A log-log plot of the area of the drainage basin, S, vs. height, h, for γ=0, 0.3, 0.6, and 1.2 [*T. Nagatani* (1992)].

Let us consider a space-time trajectory forming a particle (see Fig.2.9). Like in the case of the basic Scheidegger's model, mass of the particle is again proportional to the area of its drainage basin in the space-time (see section 2.4.1 for more details). What is different from the basic Scheidegger's model is that the area of the drainage basin, S, can not be estimated by using the theory of random walks.

In such a case let us assume the following relation between the area S and the height h.

$$S \propto h^{z(\gamma)} . \tag{3.3.3}$$

This is a natural extension since it includes the case of the basic Scheidegger's river model, in which $z(0)=3/2$ [*H. Kondoh, M. Matsushita, and Y. Fukuda* (1987); *H. Takayasu, I. Nishikawa, and H. Tasaki* (1988)]. Eq.(3.3.3) can be regarded as a dynamic scaling because it can be recognized as an equation evaluating the mean mass of particles after h time steps.

The assumption (3.3.3) is confirmed numerically for $\gamma = 0$, 0.3, 0.6, and 1.2 in Fig.3.13. The exponent $z(\gamma)$ changes continuously from 1.50 (the value for the basic Scheidegger's river model) to 1.0 (the value for a linear river) with increasing γ.

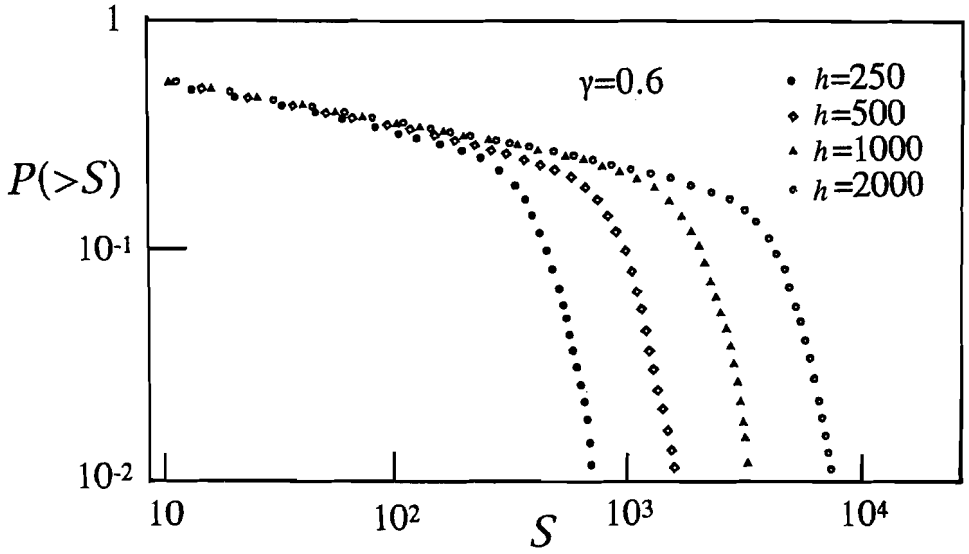

Fig.3.14 A log-log plot of cumulative mass distribution $P(>S)$ depending on the number of time steps h, h=250, 500, 1000, and 2000 for $\gamma=0.6$ [*T. Nagatani* (1992)].

In Fig.3.14 we plot mass distributions obtained for different number of time steps. We observe the tail of the curve extends according to the time steps. The mass at which the rapid decay is observed (at the larger mass range) is estimated from Eq.(3.3.3) to be proportional to $h^{z(\gamma)}$. Therefore, we propose a dynamic scaling relation as follows.

$$P_S(h) \propto S^{-\beta(\gamma)-1} f(S/h^{z(\gamma)}), \tag{3.3.4}$$

where $P_S(h)$ denotes the mass distribution depending on the time step h. From the numerical simulations Eq.(3.3.4) is confirmed for four different values of γ. The scaling function $f(x)$ is approximately a constant for $x \ll 1$ and decays faster than power-law for $x \approx 1$. Fig.3.15 shows a log-log plot of $S^{\beta(\gamma)} P_{>S}(h)$ vs. $S/h^{z(\gamma)}$ for $\gamma=0.6$.

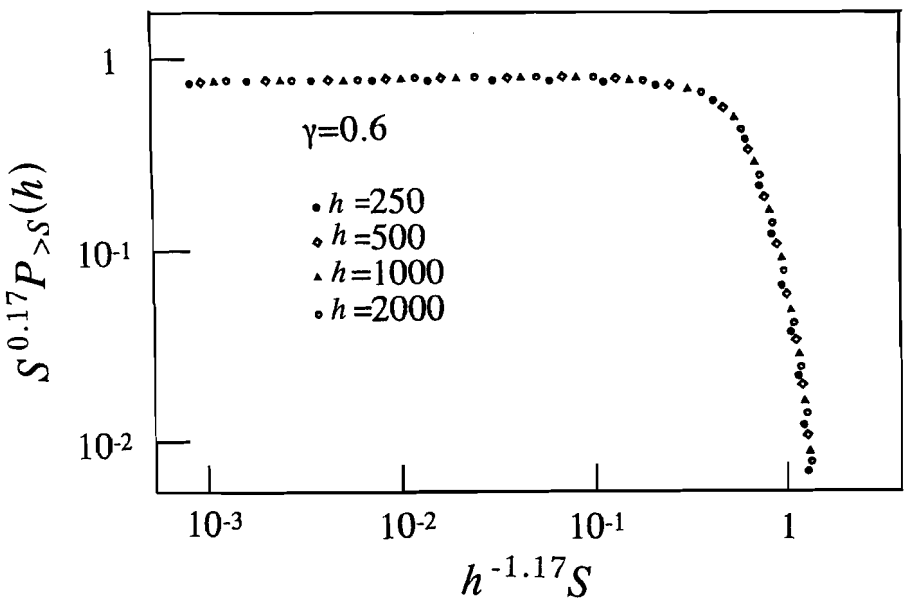

Fig.3.15 A log-log plot of the scaled cumulative mass distribution $S^{0.17} P_{>S}(h)$ vs. $h^{-1.17} S$ for $\gamma=0.6$ [*T. Nagatani* (1992)].

Since the total mass of particles in the system is proportional to the whole space-time, it is proportional to the time-step h.

$$\int_1^\infty P_S(h)SdS \propto h \quad . \tag{3.3.5}$$

Calculating the total mass by using the scaling relation as in Eq.(3.3.4), we get

$$\int_1^\infty P_S(h)SdS \propto h^{(1-\beta(\gamma))} \int_{h^z}^\infty x^{-\beta(\gamma)} f(x)dx \quad . \tag{3.3.6}$$

Comparing Eqs.(3.3.5) and (3.3.6), the following relation between exponents is derived.

$$[1-\beta(\gamma)]z(\gamma) = 1 \quad . \tag{3.3.7}$$

The exponents $\beta(\gamma)$ and $z(\gamma)$ for different γ are shown in Table 3.I. We find that the relation (3.3.7) holds nicely.

Table 3.I Exponents $\beta(\gamma)$ and $z(\gamma)$ for different γ. The errors for the exponents $\beta(\gamma)$ and $z(\gamma)$ are about ±0.02 [*T. Nagatani* (1992)].

γ	0.0	0.3	0.6	1.2
β	0.33	0.26	0.17	0.02
z	1.50	1.29	1.17	1.01

Chapter 4

Spatial correlation

4.1 Subtle spatial correlation in Scheidegger's river model

In chapter 2, we have seen that the exponents of the steady state distributions of Scheidegger's model are different in the one-dimensional cases and in the mean-field cases (except for the case of pair-creation injection). This difference indicates the importance of spatial restriction in the one-dimensional case. In this section we investigate the nature of spatial fluctuations observed in one-dimensional Scheidegger's model in order to clarify the spatial correlation in the system.

As we mentioned in chapter 2, the mass(charge) distribution of the basic model in one-dimensional space is equal to the distribution of the river size in (1+1)-dimensional space-time, while a river size is defined as the area of a drainage basin. Let us recollect Fig.2.4, which shows the ridges of the drainage basins. From the figure we find that two big drainage basins are less likely to exist adjacently than a big basin next to a small one. This gives an intuitive perception that the system has some kind of spatial correlation by which reducing the probability of two big basins come closer.

Let us see that if we can find anything about correlation from our previous analysis using the characteristic function. From the steady-state equation, Eq.(2.3.3), we can show that $Z_r(\varrho)$ can be expanded in the vicinity of $\varrho=0$ as

$$Z_r(\varrho) = 1 - c_1 r\,|\varrho|^{\beta} + \cdots \quad , \tag{4.1.1}$$

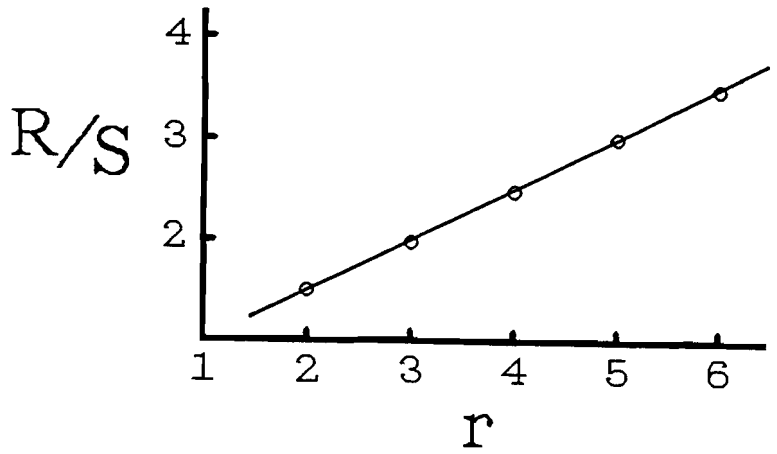

Fig.4.1 R/S diagram in log-log scale of base 2. The abscissa r gives the length of intervals. The slope of the straight line is 0.5.

where c_1 is a constant and β is either 1/3, 1/2, 2/3, or 1 depending on the spatial dimension and injection type. If the distribution is spatially independent, $Z_r(\varrho)$ should be equal to $[Z_1(\varrho)]^r$, however, it is easy to prove that these two expressions are identical only up to order ϱ^{β}, and there is a nonvanishing term of order $\varrho^{2\beta}$ as [*M. Takayasu* (1992)]

$$Z_1(\varrho)^r - Z_r(\varrho) = \frac{r(r-1)}{2}(c_1)^2\varrho^{2\beta}+\cdots \neq 0 \quad . \tag{4.1.2}$$

Therefore, we can conclude that there really exists spatial correlation. However, it is not easy to detect this correlation numerically because it is in higher order in ϱ.

R/S analysis [*J. Feder* (1988)] is one of the powerful method to find out correlation in singular fluctuations. In this method, we observe two quantities, R and S : R is the difference between the maximum and minimum of accumulated values in an interval, and

S is the variance in the same interval. So-called R/S diagram is obtained by plotting logarithm of the ratio R/S as a function of logarithm of the interval's length. In Fig.4.1 the R/S diagram of our model is shown. The points are clearly on a straight line of gradient 0.5, namely, $R/S \propto r^H$, where the Hurst exponent, H, is equal to H=0.5 which is identical to the value for the Brownian motion[*B. B. Mandelbrot* (1982)]. Hence H=0.5 means that the fluctuation has no dependency, which shows that the subtle correlation has been completely overlooked by this method.

The first reason that makes difficulties in analyzing the correlations is that it is a weak correlation which appear in higher order in ϱ as we saw in Eq.(4.1.2). The other reason is that the mass distribution follows a power-law for which the moments of the mass distribution diverge. In such a case, it is impossible to calculate the correlation function defined by the second order moments such as $<m(0, t)\cdot m(j, t)>$. Nevertheless, we can avoid this divergence by modifying the definition of the correlation function by introducing fractional moments. We show the details in the following sections.

The correlation function of the system is related to the power-spectrum by Wiener-Khinchin's theorem. However, in our model, due to the divergence of correlation function we cannot observe the correlation by power-spectrum as well. Namely, the power-spectrum of the mass configuration looks the same as in the case of white noise because a site having the largest mass acts as a delta function, and the Fourier transformation gives the same contribution at all wave numbers. Let us see how the multifractal analysis work for this problem in the next section.

4.2 Multifractal analysis

The term "Multifractality" was introduced in order to classify the fractal systems whose structures are characterized not only by a single singularity but also by an infinite number of singularities of infinitely many types. If we pay attention to a set of points on the structure corresponding to a given type of singularity, it typically forms a fractal subset whose dimension depends on the type of singularity.

The notion of multifractality was first introduced by *B. B. Mandelbrot* (1974) in connection with turbulence. Then it was developed and systematized by *H. G. H. Hentschel and I. Procaccia* (1983), and *R. Benzi et.al* (1984). Subsequently, it was discovered in percolation [*L. de Arcangelis et.al* (1985)], growth phenomena [*P. Meakin et.al* (1985)], dynamical system [*T. C. Halsey et.al* (1986)], and so on.

Now, we apply the idea of multifractality to our one-dimensional basic model. Let us divide the lattice (here, we are considering a finite size lattice) into intervals of length r and let $p_i(r)$ denote the normalized mass(charge) in the i-th interval, that is, the mass in the interval divided by the total mass of the whole finite system. Then in the limit $r \to 0$, we assume that the strength of the local singularity of i-th interval is characterized by introducing an exponent α_i as follows;

$$p_i(r) \propto r^{\alpha_i} \quad . \tag{4.2.1}$$

Namely, α_i denotes the local mass exponent. We consider the situation that α_i differs from one interval to another. In general,

the number of intervals taking the exponent between α and $\alpha+d\alpha$, $N(\alpha)d\alpha$, is expected to be scaled with r as

$$N(\alpha)d\alpha \approx r^{-f(\alpha)} n(\alpha)d\alpha \quad , \tag{4.2.2}$$

where $n(\alpha)$ denotes a constant value depending only on α, and $f(\alpha)$ is the fractal dimension of subset of intervals characterized by the local exponent α_i equal to α. The function $f(\alpha)$ is the key in the study of multifractalities.

We need a little preparation before introducing the method to get the function $f(\alpha)$. Let us introduce a fractal dimension called the information dimension, D_I, which is defined by the information entropy, $I(r)$, as;

$$D_I = \lim_{r \to 0} \frac{I(r)}{\log(1/r)} \quad , \tag{4.2.3}$$

where,

$$I(r) \equiv -\sum_i p_i(r) \cdot \log p_i(r) \quad , \tag{4.2.4}$$

and

$$\sum_i p_i(r) = 1 \quad .$$

The definition of the information entropy can be extended by considering higher order moments, such as

$$I_q(r) \equiv \frac{1}{1-q} \log \sum_i p_i(r)^q \quad . \tag{4.2.5}$$

The corresponding generalized q-th order dimension (we introduce D_q as a "dimension" although at the end of this section we show that it does not really have the physical Sense of "dimension") defined as

$$D_q = \lim_{r \to 0} \frac{I_q(r)}{\log\ (1/r)} \quad . \tag{4.2.6}$$

$I_q(r)$ is often called the q-th order Rényi information[*A. Rényi* (1970), *H. G. H. Hentshcel and I. Procaccia* (1983)] and we can easily show that $I_1(r)$ coincides with the usual information entropy defined by Eq.(4.2.4).

From Eqs.(4.2.1) and (4.2.2), we can replace the sum in logarithm in Eq.(4.2.5) by the following integral;

$$\sum_i p_i(r)^q = \int d\alpha\ n(\alpha)\ r^{-f(\alpha)+q\alpha} \quad . \tag{4.2.7}$$

In the limit $r \to 0$, the integral will be dominated by the value of α which minimizes the exponent. This leads to the conditions

$$\frac{df(\alpha)}{d\alpha}\Big|_{\alpha_q} = q \quad , \qquad \frac{d^2 f(\alpha)}{d^2 \alpha}\Big|_{\alpha_q} < 0 \quad , \tag{4.2.8}$$

where α_q is the value of α for which $q\alpha - f(\alpha)$ is minimal. So that, Eq.(4.2.7) is estimated as

$$\sum_i p_i(r)^q \approx n(\alpha_q)\ r^{-f(\alpha_q)+q\alpha_q} \quad . \tag{4.2.9}$$

Therefore, we are able to relate the problem of obtaining the function $f(\alpha)$ to the problem of observing $\sum_i p_i(r)^q$ by the following relations:

$$D_q = \frac{1}{q-1}\{q\alpha_q - f(\alpha_q)\} \quad , \tag{4.2.10a}$$

$$f(\alpha_q) = q\alpha_q - (q-1)D_q \quad , \tag{4.2.10b}$$

$$\alpha_q = \frac{d}{dq}\{(q-1)D_q\} \quad . \tag{4.2.10c}$$

$f(\alpha_q)$ is called f-α spectrum. In the case that $q=1$, $q\alpha_q - f(\alpha_q)$ should be zero otherwise the conservation of probability, $\sum p_i(r)=1$, will break up. So that, at $q=1$, f-α spectrum is tangent to the line $f(\alpha_q)=q\,\alpha_q$. From Eq.(4.2.10a), the maximum of f-α spectrum is always given at $q=0$. And for an ideal fractal with perfect self-similarity, f-α spectrum becomes a single point since the local singularities on whole space are characterized by one exponent .

We made numerical simulations of our model on 2^8 sites and adopted the data at the 5000th time step to f-α spectrum. Statistical average was taken over 10 realizations. In Fig.4.2 we plotted r vs $Q \equiv [\sum_i p_i(r)^q]^{1/(q-1)}$ for several different q 's, so that we can estimate the value D_q from the slope if we can define the linear part of such plots. Nevertheless, except for the models which are rigorously defined as multifractals, most of the stochastic models and the real systems do not show perfect linearity in such plots. Indeed, as we see in Fig.4.2 points do not fall on straight lines. In such a case, we discuss the following two methods to estimate D_q.

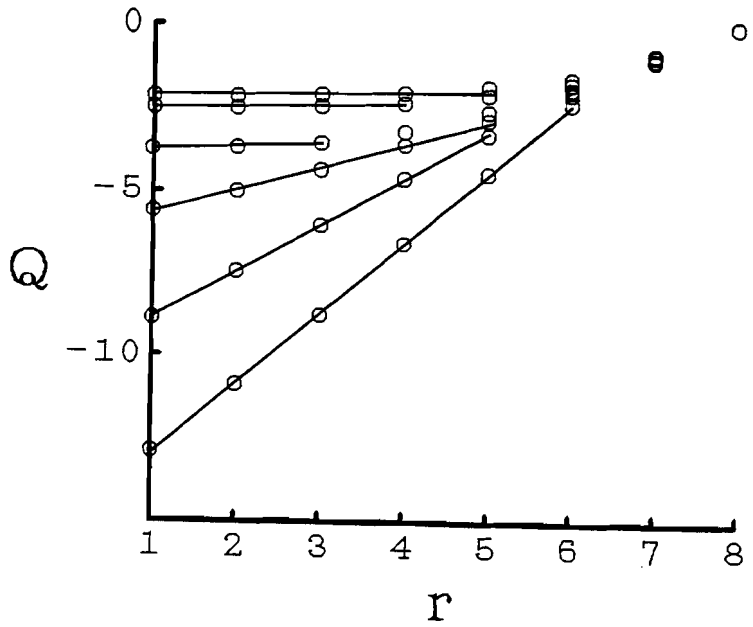

Fig.4.2 $Q \equiv [\sum_i p_i(r)^q]^{1/(q-1)}$ vs. r in log-log scale of base 2. q = 5, 2, 0.5, 0.2, -0.3 and -1.5, from top to bottom. The slope of each line gives $[q\alpha - f(\alpha)]/(q-1)$.

The first method is to approximate the r vs $Q \equiv [\sum_i p_i(r)^q]^{1/(q-1)}$ plot by its local slopes, so that we define D_q as a function of r. This approach seems to be a little forceful since the theoretical supports of multifractal analysis are defined only in the vicinity of $r \to 0$. But once we face a digital experimental data we will have a difficulty in adopting a slope for $r \to 0$. From the study of such locally defined D_q, a strange result has been found by *H. Takayasu and T. Suzuki* (1991). They show that white noise can be characterized by an r-dependent parabolic f-α spectrum due to the finite size of the system. And for white power-law fluctuations an r-independent parabolic f-α spectrum is observed nearly for two decays of r. Also the f-α spectrum is tangent to a line $f(\alpha_q) = q\,\alpha_q$ since $\sum p_i(r) = 1$ is kept by the finiteness of the system. It is a remarkable fact that an

r-independent parabolic f-α spectrum is observed not only in a multiscaled system but also in a non-correlated monofractal system.

In order to avoid treating the finite size effect, there is another method to analyze D_q. Finite size effect becomes more effective for bigger r , therefore, we adopt a slope near r=0 for the value of D_q for an arbitrary q. This corresponds to the estimation of D_q in the vicinity of r=0 which can be regarded as an asymptotic result in continuous limit of the one-dimensional lattice. Let us apply this analysis to our data.

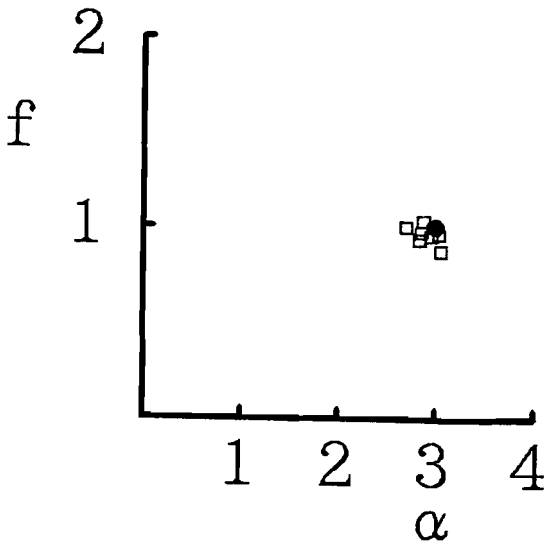

Fig.4.3 $f(\alpha)$-α diagram. Numerical results (square) and theoretical value for independent case (circle).

Analyzing Fig.4.2, we can say that for q<0.2 the estimated values of D_q change continuously with q. On the contrary, for q>0.5, D_q seems to have a constant value independent of q. It is likely that there exists a critical value for q between 0.2 and 0.5. The corresponding f-α spectrum is obtained from Eqs.(4.2.10b) and (4.2.10c), and is shown in Fig.4.3. All the points are located around

a single point $f=1$, $\alpha=3$. This result is natural since we know that the mass distribution in the model is rigorously characterized by a power-law exponent, not by multi-exponents. As we are estimating the results for continuous limit of a system following power-law, the conservation of the mass probability function is broken since $\sum_i p_i(r) \to \infty$. Consequently, the appearance of f-α spectrum is very different from the parabolic f-α spectra which are tangent to the line $f(\alpha_q)=q\ \alpha_q$. Next, we show that the single point f-α spectrum which we obtained from our model is comprehensible if we neglect any spatial correlations by using the notion of stable distribution [*M. Takayasu and H. Takayasu* (1989)].

As we mentioned in section 2.4.3 and Appendix (3), independent random variables which obey power-law distributions can be best approximated by stable distributions. Since we are considering the basic version of the model in which every site take only positive quantity(mass), we can assume that the size distribution for each site follows an independent one-sided stable distribution with the characteristic exponent, $\beta = 1/3$. From the basic property of stable distribution (see Appendix (3)) we have the following relation between the mass of a site, $m\ (1)$, and that of a sum of r sites, $m\ (r\ )$:

$$m\ (r\ ) \stackrel{d}{=} r^{\,1/\beta} m\ (1)\ , \qquad (4.2.11)$$

Where $\stackrel{d}{=}$ indicates that the distributions on both sides are identical. Taking the q-th power on both sides we have

$$m\ (r\ )^q \stackrel{d}{=} r^{\,q/\beta} m\ (1)^q\ . \qquad (4.2.12)$$

As $p_i(r)$ is proportional to m (r) by definition and the total number of intervals of size r is proportional to $1/r$, the left-hand side of Eq.(4.2.9) can be estimated as

$$\sum_i p_i(r)^q \propto r^{-1+q/\beta} \quad . \tag{4.2.13}$$

Comparing Eqs.(4.2.9) and (4.2.13) we get

$$-f(\alpha_q) + q\alpha_q = -1 + \frac{q}{\beta} \quad . \tag{4.2.14}$$

We note here that Eq.s(4.2.12)-(4.2.14) are valid only for $q < \beta$. For $q \geq \beta$ the qth-order moment of mass distribution $\langle m^q \rangle$ diverges because of the long tail. Consequently, the left-hand side of Eq.(4.2.13) does not have a definite value. Namely, for $q \geq \beta$ we cannot define D_q. This is consistent with the numerical results mentioned above and the critical value $\beta = 1/3$ is in the estimated range. The numerically observed value D_q=0 for q larger than the critical value may be an artificial value caused by the finiteness of numerical simulation. For example, if an exponentially large mass is concentrated on a single site, we may observe such behavior since $Q \equiv [\sum_i p_i(r)^q]^{1/(q-1)}$ is scaled by zero-th order power of r.

Eq.(4.2.14) agrees very nicely with numerically estimated values of $-f(\alpha_q) + q\alpha_q$ for $q < \beta$, and substituting Eq.(4.2.14) into Eqs.(4.2.10b) and (4.2.10c) we obtain the single point for the f-α spectrum:

$$\alpha_q = \frac{1}{\beta} = 3 , \quad f(\alpha_q) = 1 . \tag{4.2.15}$$

An intuitive explanation of Eq.(4.2.15) can be given as follows: From Eqs.(4.2.1) and (4.2.11) we can directly determine α_q as $\alpha_q = 1/\beta$ since $m\ (r\ ) \propto p_i(r)$. This result is applicable to any interval, so the number of elements summed in Eq.(4.2.9) is proportional to $1/r$. Therefore, we have the same result as Eq.(4.2.14). For the general D-dimensional analysis, we will have $\alpha_q = 1/\beta$ and $f\,(\alpha_q) = D$.

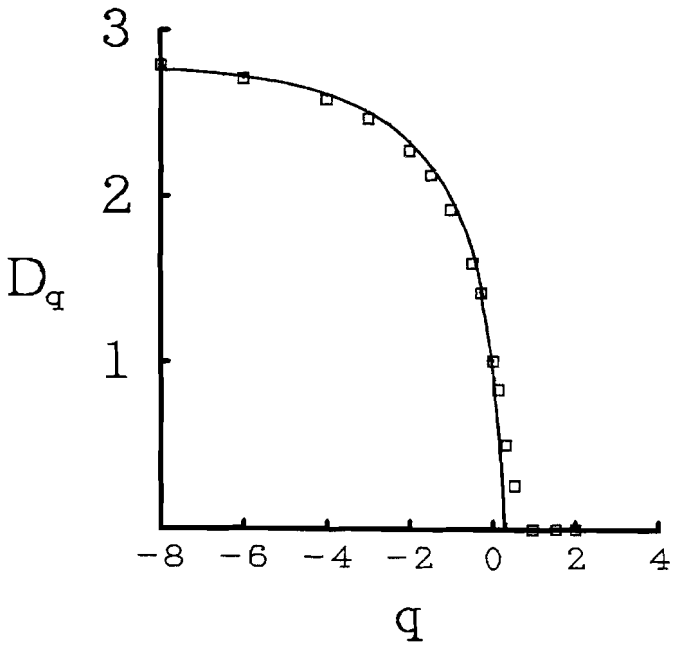

Fig.4.4 D_q - q diagram. Numerical results for the basic Scheidegger's river model(squares) and theoretical curve for the independent power-law distribution (solid line).

It is clear from the previous discussion that the property obtained by multifractal analysis holds when the mass distribution of each site is an independent power-law, which contradicts the fact that the correlation among sites really exists. Still more, we have another contradiction in our analysis. In Fig.4.4 we plotted the D_q-q diagram obtained for our model with squares and the theoretical

estimate for the independent case by a solid line. Though we are analyzing a monofractal system, which is indicated by the single point f-α spectrum, the diagram shows the existence of many different generalized dimensions D_q characterizing the system. From this inconsistency we conclude that the value D_q does not have a physical meaning of dimensions [*M. Takayasu and H. Takayasu* (1988); *B. B. Mandelbrot* (1988)].

4.3 Generalized correlation function

In the previous section we confirmed that the multifractal analysis can not detect the delicate spatial correlation in the basic Scheidegger's model. Therefore, in this section we return to the correlation function and we make an attempt to generalize the conventional definition to make it applicable to systems with diverging moments. Namely, we introduce a correlation function defined by fractional order cumulants. We will find that the weak correlation, which could not be observed by conventional methods; such as R/S analysis, power spectrum, and multifractal analysis, is observed numerically.

The divergence of the mean value and variance in mass distribution of Scheidegger's model can be explained in the following way. Assuming that the size distribution follows a power-law, $m^{-\beta-1}$, the statistical average of m^{α} is written as:

$$<m^{\alpha}> = \sum_{m=1}^{\infty} m^{\alpha} p(m) \propto \sum_{m=1}^{\infty} m^{\alpha-\beta-1} \quad . \tag{4.3.1}$$

For α which satisfies $\alpha < \beta$ the summation remains finite, however, it diverges otherwise. In this particular model, α should be smaller than 1/3 in order to avoid the divergence. Now, it is clear that the conventional correlation function cannot be defined. To control this divergence, we generalize the definition of correlation function as follows [*M. Takayasu* (1992)]:

$$C_{\alpha}(\xi) = \frac{<m(j+\xi)^{\alpha} m(j)^{\alpha}> - <m(j)^{\alpha}>^2}{<m(j)^{2\alpha}> - <m(j)^{\alpha}>^2} \quad , \tag{4.3.2}$$

where $C_1(\zeta)$ is the conventional correlation function. By this definition, $C_\alpha(\zeta)$ is observable for $\alpha < \beta = 1/3$ for the basic Scheidegger's model in one-dimension.

Fig.4.5a shows the values of $C_{0.01}(\zeta)$. Apparently, correlation can be seen for $\zeta = 1$, 2 and 3. The simulation is done on one-dimensional sites of size 1000 with 4000 time steps averaged over 10 different realizations. The negative values of correlation agree with the intuitive explanation that particles with large masses have less tendency to be located close to each other. The plot in Fig.4.5a is well approximated by exponential; $y(x) = exp(-1.3x)$.

Fig.4.5b shows the case of $\alpha=1$. In this case, it is obvious from our previous discussion that each average in the right hand side of Eq.(4.3.2) diverges if the system is infinite. In a finite system the results are a little different as the moments never take an actual infinite value. Nevertheless Eq.(4.3.2) behaves as having no correlation, and the obtained points are on the line of $C_1(\zeta)=0$ within the error bar. It is confirmed that $C_1(\zeta)$ calculated from data made by independent power-law distribution gives identical results with Fig.4.5b.

In case of negative values of α, the whole system looks entirely changed as the relative size of m is reversed; small values of m are emphasized and large values are diminished. In the limit of $\alpha \to -\infty$, the spatial sequence of $\{m^\alpha\}$ is composed of 1 or 0. $m\ (j, t)^\alpha$ takes 1 when neither the particle on the site j-1 nor j at time step t- 1 jumps to j, and it takes 0 otherwise. The probabilities of two adjacent sites taking the configurations (0,0), (0,1), (1,0), and (1,1) are obtained from the evolution rules as 1/2, 1/4, 1/4, and 0, respectively. And the probabilities of a site taking the value 0 is 3/4. Therefore, from Eq.(4.3.2), $C_{-\infty}(1)$ can be calculated as 1/3.

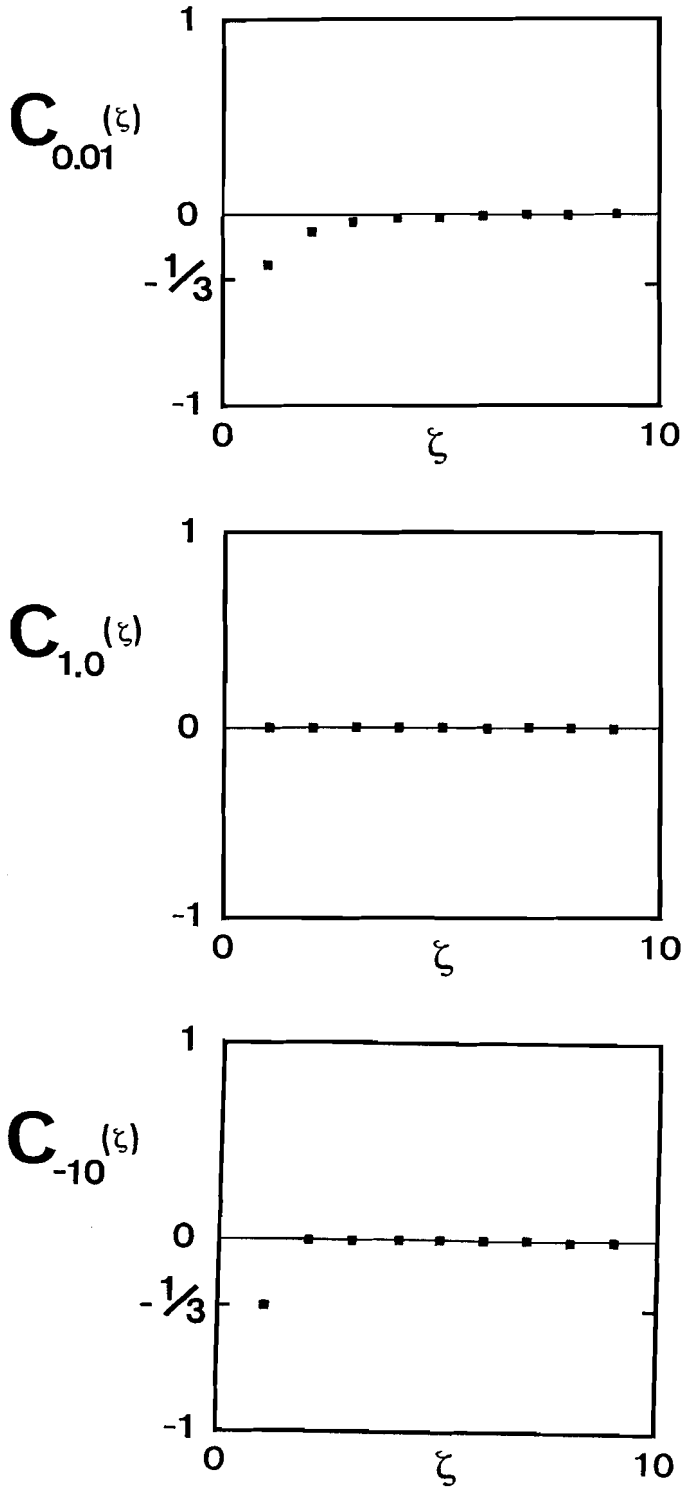

Fig.4.5a, b, c $C_\alpha(\zeta)$ vs. ζ for the Scheidegger's basic model. The error estimates are on the order of 10^{-2}, which are smaller than the size of the square points.

It is obvious that $C_{-\infty}(\zeta)=0$ for $\zeta \geq 2$, because the configuration at time step t is fully determined by the jumps between time step $t-1$ and t, since a particle can jump at most one site in one time step. As shown in Fig.4.5c the value of $C_{-10}(1)$ is very close to 1/3 and $C_{-10}(\zeta)$ for $\zeta \geq 2$ is nearly equal to 0, namely the characteristics of $\alpha=-\infty$ are realized by a relatively small absolute value, $\alpha=-10$.

Observing the behavior of $C_\alpha(\zeta)$ for different values of α, it is confirmed that non-trivial correlations are observable for $0<\alpha<1/3$. In this range of α the correlations always decay very quickly and practically no correlation can be detected for $\zeta \geq 5$.

Several authors have calculated non-integer moments in the study of random walks [*G. H. Weiss, S. Havlin, and O. Matan* (1989)], random resister networks [*L. de Arcangeles, S. Redner, and A. Coniglio* (1986), *P. Meakin, A. Coniglio, H. E. Stanley* (1986)], chaos[*P. Meakin and H. E. Stanley* (1988)], and diffusion limited aggregations [*H. G. E. Hentschel and I. Procaccia* (1983)] in order to discover multi-scaling relations. *A. P. Siebesma and L. Pietronero* (1988) show the relation between multifractal scaling and correlation function defined by fractional moments in the generalized Cantor set. Their analysis may be applicable to the mathematically rigorous multifractal models but it is suspicious whether the relation they obtained still holds in stochastic systems including our model. In fact, according to section 4.2, multifractal diagram of our model is identical to the one of an uncorrelated system, though the analysis using Eq.(4.3.2) shows correlation among sites.

In conclusion, the generalization of correlation function with non-integer α as in the form Eq.(4.3.2) enables us to observe the hidden spatial correlations which are subtle but effective enough to change the exponent of the mass distribution from that of the

mean-field case. Though we analyzed a very special example, the method is applicable to any other data. Especially, Eq.(4.3.2) with non-integer α will be powerful for the systems with power-law fluctuations.

4.4 Interval distribution of level set

We introduce a new approach to clarify the correlation in order to investigate a more vivid appearance of the spatial correlation in Scheidegger's river model. We will apply the new method not only for the mass configuration on one-dimensional lattice in Scheidegger's river model but also for the other irreversible systems having large or possibly infinite variance such as time series of earthquake magnitude and time series of energy dissipation rate in atmospheric turbulence [*M. Takayasu* (1992)].

4.4.1 IDL and its application to non-correlated systems

Distribution of gaps (the intervals between one incident and the next one) have been studied as a way of characterizing fractal properties of Cantor-sets and other sets of fractal dimension $D < 1$ [*B. B. Mandelbrot* (1982)]. It has been shown that the gap-size distribution for a fractal set follows a power-law, $P(r) \propto r^{-D-1}$, where $P(r)$ denotes the probability of finding a gap of size r. Power-law gap-size distributions are found not only in mathematical models but also in real systems such as the error occurrences in data transmission lines [*S. M. Sussman* (1963)].

The idea of examining gaps is applicable to fluctuations of a scalar quantity on 1-dimensional space by observing the level sets of intersections. Brownian trajectory in space-time coordinates is one of the examples whose gap-size distribution of the level set on the intersection of $x(t)=c$, (where c is a given constant), satisfies $P(r) \propto r^{-D-1}$ with $D=1/2$ [*W. Feller* (1966)]. As for fractional Brownian motion, the exponent D is known to be expressed as

$D=1-H$ where H is the Hurst exponent which takes a value between 0 and 1 [*B. B. Mandelbrot* (1982)].

D. ben-Avraham, M. A. Burschka, and C. R. Doering (1990) examine the inter-particle distributions (distribution of gaps between successive particles) in one-dimensional diffusion reaction model governed by a rule A+A→A. In the case when the process involves injection of particles at randomly chosen sites the system reaches a stationary state with indefinitely maintained non-zero concentration of particles. At the stationary state, the gap-size distribution shows a distinctive peak at a certain size of gap depending on the rate of injection and the diffusion coefficient.

In this section, we introduce a systematic way of investigating spatial or temporal correlations using the interval distribution of level sets (in short IDL). First, let us introduce the IDL analysis of one dimensional spatial or temporal data in general. For given discrete data, we set a threshold height Ec and pay attention only to the data points which have values higher than Ec (see Fig.4.6). The set of points chosen this way is called a level set and Ec is called a level. IDL is the size distribution of distances between nearest-neighbor elements of a level set like r_i shown in Fig.4.6. We observe IDLs with different Ec and try to scale them on a curve by considering Ec as a parameter. In that sense, the IDL curves obtained from different Ec are related to one another.

For the purposes of comparison with real data, we list the IDL of an uncorrelated white-noise system. The probability of finding an interval of length r, $Prob_{Ec}(r)$, can be estimated as follows for large r;

$$Prob_{Ec}(r) = p_{Ec}^2 (1-p_{Ec})^{r-1} \propto exp\ (r\ ln\ (1-p_{Ec})), \qquad (4.4.1)$$

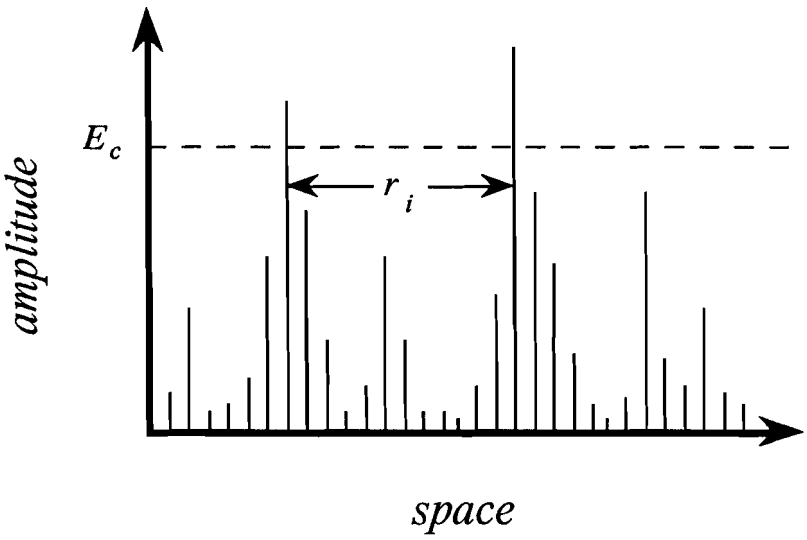

Fig.4.6 Definition of interval r_i of level Ec on one dimensional data.

where p_{Ec} denotes the probability that a chosen site is an element of the level set at level Ec . Eq.(4.4.1) shows that the IDL follows an exponential decay. An exponential probability distribution is fixed uniquely by the mean value of r , $\langle r \rangle_{E_c}$, as

$$Prob._{E_c}(r) = \frac{1}{\langle r \rangle_{E_c}} exp\ (-\frac{r}{\langle r \rangle_{E_c}}) . \qquad (4.4.1)'$$

By comparing Eqs.(4.4.1) and (4.4.1)', we can see that p_{Ec} is related to $\langle r \rangle_{E_c}$ as follows for $\langle r \rangle_{E_c} >> 1$:

$$p_{E_c} = 1 - exp\ (-\frac{1}{\langle r \rangle_{E_c}}) . \qquad (4.4.2)$$

D. ben-Avraham, M. A. Burschka, and C. R. Doering (1990) mentioned that in their one dimensional diffusion reaction model the interparticle distribution function at stationary state becomes

exponential when the reaction system includes the reverse process: A+A←A. This exponential distribution is explained by the maximum entropy principal since the system satisfies detailed balance as in the case of thermal equilibrium. Namely, in such reversible particle systems, particles are observed to behave independently.

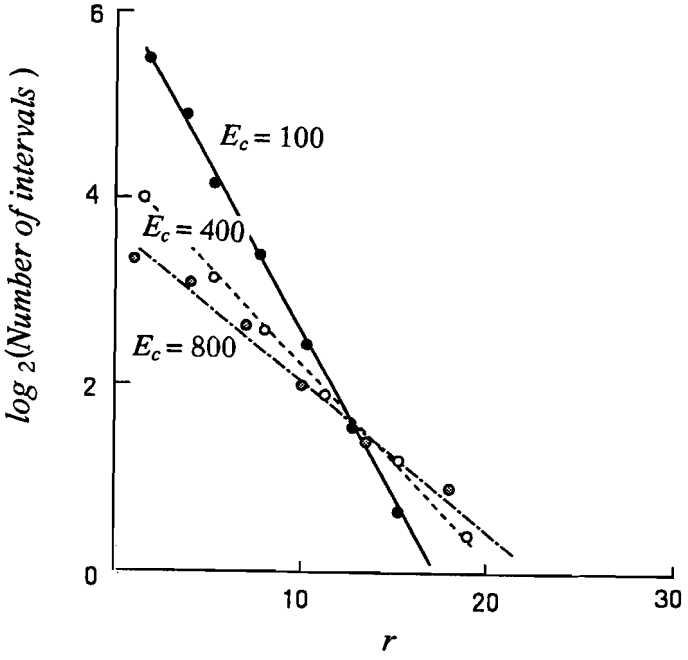

Fig.4.7 IDL of white power-law distribution in semi-log plot.

Fig.4.7 shows an IDL of a variable that obeys white power-law size distribution with exponent equal to -4/3. This corresponds to the case of non-correlated system with $p_{Ec} \propto E_c^{-\frac{1}{3}}$ in the above discussions since p_{E_c} is proportional to the cumulative size distribution of Ec. Total number of data points is 1000. We take an average over 20 realizations with three different Ec ; Ec =100, 400, and 800, the estimated values of slopes are Δ = 0.23, 0.14 and 0.11, respectively, while the slopes calculated from Eq.(4.4.1)' are

Δ =0.222, 0.137, and 0.108. We also confirm that Eq.(4.4.2) is approximately satisfied.

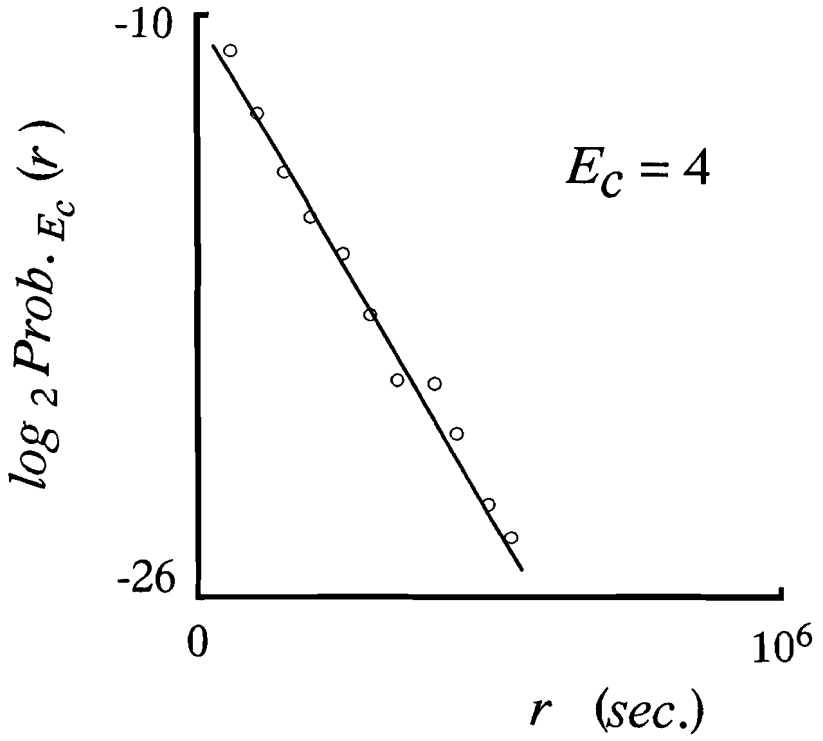

Fig.4.8 The dots show an IDL of real of real earthquake magnitude. The line shows corresponding exponential decay.

The dots in Fig.4.8 show an example of an exponential-like IDL observed in a time series of earthquake magnitudes with $Ec = 4$ which occurred in the Tohoku area in Japan from 1986 to 1989. The number of data points is 1362. The original time series data were published by the Japan Metrological Agency. The line shows an ideal exponential distribution with the same mean interval as the earthquake data. This result suggests that the time intervals between earthquakes with magnitudes greater than 4 occur almost

independently, which is consistent with the widely believed conjecture that time series of the main shock can be treated as a Poisson process. Recently, *Y. Y. Kagan and D. D. Jackson* (1991) claimed that the main shock occurrence is very close to a stationary Poisson process but weak clustering is observed, which forms a fractal set on the time axis with dimension D=0.8 to 0.9. Nevertheless, we cannot confirm it from our data. From the analysis of a numerical model of earthquake(a version of self organized criticality model), *J. Lomnitz-Adler, L. Knopoff, and G. Martinez-Mekler* (1992) report that the interval distribution has a clear peak and is very different from the exponential.

4.4.2 IDL of Scheidegger's river model

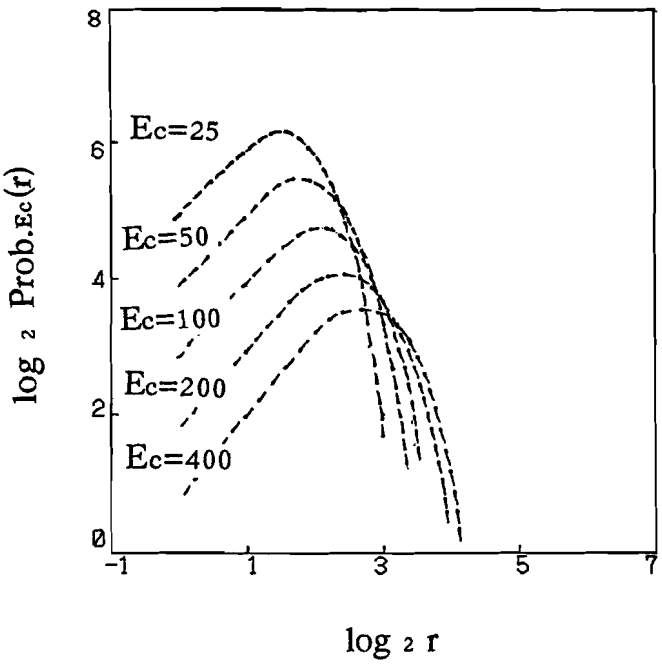

Fig.4.9 IDL of the basic Scheidegger's model for E_c=25, 50, 100, 200, and 400.

Now, let us apply IDL analysis to the subtle correlation in the basic Scheidegger's model, whose correlation cannot be detected by the following cases as we have seen in the preceding sections; R/S analysis, conventional correlation function, power-spectrum, and multifractal analysis. We are going to show that the IDL analysis is nevertheless effective in such a case.

IDL for the mass configuration in one-dimensional basic model shows a curve with a distinctive peak whose position depends on the level as shown in Fig.4.9. Namely, different level sets have different characteristic intervals and the appearance of IDL is obviously different from a non-correlated system shown in Fig.4.7.

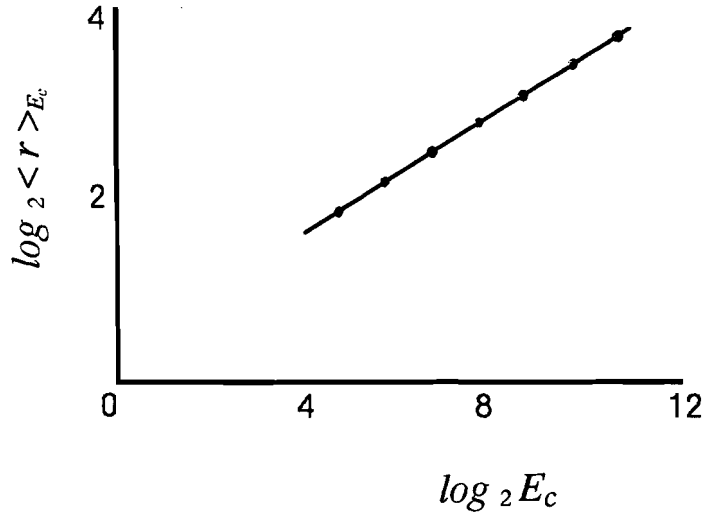

Fig.4.10 E_c vs. $<r>_{E_c}$ in log-log scale. The slope is estimated as 0.33.

The mean interval, $<r>_{E_c}$, is estimated as $<r>_{E_c} \propto E_c^{0.33}$ from the simulations(see Fig.4.10). This can be explained as follows: $<r>_{E_c}$ is

proportional to the inverse of p_{Ec} which is proportional to the number of sites having mass bigger than E_C , i.e, $p_{Ec} \propto E_c^{-\beta}$. So we have

$$\langle r \rangle_{Ec} \propto \frac{1}{p_{Ec}} \propto E_c^{\beta}, \tag{4.4.3}$$

where $\beta = 1/3$ for the basic model.

The curves for different E_C (E_C = 25, 50, 100, 200, and 400) are confirmed to be congruent(see Fig.4.9). As the value of E_C is doubled, the curve in the log-log plot shifts constantly both in horizontal and vertical directions. These curves can be scaled on a function as shown in Fig.4.11 by rescaling r and $Prob_{E_c}(r)$ as follows;

$$Prob._{E_c}(r) \propto E_c^{-2/3} f(r\, E_c^{-1/3}). \tag{4.4.4}$$

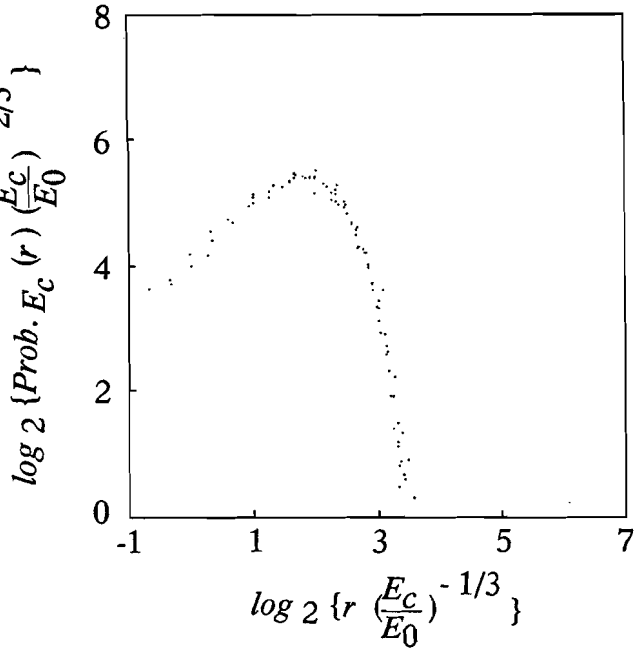

Fig.4.11 A scaling plot of IDL for the basic Scheidegger's model.

The scaling function, $f(\zeta)$, is estimated to be nearly proportional to ζ for $\zeta<1$ and it falls off faster than exponentially, as $f(\zeta) \propto \exp(-(\zeta-1)^{-2})$, for $\zeta>1$.

Scaling exponents in Eq.(4.4.4) can be obtained theoretically if we make the following scaling assumption [*T. Vicsek* (1989)]:

$$Prob._{E_c}(r) \propto E_c^{-\theta} f(r E_c^{z}) . \tag{4.4.5}$$

From the definition, p_{E_c} and $Prob._{E_c}(r)$ satisfy the following relation;

$$p_{E_c} = \int_1^{\infty} Prob._{E_c}(r)dr \propto E_c^{-\beta} . \tag{4.4.6}$$

Substituting Eq.(4.4.5) into Eq.(4.4.6) and taking into account that $E_C >>1$, we obtain

$$z - \theta = -\beta . \tag{4.4.7}$$

Also, by Eqs.(4.4.5) and (4.4.6) the mean interval, $<r>_{E_c}$, is given as

$$<r>_{E_c} \propto \int_1^{\infty} r \frac{Prob._{E_c}(r)}{p_{E_c}} dr = E_c^{z} \int_1^{\infty} \zeta f(\zeta) d\zeta \propto E_c^{z} . \tag{4.4.8}$$

Comparing Eq.(4.4.8) with Eq.(4.4.3) and using Eq.(4.4.7), we have $z = \beta = \frac{1}{3}$ and $\theta = 2\beta = \frac{2}{3}$ for the basic Scheidegger's model, which are consistent with the scaling exponents in Eq.(4.4.4).

4.4.3 IDL of turbulence

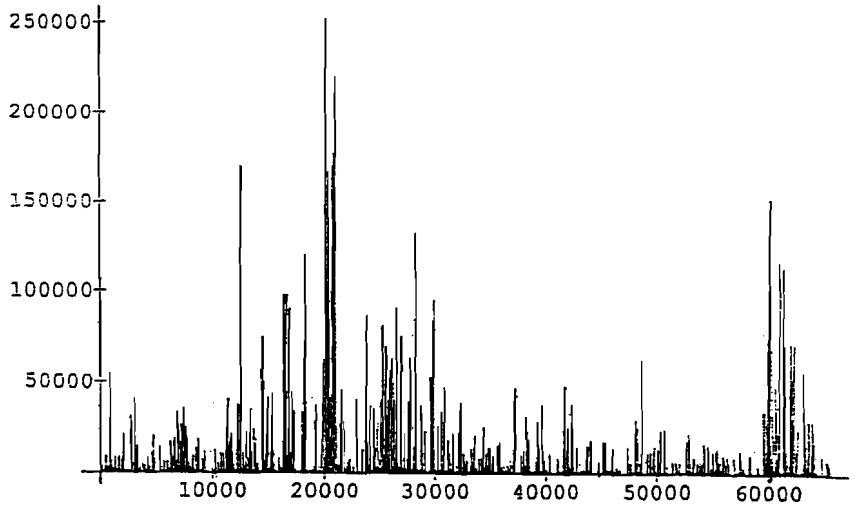

Fig.4.12 A time series of the square of velocity differences differences observed in the atmospheric turbulence.

IDL for turbulence in the atmospheric boundary layer is analyzed using data obtained by *M. Yamada and K. Ohkitani* (1991). The observation was done on a fine calm day at 2 meters above the roof of a 15 meters high building. The flow velocity was observed as signals from a hot wire anemometer at a sampling frequency 500Hz for over 3 minutes. The mean velocity $\langle v(t) \rangle$ is about 5.4 m/s and the variance $\sqrt{\langle (v(t) - \langle v(t) \rangle)^2 \rangle}$ is about 1.45 m/s. The Taylor's frozen hypothesis is considered to be valid at least for small-scale motion. The inertial range in the time scale is about 2^3 to 2^{10} (in the unit of Δt =1/500 sec.). The time series data of the square of velocity differences, $(\delta v(t))^2 = (v(t+\Delta t) - v(t))^2$, which is generally believed to be proportional to the energy dissipation rate, have violently fluctuating amplitudes as shown in Fig.4.12.

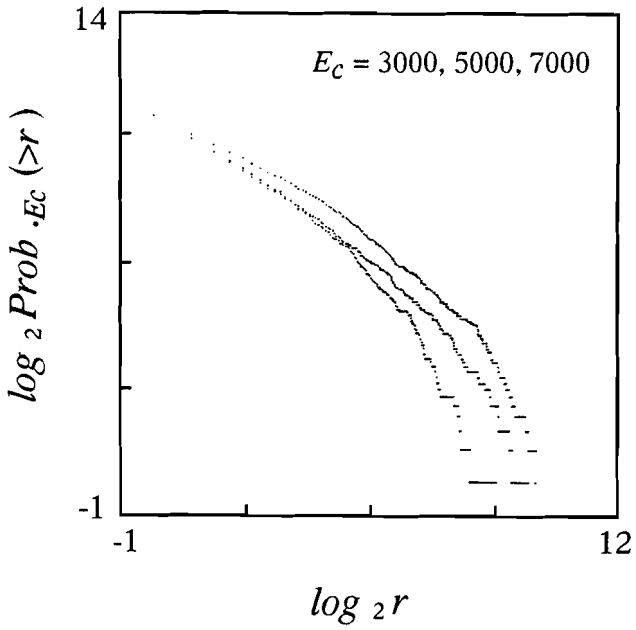

Fig.4.13 IDL of atmospheric turbulence for E_c=3000,5000, and 7000.

We observe the cumulative IDL in order to keep good statistics. The observed values of $(\delta v\ (t\ ))^2$ are in the range of $1\times10^{-2}\sim1\times10^{5}$. We set the threshold energy dissipation rate Ec as 3000, 4000, 5000, 6000, 7000 and 8000, and for each level 2000 points are observed(see Fig.4.13).

In Fig.4.14, we try to rescale the curves for different levels on the curve for Ec=3000 by using the following scale transformation;

$$r \rightarrow r\ (\frac{E_c}{E_0})^{1.5} 2^{-\alpha(E_c - E_0)}$$

$$Prob_{E_c}(>r\ ) \rightarrow Prob_{E_c}(>r\ )\, 2^{\beta(E_c - E_0)}, \tag{4.4.9}$$

where E_0 =3000, α=0.001, and β=0.00024. The line formed by dots in Fig.4.14 shows the rescaled measures for these levels in a log-log plot. We have to mention that the range of E_C showing a good fit is relatively small. For E_C >10000 and E_C <1000, rescaled measures do not overlap by the same transformation.

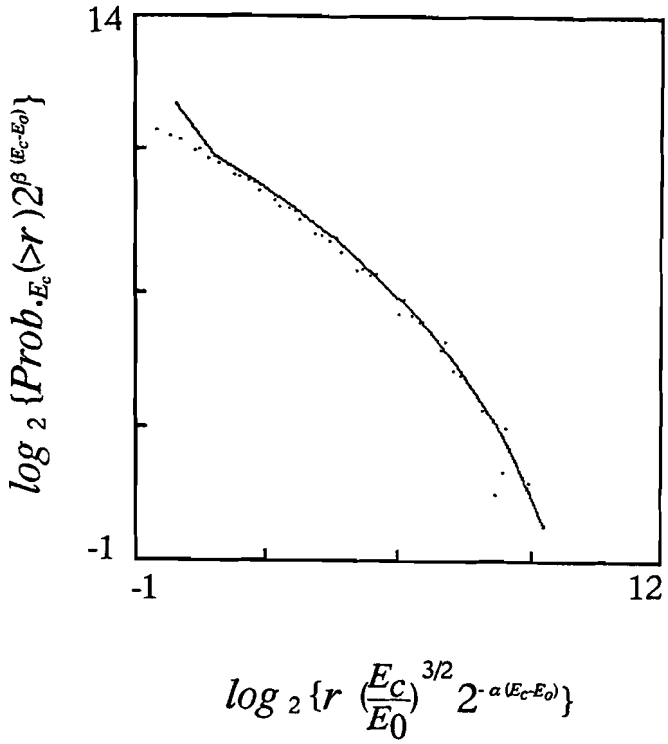

Fig.4.14 A scaling plot of IDL for atmospheric turbulence.

The above results for turbulence can be explained by assuming the multifractal structure [*C. Meneveau and K. R. Sreenivasan* (1987), (1991)]. Let us introduce a simple mathematical model called binomial multifractal measure.

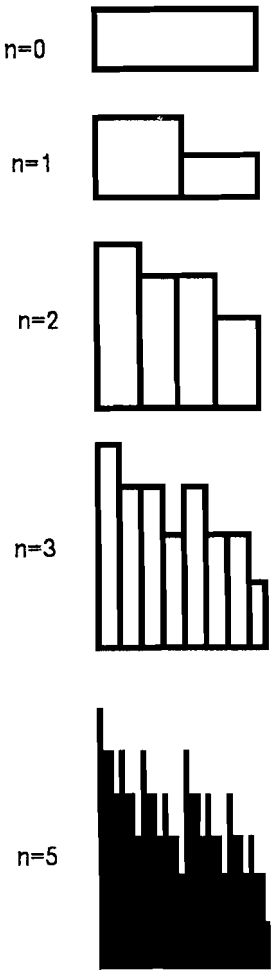

Fig.4.15

Binomial multifractal measure.

The binomial multifractal measure is constructed by spreading measure over the halves of every dyadic interval with the proportions b and $1-b$, where $0<b<1/2$ (see Fig.4.15). After n-times dyadic divisions we get 2^n small partitions with measures. The measure on x-th partition is given as $P(x) = b^{g(x-1)}(1-b)^{n-g(x-1)}$, where $g(x)$ gives the count of 1 which appear in the form of binary expansion of x [*J. Feder* (1988)]. Also $P(x)$ satisfies $\sum P(x)/2^n = 1$. In such a system, the spatial configuration consists of $n+1$ different values of $P(x)$.

Let us find some regularities hidden among a table showing the thresholds, the number of intervals, and its length (see Table 4.I). In the table we introduce a parameter τ instead of the threshold height Ec. This parameter τ shows the level presented by the order of heights such as $\tau=0$ for the highest and $\tau=1$ for the second and so on. In such a representation we find that the results do not depend on the portion b of the dyadic division. The table shows the number

of intervals satisfying the conditions of threshold τ (rows) and the length of interval in power of 2 (columns):

Table 4.I: The numbers of intervals for different lengths and thresholds.

	2^0	2^1	2^2	...	2^{n-5}	2^{n-4}	2^{n-3}	2^{n-2}	2^{n-1}	2^n
$\tau = 0$	0	0	0	...	0	0	0	0	0	1
$\tau = 1$	2	1	1	...	1	1	1	1	1	0
$\tau = 2$		n-2	n-3	...	4	3	2	1	0	0
$\tau = 3$		⋮	⋮		6	3	1	0	0	0
⋮			⋱		⋱	⋱	⋱	⋱	⋱	⋱

In this table the number of intervals of length 2^k for $\tau=\tau'$ is obtained by the sum of the number of intervals whose lengths are in the range of 2^{k+1} to $2^{n-\tau}$ for $\tau = \tau'$- 1. So that we can derive the following relations inductively, which are confirmed numerically up to n=30:

$$Prob._\tau(2^k) = N^{-1}\binom{n-k-1}{\tau-1}, \quad k \geq 1$$

$$Prob._\tau(2^0) = N^{-1}\left(2^n - \sum_{k=1}^{n-\tau} 2^k \binom{n-k-1}{\tau-1}\right), \quad k = 0 \tag{4.4.10}$$

,

where N is a normalization constant. The deviation at k=0 is due to the finiteness of the system. The line in Fig.4.14 shows the result of IDL according to Eq.(4.4.10). τ is chosen to give the same mean interval as the turbulence data for Ec =3000 , which is τ=5 for n=14. The turbulence and the binomial multifractal measure show a good fit, which indicates that the temporal structure of energy dissipation rate is very close to the binomial multifractal measure.

4.5 Conclusion

We analyzed the spatial correlation of Scheidegger's river model. The correlation is not easy to detect since the divergence caused by the singularity of power-law mass distribution disables the observations. We introduced two methods allowing to treat the divergence effectively. One is the generalized correlation which is defined by moments of fractional powers. The other is IDL analysis which succeeds in giving a clear picture of the spatial correlation. Nevertheless the model is essentially stochastic, the mass configuration on the lattice shows a distinct regularity, that is a particle with size larger than some value occupies a specified interval.

Concerned not only with our model but also with the other models involving violent fluctuations, let us discuss in more details the advantages of IDL analysis comparing to the conventional methods; R/S analysis, correlation function, power spectrum and f-α spectrum. In these conventional methods it is necessary to calculate the second or higher order moments. Sometimes errors are amplified in calculating such moments so that the results do not appear clearly; or, as in the case of the Scheidegger's river model, observing moments becomes meaningless since they are diverging. On the other hand, it is not necessary to calculate any moment to get IDL. Namely, we characterize fluctuations by focusing our attention on the distribution itself (not its moments).

Appendices

Appendix (1); Characteristic function

A characteristic function is defined by Laplacian or Fourier transformation of a distribution function, $p(m)$, such as

$$\Phi(\varrho) = \int_0^\infty p(m)\ e^{-m\varrho} d\, m \quad , \tag{A.1}$$

for a one-sided distribution ($p(m)=0$ for $m < 0$), and

$$\Phi(\varrho) = \int_{-\infty}^\infty p(m)\ e^{-im\varrho} d\, m \quad , \tag{A.2}$$

for a both-sided distribution. In the case that any order of moment is convergent the characteristic function can be expanded as follows;

$$\Phi(\varrho) = \sum_{k=0}^{\infty} <m>^k \frac{(-1)^k \varrho^k}{k\ !} \quad , \tag{A.1)'}$$

for a one-sided distribution, and

$$\Phi(\varrho) = \sum_{k=0}^{\infty} <m>^k \frac{(-i\ )^k \varrho^k}{k\ !} \quad , \tag{A.2)'}$$

for a both-sided distribution.

It is convenient to introduce a characteristic function when we are focusing on the distribution for the sum of independent variables, $\{m_j\}$. Let us show how the characteristic function works

for such a case. Let us consider distributions for two independent variables, m_1 and m_2, following the distribution function, $p(m_1)$ and $p(m_2)$, respectively. The distribution for $M = m_1 + m_2$ can be expressed as follows:

$$p(M) = \int_0^\infty dm_1 \int_0^\infty dm_2 \, p(m_1) \, p(m_2) \, \delta (M - m_1 - m_2) \quad . \qquad \text{(A.3)}$$

By performing Laplacian transformation on both sides of the equation, we get the following simple relation;

$$\Phi_2(\varrho) = \int_0^\infty dm_1 \int_0^\infty dm_2 \, p(m_1) \, p(m_2) \, e^{-(m_1+m_2)\varrho}$$

$$= \Phi (\varrho)^2 , \qquad \text{(A.4)}$$

where $\Phi_n(\varrho)$ denotes an n-body characteristic function; the characteristic function for the sum of n variables.

In general, the characteristic function $\Phi (\varrho)$, by definition, satisfies one of the following three criteria [*E. Lukacs* (1970)]:

(i) $|\Phi (\varrho)| < 1$ for all ϱ, except for $\varrho = 0$,
(ii) $|\Phi (\varrho)| = 1$ for all ϱ,
(iii) $|\Phi (\varrho)| = 1$ for countably many ϱ, and $|\Phi (\varrho)| < 1$ for the rest.

The second case (ii) corresponds to a completely degenerate distribution, *i.e.*, the distribution function is represented by a δ-function,

$$p(I) = \delta (I - I_0) \quad , \tag{A.5}$$

The third case corresponds to distributions degenerate at periodic points, *i.e.*,

$$p(I) = \sum_{j=-\infty}^{\infty} a_j \, \delta (I - jI_0 - I_1) \quad , \tag{A.6}$$

where I_0 and I_1 are constants and $\{a_j\}$ satisfy the normalization condition $\sum_j a_j = 1$ and $a_j \geq 0$. All other distributions belong to the first case (i).

Appendix (2); Continued fraction CAM

M. Suzuki (1986) proposed a new powerful method for analyzing critical phenomena which is called the coherent anomaly method (CAM). This method estimates real exponents by using a series of systematic mean-field type approximations, which always gives the classical exponents.

It was successfully applied in two and three dimensional Ising models by *M. Katori and M. Suzuki* (1987). This method is applicable to many other critical phenomena, such as, spin glasses [*M. Suzuki* (1988)], self-avoiding random walks [*X. Hu and M. Suzuki* (1988)], percolation [*M. Takayasu and H. Takayasu* (1988)], diffusion-limited aggregation [*H. Takayasu, M. Takayasu, and T. Nakamura* (1988)], contact process [*N. Konno and M. Katori* (1990)], and so on.

It is known that values of continued fractions can be estimated by the CAM theory [*M. Suzuki* (1988)]. Let us find a solution for the continued fraction, $\bar{Z}_1(\varrho)$, given in Eq.(2.3.6) [*M. Takayasu* (1988)]. We define the n-th approximation $\bar{Z}_1^{(n)}(\varrho)$ by terminating $\bar{Z}_1(\varrho)$ at the n-th order as follows;

$$\bar{Z}_1(\varrho) = \cfrac{1}{2+4\varrho - \cfrac{1}{2+8\varrho - \cdots \ddots - \cfrac{1}{2+4(n-1)\varrho - \cfrac{1}{2+4n\varrho}}}}$$

$$= \frac{A_n(\varrho)}{B_n(\varrho)}, \qquad \text{(A.7)}$$

where $A_n(\varrho)$ and $B_n(\varrho)$ are polynomials of ϱ. Generally, $B_n(\varrho)$ is expected to have a simple zero at $\varrho_c^{(n)}$ such that $B_n(\varrho_c^{(n)})=0$ and $B'_n(\varrho_c^{(n)})\neq 0$. Thus, the n-th approximation, $\bar{Z}_1^{(n)}(\varrho)$, takes the classical singularity as follows;

$$\bar{Z}_1^{(n)}(\varrho) \propto \frac{1}{\varrho - \varrho_c^{(n)}} \cdot \chi_1^{(n)}(\varrho_c^{(n)}) \quad . \tag{A.8}$$

$\varrho_c^{(n)}$ converges to a real singular point ϱ_c of the continued fraction $\bar{Z}_1(\varrho)$, as the order of approximation increases. The critical coefficient, $\chi_1^{(n)}(\varrho_c^{(n)})$, which gives a constant (do not depend on ϱ) for each approximation, is assumed to diverge as $\varrho_c^{(n)} \to \varrho_c$ following a power-law, such as,

$$\chi_1^{(n)}(\varrho_c^{(n)}) \propto \frac{1}{(\varrho_c^{(n)} - \varrho_c)^{\psi}} \quad . \tag{A.9}$$

By applying CAM, the true order of the singularity of $\bar{Z}_1(\varrho)$, φ, is estimated as follows from Eq.s(A8) and (A9):

$$\varphi = \psi + 1,$$

$$\bar{Z}_1(\varrho) \propto \frac{1}{(\varrho - \varrho_c)^{\varphi}} \quad . \tag{A.10}$$

From first three approximations (n=1 to n=3), we obtained the exponent φ by this method. The observed points fit very nicely on a linear line in $ln\ (\varrho_c^{(n)} - \varrho_c)$ *vs.* $ln\ \chi_1^{(n)}(\varrho_c^{(n)})$ plot (see Fig.A1). The obtained value is φ = -0.326, which is fairly close to the exact

value, 1/3, though the estimation is based on only a few terms in the continued fraction.

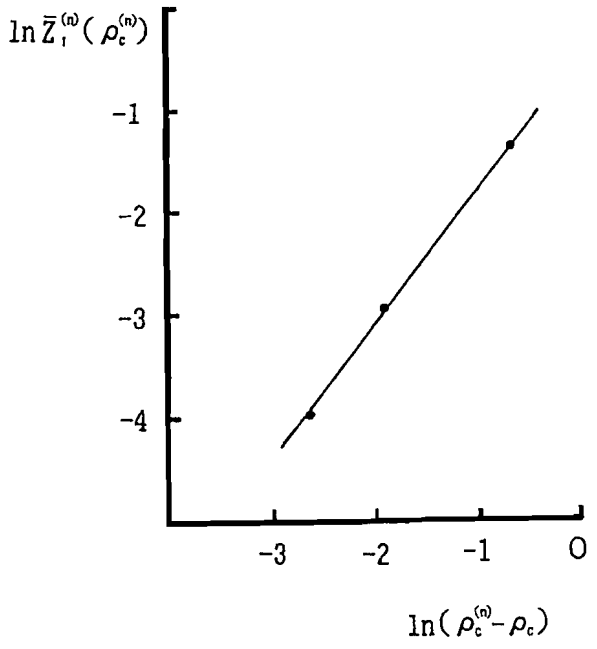

Fig.A1 *ln* $(\varrho_c^{(n)}-\varrho_c)$ *vs. ln* $\chi_1^{(n)}(\varrho_c^{(n)})$. The plotted points are the values for n=1, 2, and 3 from right to left. The slope of the line gives $\varphi = -0.326$.

Appendix (3); Stable distributions

A definition of stable distribution is given as follows [W. Feller (1966)]:

Let $X, X_1, X_2, \cdots, X_n$ be independent random variables with a common distribution R. The distribution R is stable if and only if for $Y_n \equiv X_1+X_2+\cdots+X_n$ there exist constants c_n and γ_n such that

$$Y_n \overset{d}{=} c_n X + \gamma_n , \tag{A.11}$$

where $\overset{d}{=}$ denotes that the random variables of both sides follow the same distribution.

Using the characteristic function of a distribution R, $\Phi(z) = \langle e^{-iXz} \rangle$, the relation (A.11) is transformed into

$$\Phi^n(z) = \Phi(c_n z) \cdot e^{-i\gamma_n z} . \tag{A.12}$$

The solution for Eq.(A12) is known to be given as

$$\Phi(z) = exp \{ - |z|^\alpha \cdot e^{\pm i\pi\theta/2} \} . \tag{A.13}$$

where, α is an essential parameter called the characteristic exponent which characterizes the distribution in the range $0 < \alpha \leq 2$. For $\alpha>2$, it gives unphysical result that the probability density takes negative values [to be rigorous, Eq.(A.13) is not valid for the case $\alpha=1$]. θ is another parameter for symmetric of the distribution, which takes a value in the range $|\theta| \leq \alpha$ for $0< \alpha <1$, and $|\theta| \leq 2-\alpha$ for $1<\alpha \leq 2$.

The probability density, $p(X; \alpha, \theta)$, which is define by the reverse Fourier transformation of Eq.(A.13), is given as

$$p(X; \alpha, \theta) = \frac{1}{\pi} Re \int_0^\infty dz \; exp \; \{ - iXz - z^\alpha \cdot e^{i\pi\theta/2} \} \quad . \qquad (A.14)$$

The explicit functional form of the integral of Eq.(A.14) follows Gaussian for $\alpha=2$, $\theta=0$, and Lorentzian for $\alpha=1$, $\theta=0$ [Eq.(A.14) is valid also for the case of $\alpha=1$, $\theta=0$, the case which we exclude in defining Eq.(A.13)].

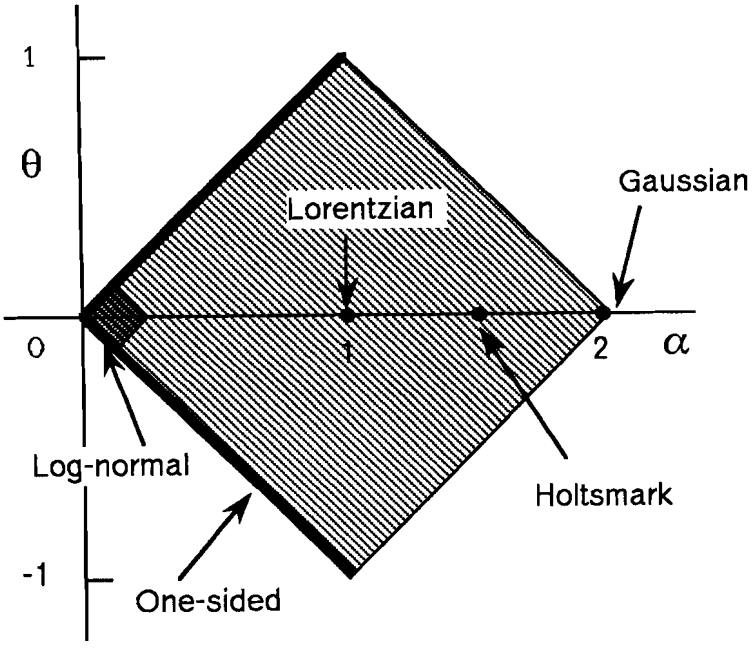

Fig.A2 The parameter space (α, θ) for stable distributions.

Typical functional forms of Eq.(A.14) depending on θ and α are shown in Fig.A2. For $\theta=0$, the distribution is symmetric, because we have the relation, $p(X; \alpha, \theta) = p(-X; \alpha, -\theta)$. On the lines of $\theta=\alpha$ and $\theta=-\alpha$, for $0<\alpha<1$, the distribution is one-sided, that the variable takes only positive or negative values. For all cases, except for $\alpha=2$(Gaussian), $p(X; \alpha, \theta)$ are known to have a power-law tails, such as $p(X; \alpha, \theta) \propto X^{-\alpha-1}$.

The constant c_n in Eq.(A11) is known to be given as $c_n=n^{1/\alpha}$ $(0 < \alpha \leq 2)$, so that we obtain the following relation for $\gamma_n=0$;

$$Y_n \stackrel{d}{=} n^{1/\alpha} Y_1. \tag{A.15}$$

In the case of basic Scheidegger's river model, Eq.(A.15) is confirmed to hold in the mass distribution with $\alpha=1/3$. Let us see Fig.2.11 in section 2.4.3. If we consider the two successive sections whose lengths are n times different, such as $r_1=k$ and $r_2=nk$, the area of basins flowing into the sections are estimated to be proportional to k^3 and $(nk)^3$, respectively, since the height, h, of a drainage basin is proportional to the square of the length of the section, namely,

$$m_{nk} \propto n^3 m_k, \tag{A.16}$$

where m_1 is the area of one particle, and m_n is the area of n particles. So that, the distributions for one particle and n particles are considered to satisfy

$$m_n \stackrel{d}{=} n^3 m_1. \tag{A.17}$$

Appendix (4); Supplement for stability of steady states

From Eq.(2.5.4), (or Eq.(2.5.7)), we have the following inequality for the perturbation:

$$\left|\tilde{Z}(\varrho, t)\right| \leq \left|\Phi(\varrho)\right|^t \cdot const. \quad . \tag{A.18}$$

In case that $\Phi(\varrho)$ satisfies criteria (i) in Appendix (1), it is trivial that $\left|\tilde{Z}(\varrho, t)\right| \to 0$ for all values of ϱ as $t \to \infty$ (remember that for $\varrho = 0, \left|\tilde{Z}(\varrho, t)\right| = 0$ by the boundary condition). In case (iii), obviously $\left|\tilde{Z}(\varrho, t)\right| \to 0$ as $t \to \infty$ for all ϱ except for the points $\{2\pi j/I_0, j = 0, \pm 1, \pm 2, \cdots\}$. Since a characteristic function is a continuous function, $\left|\tilde{Z}(\varrho, t)\right|$, must vanish for all ϱ in the limit $t \to \infty$.

In case (ii), we can assume that $I_0 > 0$ without loss of generality. The uniqueness and stability can be proven easily if we modify the definition of the characteristic function by Laplacian transformation (Eq.(A.1)), as

$$Z(\varrho, t) = \langle e^{-\varrho m} \rangle , \qquad \Phi(\varrho) = e^{-\varrho I_0} . \tag{A.19}$$

In the same way as we derived Eqs.(2.5.2) and (2.5.4), we get the following inequality:

$$\left|\tilde{Z}(\varrho, t)\right| \leq e^{-\varrho I_0 t} \cdot const. , \tag{A.20}$$

this shows that $\left|\tilde{Z}(\varrho, t)\right| \to 0$ as $t \to \infty$ for all values of positive ϱ.

Thus the perturbation $|\tilde{Z}(\varrho, t)| \to 0$ vanishes in the limit $t \to \infty$ in all cases. In other words, the aggregation system converges to the power-law steady-state for any initial distribution.

References

Abramowitz, M. and Stegun, I., *Handbook of Mathematical Functions* (Dover Publications, Inc., New York, 1965).

Anacker, L.W. and Kopelman, R. ,Phys. Rev. Lett. **58**, 289 (1987).

de Arcangeles, L., Redner, S., and Coniglio, A., Phys. Rev. B **31**, 4725 (1985).

de Arcangeles, L., Redner, S., and Coniglio, A., Phys. Rev. B **34**, 4656 (1986).

Bak, P. and Tang, C., and Wiesenfeld, K., Phys. Rev. Lett. **59**, 381 (1987).

Bak, P. and Tang, C., J. Geophys. Res. **94**, 635 (1989).

Batchelor, G. K., *Theory of Homogeneous Turbulence* (Cambridge Univ. Press, Cambridge, (1953).

ben-Avraham, D., Burschka, M. A., and Doering, C. R., J. Stat. Phys., **60**, Nos.5/6 (1990).

Benzi, R., Paladin, G., Parisi, G., and Vulpiani, A., J. Phys. A **17**, 3521 (1984).

Bleistein, N. and Handelsman, R. A., *Asymptotic Expansions of Integrals* (Dover, New York, 1986).

Cheng, Z., Redner, S., and Levraz, F., Phys. Rev. Lett. **62**, 2321 (1989).

Dhar, D. and Ramaswamy, R., Phys. Rev. Lett. **63**, 1659 (1989).

Doering, C. R. and ben-Avraham, D., Phys. Rev. A **38**, 3035 (1988).

Doering, C. R. and ben-Avraham, D., Phys. Rev. Lett. **62**, 2563 (1989).

Domany, E. and Kinzel, W., Phys. Rev. Lett. **53**, 311 (1984).

Durret, R., *Lecture Notes on Particle Systems and Percolation* (Wadsworth, Belmont, 1988).

Family, F. and Landau, D. P. (eds), *Kinetics of Aggregation and Gelation* (North-Holland, Amsterdam, 1984).

Feder, J., *Fractals* (Plenum, New York, 1988).

Feller, W., *An Introduction to Probability Theory and Its Applications* (Willey, New York, 1966).

Friedlander, S. K., *Smoke, Dust and Haze* (Willy-Int.Sci., New York, 1977).

Grassberger, P., Phys. Lett. A **97**, 227 (1983).

Halsey, T. C., Jensen, M. H., Kadanoff, L. P., Procaccia, I., and Shraiman, B. I., Phys. Rev. A **33**, 1141 (1986).

Havlin, S. and ben-Avraham, D., Adv. in Phys. **36**, 695 (1987).

Hayakawa, H., Yamamoto, M., and Takayasu, H., Prog. Theor. Phys. **78**, 1 (1987).

Hayakawa, H., J. Phys. A **22**, 571 (1989).

Hendriks, E. M. and Ernst, M. H., J. Colloid. Interface **97**, 196 (1984).

Hentschel, H. G. E., and Procaccia, I., Physica D **8**, 435 (1983).

Hu, X. and Suzuki, M., Physica A **150**, 310 (1988).

Huber, G., Physica A **170**, 463 (1991).

Ito, K. and Matsuzaki, M., J. Geophys. Res. **95**, 6853 (1990).

Jullien, R. and Botet, R., *Aggregation and Fractal Aggregates* (World Scientific Publishing, Singapore, 1987).

Kagan, Y. Y. and Jackson, D. D., Geophys. J. Intern. **104**, 117 (1991).

Kang, K. and Redner, S., Phys. Rev. A **30**, 2833 (1984).

Karder, M., Parisi, G., and Zang, Y.-C. (1986).

Katori, M. and Suzuki, M., J. Phys. Soc. Jpn. **56**, 3092 (1987)

Kida, S. and Murakami, Y., Fluid Dynamics Research **4**, 347 (1989).

Kondoh, H., Matsushita, M., and Fukuda, Y., J. Phys. Soc. Jpn, **56**, No.6, 1913 (1987).

Konno, N. and Katori, M., J. Phys. soc. Jpn. **59**, 1581 (1990)

Korvin, G., *Fractal Models in the Earth Sciences* (Elsevier Science Publishers B. V, Amsterdam, 1992).

Liggett, T. M., *Interacting Particle Systems* (Springer-Verlag, New York, 1985).

Lindenberg, K., West, B. J., and Kopelman, R., Phys. Rev. Lett. **60**, 1777 (1988).

Lindenberg, K., West, B. J., and Kopelman, R., Phys. Rev. A42, 890 (1990).

Lindenberg, K., Sheu, W.-S., and Kopelman, R., J. Stat. Phys. 65, 1269 (1991).

Lomnitz-Adler, J., Knopoff, L., and Martinez-Mekler, G., Phys. Rev. A45, 2211 (1992).

Lukacs, E., *Characteristic Functions* (Griffin, London, 1970).

Mandelbrot, B. B., J. Fluid. Mech. **62**, 331 (1974).

Mandelbrot, B. B., *Les Objects Fractals: Forme, Hasard et Dimension* (Flammarion, Paris, 1975).

Mandelbrot, B. B., *The Fractal Geometry of Nature* (W. H. Freeman, San Francisco, 1982).

Mandelbrot, B. B., *Fractals and Multifractals: Noise, Turbulence and Galaxies* (Springer, New York, 1988).

Matsushita, M., Sano, M., Hayakawa, Y., Honjo, H., and Sawada, Y., Phys. Rev. Lett. **53**, 286 (1984).

Mcleod, J. B., Quart. J. Math. Oxford **13**, 119, 193 (1962).

Meakin, P., Phys. Rev. A **26**, 1495 (1983).

Meakin, P., J. Colloid Interface Sci. **105**, 240 (1985).

Meakin, P., Stanley, H. E., Coniglio, A., and Witten, T. A., Phys. Rev. A **32**, 2364 (1985).

Meakin, P., Coniglio, A., Stanley, H. E., and Witten, T. A., Phys. Rev. A **34**, 3325 (1986).

Meakin, P. and Stanley, H. E. , Nature, **335**, 405(1988).

Meneveau, C. and Sreenivasan,K. R., Phys. Rev. Lett. **59**, 1424 (1987)C.

Meneveau, C. and Sreenivasan, K. R., J. Fluid Mech. **244**, 429 (1991).

Monin, A. S. and Yaglom, A. M., *Statistical Fluid Mechanics* (MIT, Cambridge, 1975).

Montroll, E. W. and Bendler, J. T. , J. Stat. Phys. **34**,129 (1984).

Nagatani, T., Private communication (1992).

Obukhov, S. P., Private comunication (1989).

Park, H. K. and Goldburg, W. I., Phys. Rev. Lett. **68**, 938(1992).

Pietronero, L. and Tossati, E. (eds), *Fractals in Physics* (North-Holland, Amsterdam, 1986).

Pumir, A., Shraiman, B., and Sigga, E. D., Phys. Rev. Lett. **66**, 2984 (1989).

Racz, Z., Phys. Rev. Lett. **55**, 1707 (1985).

Rényi, A., *Probability Theory* (North-Holland, Amsterdam, 1970).

Scheidegger, A. E., Bull. Int. Assoc. Sci. Hydrol. **12**, 15 (1967).

She, Z-S., Jackson, E., and Orszag, S. A., J. Sci. Comp. 3, 407 (1988).

Sinai, E. D. and Yakhot, V., Phys. Rev. Lett. **63**, 1962 (1989).

Siebesma , A. P. and Pietronero, L., J. Phys. A: Math. Gen. **21**, 3259 (1988).

von Smoluchowski, M., Z. Phys. **17**, 557 (1916).

von Smoluchowski, M., Z. Phys. Chem. **92**, 129 (1917).

Spouge, J. T., Phys. Rev. Lett. **60**, 871(1988).

Sussman, S. M., IEEE, Trans. Commun. System, 213 (1963).

Suzuki, M., J. Phys. Soc. Jpn. **55**, 4205 (1986).

Suzuki, M., Phys. Lett. A **127**, 410 (1988).

Suzuki, M., J. Phys. Soc. Jpn. **57**, 1 (1988).

Taguchi, Y., and Takayasu, H., Phys. Rev. A **41**, 2249 (1990).

Takahashi, T., *Physics of clouds* (in Japanese, Tokyo-do Publishing Inc., 1987).

Takayasu, H. and Nishikawa, I., Proc. 1st Int. Symp. for Science on Form, S. Ishizaka, ed. p. 15 (KTK Scientific, Tokyo, 1986).

Takayasu, H. and Nishikawa, I. and Tasaki, H., Phys. Rev. A **37**, 3110 (1988).

Takayasu, H., Takayasu, M., and Nakamura, T., Phys. Lett. A **132**, 429 (1988).

Takayasu, H., Phys. Rev. Lett. **63**, 2563 (1989).

Takayasu, H., Provata, A., and Takayasu, M., Phys. Rev. A **42**, 7087 (1990).

Takayasu, H., *Fractals in the Physical Sciences* (Manchester University Press, 1990).

Takayasu, H., Takayasu, M., Provata, A., and Huber, G., J. Stat. Phys. **65**, Nos.3/4 (1991).

Takayasu, H. and Suzuki, T., J. Phys. A: Math. Gen. **24**, L1309 (1991).

Takayasu, H. and Inaoka, H., Phys. Rev. Lett. **68**, 966 (1992).

Takayasu, H. and Taguchi, Y., Phys. Rev. Lett. **70**, 782 (1993).

Takayasu, M. and Takayasu, H., *What's are fractals?* (in Japanese, Diamond publishing Inc., Tokyo, 1988).

Takayasu, M. and Takayasu, H., Phys. Lett. A **128**, 45 (1988).

Takayasu, M., Master's thesis (1989).

Takayasu, M. and Takayasu, H., Phys. Rev. A **39**, 4345 (1989).

Takayasu, M., Phys. Rev. A **45**, 8965 (1992).

Takayasu, M., Phys. Rev. A **46**, 782 (1992).

Takayasu, M., submitted to Physica A (1992).

Vicsek, T., Meakin, P., and Family, F., Phys. Rev. A **32**, 1122 (1985).

Vicsek, T., *Fractal Growth Phenomena: The second version* (World Scientific, Singapore, 1992).

Watson, G. N., *A Treatise on the Theory of Bessel Functions* (Cambridge University Press, Cambridge, 1944).

Weiss, G. H., Havlin, S., and Matan, O., J. Stat. Phys. **55**, 435(1989).

White, W. H., J. Colloid. Interface Sci. **87**, 204 (1982).

Witten, T. A. and Sander, L. M., Phys. Rev. Lett. **47**, 1400 (1981).

Yamada M. and Ohkitani, K., Prog. Theo. Phys. **86**, 799 (1991).

Ziff, R. M., J. Stat. Phys. **23**, 241(1980).

Ziff, R. M. and Ernest, M. H., J. Stat.Phys., **31**, 519 (1983).

Zipf, G. K., *Human behavior and the principle of least-effort* (Addison Wesley, Cambridge.MA, 1949).

Zolotarev, V. M., Dokl. Akad. Nauk. SSSR. **98**, 735 (1954).

Zolotarev, V. M., *One-dimensional stable distributions* (American math. Soc., Providence, 1986).